ROLE OF THE N-END RULE PATHWAY IN

CARDIOVASCULAR DEVELOPMENT, SIGNALING, AND HOMEOSTASIS

by

Min Jae Lee

Bachelor of Science, Seoul National University, 2000

Master of Science, Seoul National University, 2002

Submitted to the Graduate Faculty of

the School of Pharmacy in partial fulfillment

of the requirements for the degree of

Doctor of Philosophy

University of Pittsburgh

2007

UNIVERSITY OF PITTSBURGH

SCHOOL OF PHARMACY

This dissertation was presented

by

Min Jae Lee

It was defended on

August 7, 2007

and approved by

Yong Wan, PhD., Assistant Professor, Cell Biology & Physiology

Jeffrey L. Brodsky, PhD., Professor, Biological Sciences

Wen Xie, MD., PhD., Assistant Professor, Pharmaceutical Sciences & Pharmacology

Dexi Liu, PhD., Professor, Pharmaceutical Sciences

Dissertation Advisor: Yong Tae Kwon, PhD., Assistant Professor, Pharmaceutical Sciences

ROLE OF THE N-END RULE PATHWAY IN

CARDIOVASCULAR DEVELOPMENT, SIGNALING, AND HOMEOSTASIS

Min Jae Lee, PhD

University of Pittsburgh, 2007

The N-end rule pathway relates the *in vivo* half-life of a protein to the identity of its N-terminal residue. In this pathway, a substrate bearing an N-degron is recognized and ubiquitylated by a family of E3 ubiquitin ligases named UBR proteins. The N-end rule pathway is implicated in various physiological and pathological processes including cardiac development and angiogenesis. It has been previously shown that mice lacking ATE1, which mediates N-terminal arginylation, die during embryogenesis associated with various defects in cardiovascular development. The goal of my graduate research was to understand the function of the N-end rule pathway in cardiovascular development, signaling, and homeostasis. In my first project, I employed a genome-wide functional proteomic approach to identify physiological substrates of ATE1 that potentially underlie the above cardiovascular phenotypes. I found that RGS4, RGS5, and RGS16 are *in vivo* substrates of the N-end rule pathway, the first to be identified in mammals. These RGS proteins, emerging regulators for cardiovascular G protein signaling, were degraded through sequential N-terminal modifications including N-terminal exposure of their Cys-2, its oxidation, and arginylation. In the second project, to understand the physiological meaning of ATE1-mediated RGS proteolysis in cardiac development and signaling, I characterized $ATE1^{-/-}$ mice and embryonic cardiomyocytes with an emphasis on GPCR signaling. I found that a cell-autonomous function of ATE1 regulates the proliferation of cardiomyocytes and the homeostasis of Gq-dependent cardiac signaling. In the third project, I explored a model of heterovalent interaction by developing RF-C11, a small molecule inhibitor of the N-end rule pathway. The two heterovalent ligands in RF-C11 were designed to cooperatively target two cognate sites of N-recognins. RF-C11 showed higher inhibitory efficiency than its homovalent controls, providing a molecular basis of designing multivalent inhibitors for specific intracellular pathways. Moreover, addition of RF-C11 reduced cardiac proliferation and hypertrophy in cardiomyocytes, unveiling a previously unknown function of the pathway in cardiac proliferation and signaling. In summary, my graduate research contributes to a comprehensive understanding of the function of the N-end rule pathway in the cardiovascular system.

TABLE OF CONTENTS

LIST OF TABLES

LIST OF FIGURES

ACKNOWLEDGEMENTS

I have been blessed with the peoples around me. Without them, this work and my PhD training would not have been possible. I cannot thank you enough……

My wife, Jung Hoon Lee, for being a rock in my life. I love you more than anyone in the world.

My dissertation advisor, Dr. Yong Tae Kwon, for showing me the way of "true" scientists. To make up my mind to join your lab, it was one of the best decisions in my life. Thank you.

My parents in Ilsan, Korea for always believing me and praying for me. Mom, I just want to cry in your arms right now. I love you and I miss you.

My brother and sister for being my brother and sister. You are the best and I'm so proud of you. Let's try together not to disappoint each other.

My in-laws in Seoul, Korea for showing their endless love to me.

My late grandparents in Namwon, Korea for all the happy memories.

My grandfather at a small temple in Korea for being my first mentor (you may don't know).

My relatives for sharing good time and hard time with my family.

My lab members, specially Jee Young An and Takafumi Tasaki, for taking their time to help me. I learned a lot from you. Thank you.

My friends of Year 1993 School of Chemistry, Seoul National University.

All the grad students in the Department of Pharmaceutical Sciences, School of Pharmacy, University of Pittsburgh.

Admission committee for the year of 2002, School of Pharmacy, University of Pittsburgh for giving me a chance to study in the United States.

All the members of the Center for Pharmacogenetics. Thanks to you, 6th floor of the Salk Hall is the fun place to work on.

Collaborators all over the world.

Last but not the least, my doctoral committee members for all the support and guidance.

Thanks to your love and concern, I believe I have grown not only scientifically but also humanly. The five years in Pittsburgh. It was the best time in my life. Thank you so much. Thank you so much…….

PREFACE

"The deeper the waters are, the more still they run."

Korean proverb

CHAPTER I

1.0   THE MAMMALIAN N-END RULE PATHWAY

The rates of proteolysis are a function of the cell's physiological state and are controlled differentially for specific proteins. Regulatory proteins are often short-lived *in vivo*, providing a way to generate their spatial and temporal gradients and to rapidly adjust their concentrations through changes in the rates of their degradation. Ubiquitin (Ub) is a highly conserved 76-residue protein and Ubiquitin-dependent proteolysis plays essential roles in controlling the levels of regulatory proteins *in vivo* for cell viability, cell cycle, DNA repair, protein synthesis, transcriptional regulation, and stress responses (Hershko et al. 2000; Finley et al. 2004; Ciechanover 2005; Ciechanover 2005; Varshavsky 2006). Ubiquitin is covalently attached to the substrates through a cascade of enzyme actions, and this process repeats to generate a polyubiquitin chain (Glickman and Ciechanover 2002). The internal lysine (Lys) residue of a substrate is the site of formation of a substrate-linked multiubiquitin chain.

Ub-activating enzyme (E1) first uses ATP to form a thiol ester between an E1 cysteine residue and the C-terminus of Ubiquitin. Ubiquitin is then transferred to the active site cysteine of a Ub-conjugating enzyme (E2). The Ub in this thiol ester is then attacked by the ε-amino group of a substrate Lys. The final step is usually facilitated by a Ub–protein ligase (E3) that binds the E2–ubiquitin thiol ester and the substrate at distinct sites. This three step mechanism initiates most ubiquitylation reactions, regardless of whether the substrate-bound ubiquitin will signal proteasomal proteolysis, endocytosis, or some other fate (Pickart 2001). The polyubiquitin chain is recognized by the 26S proteasome complex, an ATP-dependent multisubunit protease, and degraded into small peptides with length of 3 to 24 amino acids (Rechsteiner et al. 1993; Coux et al. 1996; Rubin et al. 1997; Baumeister et al. 1998; Saric et al. 2004). Polyubiquitin chains linked by K48-G76 isopeptide bonds are usually destined for proteasomal degradation, while K63-G76 chains are strongly implicated in nonproteolytic signaling (Hochstrasser 2006).

The selective targeting of individual substrates for ubiquitylation is facilitated by multiple

E2 and E3 enzymes. Most E3 enzymes belong to two protein families. RING E3s utilize a globular zinc-binding domain to recruit the E2–Ub intermediate (Deshaies 1999; Joazeiro and Weissman 2000) and HECT domain E3s accomplish this by using a different globular domain (Huibregtse et al. 1995; Huang et al. 1999). The HECT domain has a strictly conserved cysteine residue that forms an essential thiol ester intermediates during catalysis. RING finger includes a set of cysteine and histidine residues that have a distinctive spacing owing to their roles as the ligands of two zing ions that stabilize a characteristic globular conformation. The two families are also mechanistically distinct, in that each uses a different source of activated Ub in the isopeptide bond formation step. In RING E3-dependent reactions, the substrate Lys directly attacks the RING-bound E2–Ub intermediate, while, in HECT E3-dependent reactions, Ub must be transferred to a conserved cysteine of the E3 before it can be attacked by the substrate Lys.

The first degradation signals (degrons) were discovered by Varshavsky and coworkers (Bachmair et al. 1986). Certain amino acids located on the N-termini of proteins functioned as an essential and sufficient determinant of a protein's half-life, yielding the N-end rule pathway. N-degrons are recognized by specific E3 Ub ligases called N-recognins, and precursor form of N-degrons, pre-N-degron, can be converted into N-degron through specific N-terminal modifications, providing a means to conditionally destabilize otherwise stable polypeptides (Bachmair et al. 1986; Varshavsky 1996; Kwon et al. 2003; Tasaki et al. 2005; Hu et al. 2006; Hu et al. 2006; Varshavsky 2006). The N-end rule pathway is present in all organisms examined so far, including the Gram-negative model bacterium *E. coli*, the yeast *S. cerevisiae*, the plant *Arabidopsis thaliana* and mammalian cells (Mogk et al. 2007). However, N-degrons in these organisms show distinct differences. Recent identification of mammalian N-end rule components and construction of knockout mice lacking specific components reveal that this proteolytic pathway is implicated in many important processes such as cardiac development, angiogenesis, meiosis and pathogenesis of human genetic diseases(Varshavsky 2000; Mogk et al. 2007).

1.1   N-TERMINAL MODIFICATION IN THE N-END RULE PATHWAY

The N-terminal amino acid of a newly synthesized protein is methionine (Met). Therefore, the exposure of different amino acids on the N-terminus by endopeptidases or methionine

Term	Definition
N-end rule	A relation between the metabolic stability of a protein and the identity of its N-terminal residue
N-degron	Destabilizing N-terminal residue which can be recognized by N-recognin, an internal lysine of a substrate, and structural flexibility
N-recognin	E3 enzyme for the N-end rule pathway; UBR box protein
Destabiizing residue	N-terminal amino acids which leads to degradation of a substrates; primary, secondary, and tertiary
Stabilizing residue	Amino acids which is not bind to N-degron or modified to bind to N-degron, e.g. Met, Val, and Gly
Type 1 / type 2	Primary destabilizing amino acids which are basic, e.g. Arg, Lys, and His / which are bulky hydrophobic, e.g. Phe, Leu, and Trp
ATE1	Encoding Arg-tRNA-Protein transfere, which utilizes Arg-tRNA to arginylate N-termini of protein that bear Asp, Glu, or oxidezed Cys
UBR box	70 amino acid, zinc finger-like domain which is common feature of known and putative N-recognin, probably serves as recognition sites

Table 1. Definition of terms in the N-end rule pathway. Only mainly used terms in this paper are shown. For more detail, see Varshavsky, 1996 and Tasaki, 2007.

aminopeptidases (MetAPs) is a prerequisite for the creation of the N-degron (Table 1) as a post-translational modification. MetAPs remove Met from the N-terminus of a polypeptide if the residue at position 2 is valine (Val), glycine (Gly), proline (Pro), alanine (Ala), serine (Ser), threonine (Thr), or cysteine (Cys) (Kendall and Bradshaw 1992). Among them, only Cys can function as a tertiary destabilizing residue in the N-end rule pathway. The mammalian genome encodes approximately 500 proteins bearing an N-terminal Met-Cys sequence (Yonghua Jiang, Kwon Lab). It remains to be determined whether their secondary Cys acts as a degradation signal. Similar to the N-end rule pathway, the specificity of MetAPs is also conserved from prokaryotes to eukaryotes. A protein's C-terminal fragment after cleavage events by intracellular endopeptidases, such as caspases, Separase and calpains, can also have an N-degron exposed on its new N-terminus.

In the mammalian N-end pathway (Fig. 1), N-terminal aspartate (Asn) and glutamine (Gln) can be enzymatically modified by N-terminal amidohydrolases, NTAN1 and NTAQ1, into N-terminal aspartic acid (Asp) and glutamimc acid (Glu), respectively (Stewart et al. 1995; Grigoryev et al. 1996; Kwon et al. 2000), while a single enzyme, NTA1, deamidates the same residues in *S. cerevisiae* (Kwon et al. 2000). There is no significant sequence similarity between
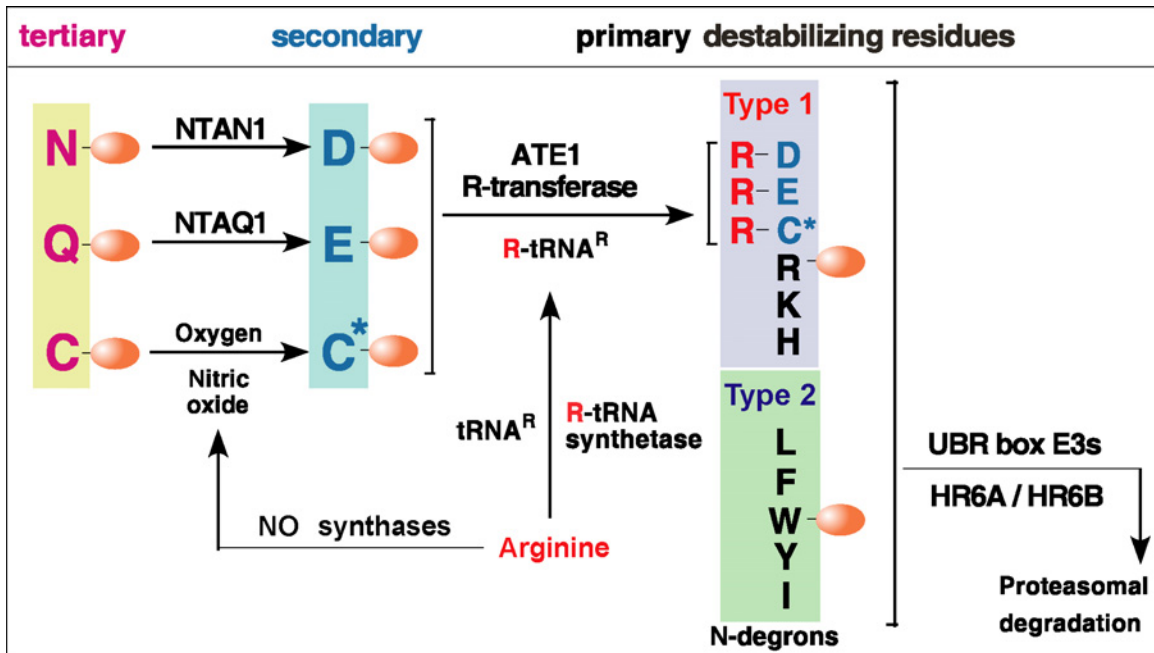
Figure 1. The mammalian N-end rule pathway. N-terminal residues are indicated by single-letter abbreviations for amino acids. Secondary and tertiary destabilizing residues are highlighted with yellow and blue boxes, respectively. Type 1 and type 2 primary destabilizing residues are with purple and green, respectively. The orange ovals denote the rest of a protein substrate. C* denotes oxidized N-terminal Cys, either Cys-sulfinic acid or Cys-sulfonic acid, produced in reactions mediated by nitric oxide and oxygen as indicated, with subsequent arginylation of oxidized Cys by the ATE1-encoded isoforms of Arg-tRNA-protein transferase (R-transferase). The type 1 and type 2 primary destabilizing N-terminal residues are recognized by UBR box E3s of the N-end rule pathway along with E2s, HR6A and HR6B.

S. cerevisiae NTA1 and mammalian NTAN1. N-terminal Asp, Glu, and Cys are destabilizing through their arginylation by the ATE1 Arg-transferase, creating an N-terminal Arg, one of primary destabilizing residues (Kwon et al. 1999; Hu et al. 2005). Arginylation of N-terminal Cys requires its prior oxidation in a manner depending on nitric oxide and oxygen (Kwon et al. 2002; Hu et al. 2005; Lee et al. 2005). In *S. cerevisiae*, an N-terminal Cys is stabilizing in contrast to in the mammalian system. N-terminal Arg together with other primary destabilizing residues are recognized for ubiquitylation by N-recognins (Kwon et al. 1998; Kwon et al. 2001; Kwon et al. 2003). NTAN1-deficient mice were found to be impaired in spontaneous activity, spatial memory and a socially conditioned exploratory behavior (Table 2). However, *S. cerevisiae* strains mutant were found to have only mild phenotypes (Kwon et al. 2000). N-terminal arginylation mediated by ATE1, one of the posttranslational modifications in eukaryotes, was identified ~40 years ago (Kaji et al. 1963) and has been recognized to have important roles in controlling the half-lives of various putative substrates which can be generated by specific proteases including endopeptidases. ATE1-encoded R-transferases are evolutionarily

4

conserved protein observed in all eukaryotes from fungi to animal (Hu et al. 2006). In prokaryotes, Leu/Phe-transferase, a functionally analogous enzyme to ATE1, transfers Leu or Phe to N-terminal Arg, or Lys, distinguished from Asp, Glu, or oxidized Cys in eukaryotes, which are recognized by the ClpAP protease (Graciet et al. 2006).

S. cerevisiae mutants lacking the ATE1-encoded Arg-transferase are viable and phenotypically normal (Balzi et al. 1990). However, ATE1-deficient mice died at a late stage of cardiac development, in which differentiating cardiomyocytes undergo 'compaction' and gradually become part of the compact wall and interventricular septum. This is associated with cardiovascular defects resembling human congenital heart disease (CHD) including ventricular hypoplasia, ventricular septal defect, and impaired angiogenesis (Kwon et al. 2002). In addition to the cardiac defects, the mutant embryos were also perturbed in late angiogenesis. These results suggest that ATE1-dependent proteolysis of unknown substrate(s) is a crucial regulatory mechanism for myocardial growth and blood vessel integrity/maturation. However, the underlying molecular mechanism to explain how knocking out the *ATE1* gene in mice causes characteristic features of CHD remains elusive. However, the details of heart formation in mouse embryos have been known for decades and more and more genes that control its developmental program has been identified, including GATA4, Nkx2.5, TBX5, and MEF2 (Fishman and Chien 1997; Srivastava and Olson 2000). Novel isoforms of ATE1 (ATE1-3, or ATE1^{1A7A}, ATE1-4, or ATE1^{1A7B}, ATE1^{1A7AB}, and ATE1^{1B7AB}) in mammalian system, in addition to the two previously known ATE1-1, or ATE1^{1B7A}, and ATE1-2, or ATE1^{1B7B}, from alternative exon splicing have been known (Rai and Kashina 2005; Hu et al. 2006). Nonetheless, the individual enzymatic activity of each R-transferase on unmodified N-terminal Cys, Asp, or Glu (Rai and Kashina 2005; Hu et al. 2006) and its physiological function remain to be evaluated.

The known functions of the N-end rule pathway in yeast include the regulation of peptide import through degradation of CUP9, which controls the expression of a peptide transporter (Byrd et al. 1998), and osmoregulation by controlling Sln1p-dependent phosphorylation (Ota and Varshavsky 1993). Moreover, it was also reported to regulate the degradation of Gpa1p, a Gα protein of *S. cerevisiae (Madura and Varshavsky 1994)*, and alphaviral RNA polymerase in virus-infected metazoan cells (de Groot et al. 1991). Inhibition of the N-end rule pathway interfered with mammalian cell differentiation (Hondermarck et al. 1992) and limb degeneration in amphibians (Taban et al. 1996). More recently, a few *in vivo* ATE1 substrates, in common

with N-end rule substrates, have been identified. Yeast *S. cerevisiae* SCC1, a subunit of the cohesin complex, is cleaved by the ESP1 separase at the metaphase-anaphase transition, yielding a C-terminal Arg-SCC1 fragment which is degraded by yeast UBR1 (Rao et al. 2001). In *S. cerevisiae*, perturbation of SCC1 degradation resulted in chromosome instability. *Drosophila melanogaster* DIAP1, an apoptosis inhibitor has been identified as an ATE1 substrate, which is implicated in the regulation of Rpr and Hid-mediated apoptosis (Ditzel et al. 2003). Caspase-mediated cleavage of *Drosophila* DIAP1 produces a C-terminal Asn-DIAP1 fragment that is deamidated by dNTAN1 into Asp-DIAP1, and subsequently arginylated for proteolysis by dATE1 into Arg-Asp-DIAP1 (Baker and Varshavsky 1995; Kwon et al. 2000). In mammals, arginylation of β-actin in mouse embryonic fibroblasts was reported, but, surprisingly, the stability of β-actin was unchanged regardless of arginylation (Karakozova et al. 2006). Instead, ATE1 regulates actin filament polymerization and lamella formation by preventing aggregation of the filament through electrostatic repulsion. A unique form of arginylation which is linked to the γ-carboxyl of internal Glu, instead of N-terminal amine, of neurotensin was also reported to control neurotensin's binding affinity with its receptors (Eriste et al. 2005).

1.2   N-TERMINAL RECOGNITION IN THE N-END RULE PATHWAY

Even in prokaryotes where no ubiquitin exists, the N-end rule pathway is functional, indicating the ancient origin of the N-end rule pathway. However, the destabilizing residues in the N-end rule show organism specificity. While basic amino acids, such as Arg, Lys, and His, serve as type 1 and bulky hydrophobic amino acids, such as Leu, Phe, Trp, Tyr, and Ile, serve as type 2 primary destabilizing resides in eukaryotes, similar but smaller number of amino acids, including Leu, Phe, Trp, and Tyr, function as primary destabilizing residues in *E. coli*. In plants, the N-degron includes basic and aromatic residues. In eukaryotes, N-terminal Asn and Gln can act as tertiary destabilizing residues of the N-end rule pathway through deamidation by N-terminal amidohydrolases (Nt-amidases) into the secondary destabilizing N-terminal residues Asp and Glu, respectively (Fig. 1). N-terminal Asp and Glu function as secondary destabilizing residues through arginylation by *ATE1*-encoded R-transferase, creating the primary destabilizing residue

6

Component	Knockout mouse phenotype
NTAN1	Behavioral alteraltion
ATE1	Impaired cardiogenesis
UBR1	Mouse version of Johanson-Blizzard Syndrome
UBR2	Female-specific lethality / male-specific infertility
UBR1/UBR2	Impaired neurogenesis / cardiogenesis
UBR3	Abnormality in olfactory sensor

Table 2. Phenotypes of N-end rule-related knockout mice. For more detail, see references, Kwon, 2000 for NTAN1; Kwon, 2002 for ATE1; Kwon, 2001 for UBR1; Kwon, 2003 for UBR2; and Tasaki, 2007 for UBR3.

Arg at the N-terminus (Balzi et al. 1990; Kwon et al. 1999).

In mammals, Arg, one of the primary destabilizing residues can be conjugated to secondary destabilizing residues by *ATE1*-encoded Arg-transferases (Kwon et al. 1999). The N-terminal Arg and other N-terminal destabilizing residues, which can be categorized into type 1 and type 2, are recognized and ubiquitylated by a family of E3 Ub ligases, UBR proteins (Kwon et al. 1998; Tasaki et al. 2005). UBR1/E3α has long been known as the only N-recognin in mammals. It has been characterized biochemically in rabbit reticulocyte extracts (Hershko et al. 2000) and its cloned mouse gene, *UBR1*, encodes a 200-kDa protein that was similar to sc-UBR1 not only in sequence but also in the substrate-binding properties as well (Kwon et al. 1998). Soon after that, additional N-recognins have been suggested and identified. The common feature of the UBR proteins is a 70-amino acid, zinc finger-like domain (termed the UBR box) for N-degron recognition, and another specific body structure (the RING domain in UBR1, UBR2, and UBR3; the HECT domain in UBR5; the F-box in UBR6; the PHD domain in UBR7) for Ub transfer and/or additional substrate recognition site (Tasaki et al. 2005). A genetic screen with *S. cerevisiae* UBR1 identified type 1-specific residues in the UBR box and type 2-specific residues scattered outside the UBR box. In the case of *Arabidopsis* UBR4, a conserved Cys in the UBR box was implicated in auxin transport and growth (Gil et al. 2001). UBR5/EDD is a 300 kDa nucleic E3 ligase with a HECT domain. UBR6 is a 90 kDa-F-box protein and UBR7 is a 50-kDa protein with the plant homeodomain (PHD), a conserved zinc finger that resembles the RING finger domain.

The N-end rule pathway exists even in prokaryotes which lack Ub and Ub-proteasome

proteolytic system (Tobias et al. 1991; Shrader et al. 1993), suggesting that the N-end rule pathway existed prior to the evolution of the Ub-proteasome system. In *Escherichia coli*, N-end rule substrates are degraded by collective function of ClpA and ClpP (together forming ClpAP), and ClpS (recognizing destabilizing N-terminal residue) (Erbse et al. 2006). The substrate recognition domain of ClpS and a part of the type 2 binding site of *S. cerevisiae* UBR1 showed significant homology, suggesting an evolutionary conserved mechanism for the recognition of N-degrons. Therefore, it is increasingly clear that the UBR box is essential for the recognition of both type 1 and type 2 N-degrons, probably providing a common structural element.

Mutation in human UBR1 causes Johanson-Blizzard Syndrome (JBS) (Zenker et al. 2005) and mice lacking UBR1 developed exocrine pancreatic insufficiency, despite normal synthesis of zymogens such as trypsinogen and proelastase, subtle growth retardation, altered fat metabolism, and behavioral abnormality, all related with the diagnostics of human JBS (Kwon et al. 2001; Zenker et al. 2005). In the mutant mice, endogenous skeletal muscle proteins also showed impaired degradation and ubiquitylation (Solomon et al. 1998; Lecker et al. 1999). The mild phenotypes of *UBR1*$^{-/-}$ mice were attributed to the functional compensation by UBR2. It was reported that *UBR2*$^{-/-}$ male mice are infertile as a result of testis degeneration due to defects in homologous chromosome pairing during meiotic prophase 1, whereas a majority of *UBR2*$^{-/-}$ female embryos were lethal without specific terminal phenotypes (Kwon et al. 2003). Spermatocytes lacking UBR2 are arrested before the pachytene status and undergo extensive apoptosis. Interestingly, in *S. cerevisiae*, the cleaved cohesin component SCC1 has N-terminal Arg and degraded by UBR1. This cleavage event by Separase is required to initiate sister chromatid separation at the metaphase-to-anaphase transition during mitosis and consequently for chromosome stability.

UBR1 and UBR2 appear to cooperate with each other for ubiquitylation of N-end rule substrates. Mice lacking both UBR1 and UBR2 also died at early midgestation associated with severe abnormality in cardiogenesis and neurogenesis, where precocious differentiation and impaired proliferation of neural precursor cells were observed (An et al. 2006). In the double mutants, the balance between proliferation and differentiation of neural stem cells in the forebrain shifted toward decreased proliferation and increased differentiation. In contrast to UBR1 and UBR2, UBR3 does not bind to known destabilizing N-terminal residues (Tasaki et al. 2007). UBR3 is prominently expressed in sensory cells and, especially, UBR3-deficient mice in

a C57BL/6 genetic background are impaired in the olfactory sensor system. Consequently, new-born UBR3$^{-/-}$ pups cannot feed themselves with mother's milk and die within two days. In another study, UBR5/EDD-deficient mice showed embryonic lethality due to impaired development in yolk sac vessel and abnormal cell proliferation in extraembryonic tissues (Saunders et al. 2004).

CHAPTER II

2.0 IDENTIFICATION OF RGS4, RGS5, AND RGS16 AS *IN VIVO* SUBSTRATES OF THE N-END RULE PATHWAY

2.1 OVERVIEW

Mice lacking ATE1, which mediates N-terminal arginylation, die during embryogenesis associated with various defects in cardiovascular development. However, its underlying molecular mechanism remains elusive. To understand the function of ATE1 in the cardiac development, this study employed a functional proteomic approach. I demonstrate that ATE1 Arg-transferase mediates the *in vivo* degradation of RGS4, RGS5, and RGS16. They function as negative regulators of specific G proteins which are implicated in cardiac growth and angiogenesis. Mutant RGS proteins in which the conserved Cys-2 residue could not become N-terminus were long-lived *in vivo*. The proteolysis of these RGS proteins was perturbed in cells lacking Ub ligases UBR1 and/or UBR2. Hypoxia decreased the ubiquitylation of these RGS proteins both *in vitro* and *in vito*. These results together suggest that the sequential modifications of RGS4, RGS5, and RGS16 (N-terminal exposure of their Cys-2, its oxidation, and subsequent arginylation) act as a licensing mechanism in response to extracellular and intracellular signals prior to the targeting for proteolysis by UBR1 and UBR2. I also found that *ATE1* $^{-/-}$ embryos were impaired in the activation of ERK mitogen-activated protein kinases and in the expression of G protein-induced downstream effectors such as Jun, cyclin D1, and β-myosin heavy chain. The mRNA level of βMHC, a downstream gene of the GPCR pathway regulating cardiac development, was also decreased in *ATE1* $^{-/-}$ embryos and embryonic hearts. These results established RGS4, RGS5, and RGS16 as *in vivo* substrates, the first to be identified, of the mammalian N-end rule pathway, and also suggested that the O_2-ATE1-UBR1/UBR2 proteolytic circuit plays a role in RGS-regulated G protein signaling in the cardiovascular system.

2.2   BACKGROUND

In mammals, Asp and Glu, the two N-terminal residues known to be arginylated by ATE1-encoded R-transferase, were shown to be destabilizing residues in the N-end rule pathway (Bachmair et al. 1986). Therefore, it was proposed that the function of R-transferase is to target proteins for degradation by conjugating Arg, one of the primary destabilizing residues, to secondary destabilizing N-terminal residues, which are Asp and Glu in fungi, and Asp, Glu, and Cys in metazoans (Gonda et al. 1989). It was also proposed that the analogous prokaryotic enzyme Leu, Phe-tRNA-protein transferase (L, F-transferase) mediates the activity of N-terminal Arg and Lys, which, in prokaryotes, would be secondary destabilizing residues (Hu et al. 2006). The physiological function of N-terminal arginylation has been known to be implicated in cardiovascular development (Kwon et al. 2002). $ATE1^{-/-}$ embryos died associated with various cardiovascular defects including those resembling human congenital heart disorders. The mutant ventricular myocardium displayed severe hypoplasia, resembling thin myocardium syndrome, associated with ventricular septal defect. In addition to cardiac defects, the mutant embryos were also perturbed in late angiogenesis. These results suggest that ATE1-dependent proteolysis of unknown substrate(s) is a crucial regulatory mechanism for myocardial growth and blood vessel integrity/maturation. Given that myocardial diseases account for the leading causes of death in western society, a fundamental question is the identity of molecules underlying ATE1-dependent myocardial growth.

Heterodimeric G proteins are signal transducers that connect the ligand-activated G protein-coupled receptors (GPCRs) to effectors for the intracellular signaling pathways (Neves et al. 2002). Ligand-activated GPCRs stimulate the Gα subunit to exchange GDP to GTP, and thereby dissociate the inactive Gαβγ heterotrimer into the active Gα and Gβγ subunits, both of which activate independently second messenger-producing enzymes and ion channels. Signaling by Gα and Gβγ continues until Gα hydrolyzes GTP and the heterotrimer reassociates. The duration of signaling by G proteins is tightly controlled to produce appropriate cellular responses. The slow intrinsic rate of GTP hydrolysis by Gα can be drastically increased by G protein signaling (RGS) proteins (Berman et al. 1996), which contain a 120 amino acid RGS domain responsible for GTPase activation. RGS4, RGS5, and RGS16 act as GTPase activating proteins (GAPs) for Gαq and Gαi and have a crucial role in shutting off G protein-mediated

11

responses in all eukaryotes (Berman et al. 1996). GTP-bound Gαq activates phospholipase C (PLC) and mediates IP$_3$-mediated calcium release and diacylglycerol-mediated protein kinase C (PKC) activation. G$\beta\gamma$ mediates activation of the small GTP-binding protein Ras and initiate a tyrosine kinase, leading to activation of mitogen-activated protein kinases (MAPKs) (Molkentin and Dorn 2001). Although the role of RGS5 and RGS16 in the heart is yet to be explored, given that RGS4, RGS5, and RGS16 are all prominently expressed in the ventricle (Wieland and Mittmann 2003), the potential role of RGS5 and RGS16 in the Gq- and Gi-activated cardiovascular signaling has been anticipated.

In this study, a functional proteomic approach was employed in collaboration with Meso Scale Discovery (Gaithersburg, MD) to identify physiological substrates of the N-end rule pathway. I identified a set of RGS proteins, RGS4, RGS5, and RGS16, as *in vivo* substrates of the pathway, the first to be identified. These RGS proteins were degraded through sequential N-terminal modifications including N-terminal exposure of their Cys-2, its oxidation, and arginylation. Consistent with the function of RGS proteins as negative regulator of GPCR signaling, downstream signal transducers of G protein signaling pathway, MAPKs, were impaired in *ATE1*$^{-/-}$ and *UBR1*$^{-/-}$*UBR2*$^{-/-}$ embryos and/or cells. These data indicate that the ATE1-dependent N-end rule pathway plays a crucial role for RGS-regulated G protein signaling in the cardiovascular system and possibly in other biological processes as well.

2.3   METHODS

***In vitro* ubiquitylation and degradation assays of RGS proteins.** For *in vitro* degradation assay, RGS proteins were expressed and biotin-labeled, in the absence or presence of 2 mM dipeptides, using the rabbit reticulocyte lysate TnT system (Promega), followed by a time-course Western blotting with horseradish peroxidase (HRP)-conjugated streptavidin (Pierce). *In vitro* ubiquitylation of RGS proteins was similarly determined except that the reaction was done in the presence of MG132, followed by anti-Ub immunoprecipitation and subsequent Western blotting with HRP-conjugated streptavidin. Anti-Ub antibody (Biomol International) recognizes both mono- and multi-ubiquitinated proteins but not free Ub. Bestatin (Sigma-Aldrich) with 150 μM concentration was added to decrease degradation of dipeptides. The RGS4, C2V-RGS4, and

C2G-RGS4 constructs were previously described (Davydov and Varshavsky 2000) as were the RGS5, Myc-RGS5, and C2A-RGS5 constructs (Zhou et al. 2001). The C2A-RGS5 construct was generated by PCR-mediated mutagenesis. The RGS16 construct was generated by using RT-PCR, subcloning into pENTR vector (Invitrogen), and subsequent recombination into pcDNA-cLumio-DEST vector (Invitrogen). Anti-RGS5 antibody was previously described (Zhou et al. 2001), while anti-RGS4 antibody was purchased (Santa Cruz Biotechnology). For pulse chase analysis, mouse embryonic fibroblasts were transiently transfected with RGS4 or RGS5-expressing plasmid and control plasmid. After 24 hr post-transfection, mouse embryonic fibroblasts were labeled with [^{35}S]methionine/cysteine for 12 min, followed by chase for 0, 30 min, and 60 min in the presence of cycloheximide. Extracts were prepared and immunoprecipitated with anti-RGS4 or RGS5 and V5 (for luc) antibodies, and SDS-PAGE, autoradiography, and quantification were sequentially performed. $ATE1^{-/-}$, $UBR1^{-/-}$, and $UBR2^{-/-}$ embryonic fibroblasts were previously described(Kwon et al. 2001; Kwon et al. 2002; Kwon et al. 2003), while $UBR1^{-/-}UBR2^{-/-}$ mouse embryonic fibroblasts will be described elsewhere (An et al. 2006). The ATE1-1 and ATE1-2 constructs were generated by subcloning their open reading frames (ORFs) from the yeast expression constructs into pcDNA3 vector (Invitrogen).

***In vitro* oxygen depletion.** To generate oxygen-depleted reaction condition, a nitrogen-containing balloon was connected to microtube with rubber-O-ring cap (Axygen Scientific) through a 10-mL syringe and a 23-gauge needle. Before the reaction, nitrogen was introduced into the tube by pulling out another plunger gently several times to vent out inside air. For control, luciferase-expressing plasmid was cotranslated with RGS-expressing plasmid to determine more precise comparison of stability of RGS proteins between in the presence and absence of oxygen. For *in vivo* hypoxic treatment, wild type and $ATE1^{-/-}$ mouse embryonic fibroblasts were co-transfected with RGS5 and control LacZ plasmids. After 6 hr post-transfection, cells were exposed to either normoxia or hypoxia for 24 h. Hypoxia was achieved by exposing cells to 0.1% O_2 and 5% CO_2 balanced with N_2 in an anaerobic incubator (Thermo Electron). Reticulocytes in hypoxic condition could be distinguished from those in normoxic condition by its dark color, probably from less oxidized heme in red blood cells.

Western Blot Analysis, Kinase Assay, and Expression Analysis. To examine the activities of

13

MAPKs, total embryonic or embryonic heart extracts from wild type and *ATE1*^{-/-} embryos and mouse embryonic fibroblasts were subjected to immunoblotting using antibodies against ERK1/2, phospho-ERK1/2, JNK1, JNK2, phospho-JNK1/2 (Santa Cruz Biotechnology), p38, and phospho-p38 (Cell Signaling Technology), MEK1/2, phospho-MEK1/2, Gαq (Santa Cruz Biotechnology), and actin (Sigma-Aldrich). The whole embryos and embryonic hearts were isolated in ice-cold PBS and homogenized in lysis buffer (20 mM Hepes, pH 7.5, 150 mM KCl, 10 % glycerol, 0.1 mM EDTA) containing protease inhibitor cocktail, sodium orthovanadate, and sodium fluoride (Sigma). A soluble fraction was separated by a two-step centrifugation (9,000 *g* and 100,000 *g*). The signals were visualized by Supersignal West Pico Chemiluninescent Substrate (Pierce) and the membranes were reprobed with anti-actin antibody (Sigma). *In vitro* ERK kinase assay was performed using an assay kit from Upstate Biotechnology. Mouse embryonic fibroblasts were grown were grown as monolayers in Dulbecco's modified Eagle medium (GIBCO) supplemented with 10% fetal bovine serum. Genotyping of each embryo and mouse embryonic fibroblasts were performed using standard polymerase chain reaction (PCR) with primers F1 (CCAGCTCATTCCTCCCACTCATGATC), R1 (GGTATTTGCTGCCGTCCTTTGGTGGTC), and R2 (CTGGAGACAAAGCCCCAGCCA-GAC), amplifying 570-bp and 430-bp fragments for wild type allele and knockout allele, respectively. For Northern blot analysis, total RNA was subjected to hybridization with cDNA fragment probes. Microarray analysis was done using the GPCR signaling pathway GE array (SuperArray Bioscience) with a size of 96 genes.

2.4   RESULTS

2.4.1   RGS4, RGS5, and RGS16 as Substrates of the N-end Rule Pathway

ATE1^{-/-} mouse embryos die *in utero* due to various cardiovascular defects (Kwon et al. 2002), suggesting that ATE1-dependent proteolysis of cardiovascular regulators may be an essential regulatory mechanism for appropriate cardiovascular function. Therefore, I asked whether there

Proteins	Sequences	Predicted N-termini
RGS4, -5, -16	Met—**Cys**—RGSs	Cys
Myc-RGS5	**Met**—Glu—Myc—Met—Cys—RGS5	Met
C2A-RGS5	Met—**Ala**—RGS5	Ala
C2V-RGS4	Met—**Val**—RGS4	Val
C2G-RGS4	Met—**Gly**—RGS4	Gly

Table 3. RGS constructs and their expected N-terminal residues. MetAPs remove Met from the N-terminus of a polypeptide if the residue at position 2 is Val, Gly, Pro, Ala, Ser, Thr, or Cys. Among them, only Cys can function as a tertiary destabilizing residue in the N-end rule pathway. Ala, Val, and Gly are stabilizing residues in the N-end rule pathway. N-terminal Myc tag blocks the recognition and cleavage by MetAPs, resulting in a stable form of RGS proteins.

are cardiac regulators amongst candidate N-end rule substrates which were identified through a recent functional proteomic approach (Meso Scale Discovery, Gaithersburg, MD). In this screening, ~18,000 cDNAs encoding ~14,000 distinct proteins were expressed in rabbit reticulocyte lysates, labeled with biotin, and allowed to be ubiquitylated. Polyubiquitylated proteins were immobilized and detected by using electrochemiluminescence (ECL) technique. Approximately 500 proteins were identified to be highly ubiquitylated. Subsequent dipeptide treatment to the ubiquitylation reaction further identified 42 candidate substrates for the N-end rule pathway (Data not shown).

In eukaryotes, Met aminopeptidases (MetAPs) can cleave off N-terminal Met when the second residue is Cys (pro-N-degron), Ala, Ser, and Thr (type 3 N-degron), Pro (UFD substrate), Gly, or Val (stabilizing) (Kendall and Bradshaw 1992). Previous reports indicated that in mammals N-terminal Cys can serve as a pro-N-degron through ATE1-dependent N-terminal arginylation (Kwon et al. 2002). MetAPs can therefore potentially destabilize, via the *ATE1* gene activity, a protein only when the second residue is Cys. Analysis of known or predicted open reading frames (ORFs) of candidate N-end rule substrates suggested that only RGS4, RGS5, and RGS16 bore the Cys_2 residue, indicating that their half-lives may be controlled by ATE1-dependent N-terminal arginylation. Consistent with this finding, RGS4 was previously reported to have a short half-life, and its *in vitro* degradation is inhibited by type 1 dipeptide inhibitors (Davydov and Varshavsky 2000). However, it remains unknown whether RGS4 is an *in vivo* N-end rule substrate. These results suggested that the remaining 32 proteins (except for RGS4, RGS5, and RGS16) are likely to be destabilized via cleavage events by endopeptidases (e.g.,
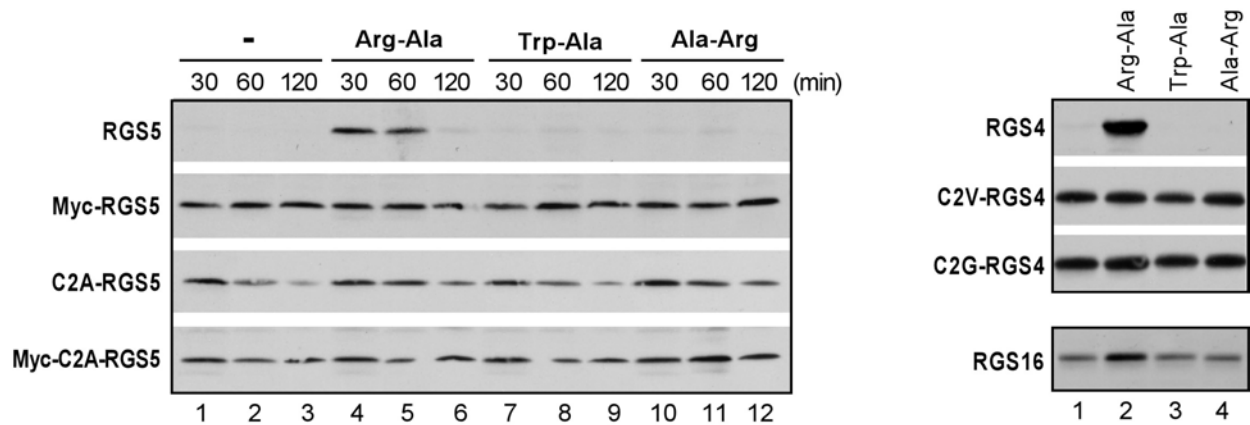
Figure 2. *In vitro* degradation RGS4, RGS5, and RGS16. RGS5 and its mutations (left panel), RGS4 and its mutation (right panel, upper), and RGS16 (right panel, lower) were expressed in reticulocyte lysates in the presence of different dipeptides N-end rule inhibitors, and their degradation was analyzed using anti-biotin Western blotting. Reactions were allowed for 60 min in RGS4 and RGS5. Inhibition of RGS5 proteolysis by Arg-Ala diminished after 120 min perhaps due to instability of dipeptides. These RGS proteins act as type 1 substrate. Therefore, non-cognate dipeptides, such as Trp-Ala and Ala-Arg exert no effect on the stability of the proteins. The stabilization degree of RGS16 protein is lower than those of RGS4 and RGS5.

caspases) that produces C-terminal fragments bearing N-degrons, which should be the major mechanism that destabilizes proteins for the N-end rule pathway.

RGS4, RGS5, and RGS16 belong to structurally related R4 RGS subfamily and are considered prototypical because they have a 120 residue RGS domain with no other identifiable features except for a conserved N-terminal 33 residue amphipathic helix enriched in basic residues. Accumulating evidence suggests that RGS4, RGS5, and RGS16 are emerging counter regulators of Gq- and Gi-activated cardiovascular signaling pathways (See Background). Therefore, it was hypothesized that ATE1-dependent proteolysis of these RGS proteins may be a novel regulatory mechanism for the cardiovascular GPCR signaling pathways. RGS4, RGS5, and RGS16 were all short-lived in reticulocyte lysates and their degradation was perturbed by MG132 or Arg-Ala, but not by Trp-Ala or the control dipeptide Ala-Arg (Fig. 2), suggesting that their proteolysis requires type 1 N-degron(s). Inhibition of RGS5 proteolysis by Arg-Ala diminished after 120 min (Fig. 2, lane 6) perhaps due to instability of dipeptides (Fig. 16). Without an endopeptidase inhibitor, bestatin, dipeptides showed no inhibitory activity on the degradation of model substrates. Bestatin itself did not change their stability. The results with RGS4 are largely consistent with the previous observation (Davydov and Varshavsky 2000). Notably, RGS16 was less destabilizing thanRGS4 and RGS5. The Cys_2 residue of RGS16 can be palmitolylated, which appears to be important for plasma membrane localization but not for GAP
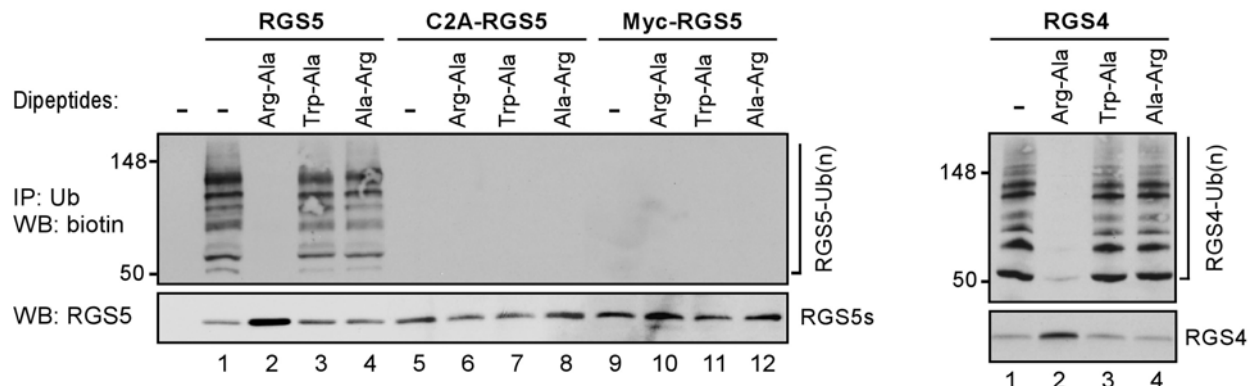
Figure 3. *In vitro* ubiquitylation of RGS4, RGS5, and RGS16. RGS proteins were expressed in reticulocyte lysates in the presence of MG132. After 15 min, their ubiquitylation was analyzed using anti-Ub immunoprecipitation and subsequent anti-biotin Western blotting (top panels), while their expression levels were determined using anti-biotin Western blotting (bottom panels). Consistent with the degradation assay result (Fig. 2), ubiquitylation of RGS4 and RGS5 were active without Arg-Ala dipeptides. Mutated RGS5, which cannot expose N-terminal Cys, showed no ubiquitylation.

activity. Thus, Cys_2 palmitoylation may be a regulatory mechanism that prevents Cys_2 recognition by *ATE1*-encoded Arg-transferases.

The Cys_2 residue of RGS4, RGS5, and RGS16 has been expected to be a common degradation determinant. To examine this, wild type RGS proteins and their mutant with different N-terminal amino acids were constructed (Table 3). N-terminally Myc-tagged RGS5 (Myc-RGS5) where the original Cys_2 residue cannot be exposed at the N-terminus became long-lived (Fig. 2) and was insensitive to Arg-Ala. Further, C2A-RGS5, Myc-C2A-RGS5, C2V-RGS4, and C2G-RGS4, whose predicted N-terminal residues were Ala, Met, Val, and Gly (Table 3), were all significantly stabilizing (Fig. 2). C2A-RGS5 was more destabilizing than Myc-RGS5 both in the absence and presence of dipeptides perhaps because of an elusive E3 called E3β that targets N-terminal Ala, Ser, or Thr (Heller and Hershko 1990) or a yet unknown E3. Consistent with the degradation assay, RGS5 and RGS4 were rapidly ubiquitinated (Fig. 3), and their ubiquitylation was inhibited by Arg-Ala but not by Trp-Ala or Ala-Arg, while ubiquitylation of C2A-RGS5 and Myc-RGS5 was barely detected (Fig. 3). Altogether these data indicated that RGS4, RGS5, and RGS16 are commonly degraded by the type 1 N-end rule pathway, and their degradation requires the expose of Cys_2 at the N-terminus.

2.4.2 ATE1-mediated *In Vivo* RGS protein Degradation
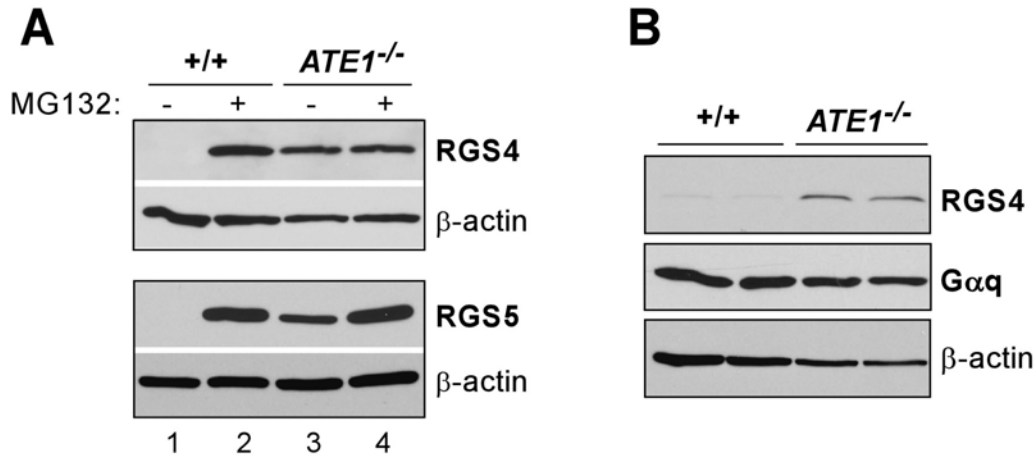
Figure 4. *In vivo* degradation assay of RGS4 and RGS5 in wild type and *ATE1*^{-/-} cells. Anti-RGS4 and RGS5 immunoblotting of overexpressed RGS4 and RGS5 (A) and endogenous RGS4 (B) in wild type and *ATE1*^{-/-} cells in the absence and presence of MG132. In *ATE1*^{-/-} mouse embryonic fibroblasts, otherwise unstable RGS4 and RGS5 were long-lived. MG132 stabilized the proteins in wild type mouse embryonic fibroblasts. Slightly increased RGS protein level in *ATE1*^{-/-} mouse embryonic fibroblasts with MG132 suggests that there may be another controlling mechanism of the proteins' half-lives. Since antibodies sufficient for endogenous RGS5 and RGS16 were unavailable, only endogenous RGS4 levels were compared in wild type and *ATE1*^{-/-} mouse embryonic fibroblasts.

N-terminal Cys$_2$ residue of RGS4 purified from mouse L cells was reported to be arginylated (Kwon et al. 2002). However, it remains unknown whether N-terminal Cys$_2$ arginylation is required for Ub-dependent proteolysis. I asked whether RGS4 and RGS5 are short-lived in mouse embryonic fibroblasts and, if so, whether their degradation is perturbed in *ATE1*^{-/-} cells. RGS4 and RGS5 were expressed in wild type and *ATE1*^{-/-} cells, and their levels were monitored in the absence or presence of MG132. RGS4 and RGS5 were short-lived in wild type cells (Fig. 4, lane 1), and their degradation was perturbed by either MG132 treatment (lanes 2 and 4) or *ATE1* knockout (lane 3). Partial degradation of RGS5 in *ATE1*^{-/-} cells (Fig. 4, lane 3) is perhaps due to non-ATE1-dependent E3 activity present in mouse embryonic fibroblasts. Next, the *in vivo* half-lives of RGS4 and RGS5 in wild type and *ATE1*^{-/-} cells were determined using pulse chase analysis. While less than 1% of RGS5 (compared with the level of Myc-RGS5 at the beginning of chase) remained intact after the 60 min-chase in wild type cells, 71% remained in *ATE1*^{-/-} cells under the same condition (Fig.5). Further, 51% and 45% of C2A-RGS5 and Myc-RGS5, respectively, remained intact after the 60 min- chase even in wild type cells (Fig. 5). Similarly, RGS4 also was rapidly degraded in wild type cells, and its degradation was perturbed in *ATE1*^{-/-} cells (Fig. 5). Then, I examined whether the levels of endogenous RGS4, RGS5, and

18
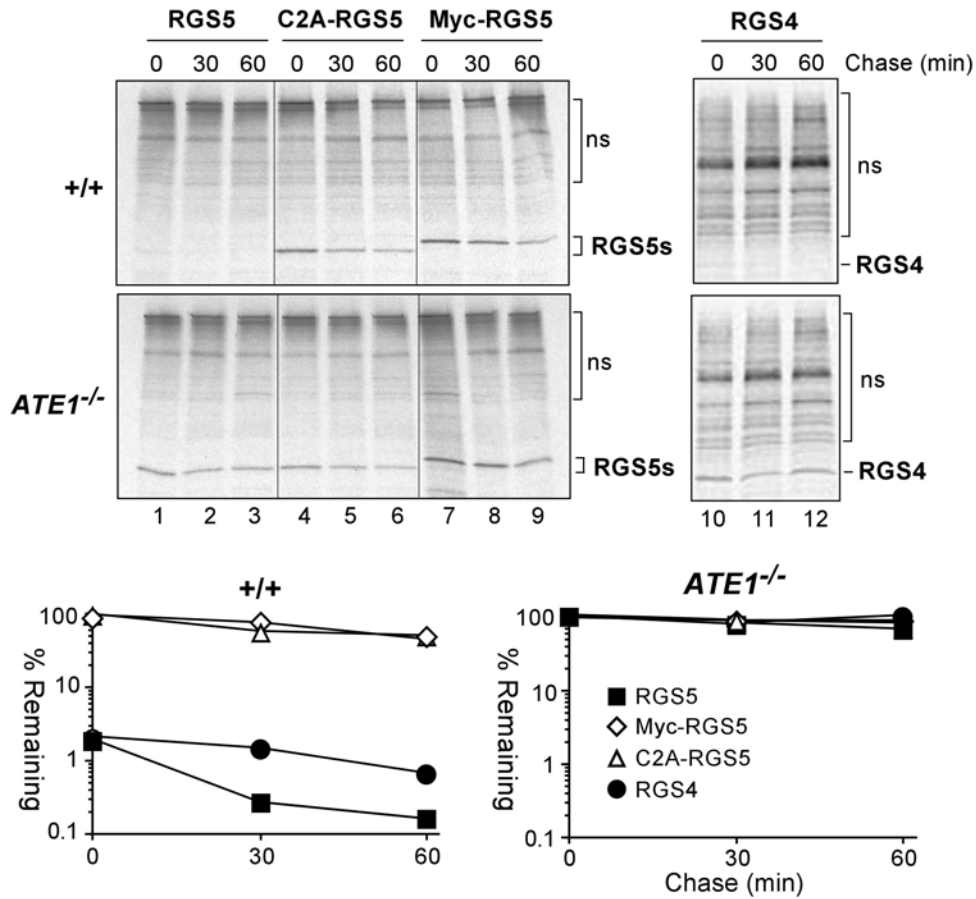
Figure 5. Pulse chase analysis of RGS5, C2A-RGS5, Myc-RGS5, and RGS4 in wild type and $ATE1^{-/-}$ cells. The transfected cells were labeled for 12 min with ^{35}S-Met/Cys, followed by anti-RGS4 or RGS5 immunoprecipitation and SDS-PAGE analysis. Quantitation of autoradiography using PhosphorImager was shown in right. Consistent with the *in vivo* degradation assay (Fig. 4), which measured steady-state level of the proteins, the newly synthesized RGS4 and RGS5 exhibited short half-lives in wild type mouse embryonic fibroblasts, while the secondary Cys mutations were stable. In ATE1-deficient cells, wild type proteins showed almost same half-lives as the mutant proteins.

RGS16 are increased in $ATE1^{-/-}$ cells using anti-RGS4, RGS5, and RGS16 immunoblotting. The level of endogenous RGS4 was higher in $ATE1^{-/-}$ cells than in wild type cells (Fig. 4), though anti-RGS5 and RGS16 antibodies did not detect endogenous proteins in wild type and $ATE1^{-/-}$ cells. (However, more recently, endogenous levels of RGS5 and RGS16 were detected in embryonic hearts and brains. See details in Chapter III). Therefore, RGS4 and RGS5 (and perhaps RGS16 as well) are suggested to be the physiological substrates, the first to be identified, of the ATE1-dependent N-end rule pathway.

ATE1 produces, through alternative splicing, the 60 kDa ATE1-1 and ATE1-2 that contain one of two homologous exons and differ in cellular localization and tissue distribution

19
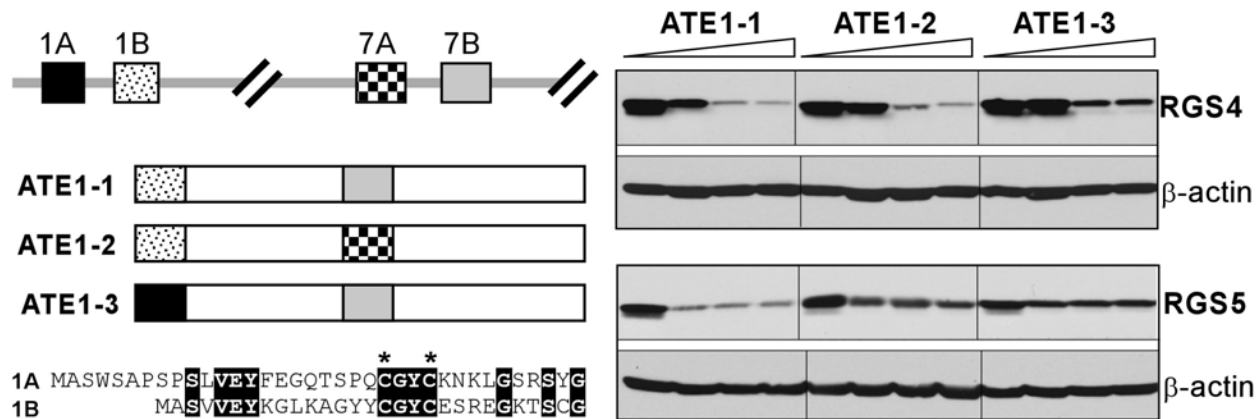
Figure 6. Rescuing ATE1 function on RGS proteolysis in $ATE1^{-/-}$ cells. (Left panels) Structure of $ATE1$ (top), schematics of ATE1-1, ATE1-2, and ATE1-3 (middle), and comparison of sequences encoded by alternative exons 1A and 1B (bottom). (Right panels) An ATE1 isoform and an RGS protein were coexpressed in $ATE1^{-/-}$ cells, followed by anti-RGS immunoblotting. Total 4 μg of the plasmid mixture (RGS4 or RGS5, 2 μg; ATE1-1 or ATE1-2, 0, 0.25, 0.5, or 2 μg, respectively; pcDNA3, 2, 1.75, 1.5, 0 μg, respectively) was transfected into cells in a 6-well plate. As in Figure 4, RGS4 and RGS5 levels in $ATE1^{-/-}$ cells were significant in a normal condition. However, with overexpression of an ATE1 isoform, these protein levels were reduced in concentration-dependent manner. There are slightly different rescuing degrees depending on isoforms.

(Kwon et al. 1999). Sequences encoded by alternative exons 1A and 1B shared two highly

conserved Cys residues (Fig. 6), and a truncated ATE1-1 mutant lacking exon 1B did not exhibit

Arg-transferase activity for N-terminal Asp and Glu. To answer whether and to what degree

individual ATE1 isoforms promote the proteolysis of RGS4 and RGS5 whose common

degradation determinant is N-terminal Cys, a combination of RGS proteins and increasing

amounts of ATE1 isoforms was expressed in $ATE1^{-/-}$ cells where RGS4 and RGS5 are stabilized

(Fig. 6). ATE1-1 was the major Arg-transferase that efficiently promotes proteolysis of both

RGS4 and RGS5 in mouse embryonic fibroblasts, as answered by anti-RGS4 and RGS5

immunoblotting (Fig. 6). In contrast, ATE1-2 facilitated degradation of RGS4 but not efficiently

of RGS5, whereas ATE1-3-dependent degradation was inefficient for both RGS4 and RGS5.

These results suggest that RGS4, RGS5, and RGS16 are physiological substrates of $ATE1$-

encoded Arg-transferases and that two pairs of alternative exons (1A/1B and 7A/7B) are

important for the enzymatic specificity in a substrate-specific manner. The detailed biochemical

mechanism and the role in cardiovascular development of individual ATE1 isoforms are to be

further investigated.

2.4.3   Perturbation of RGS protein Degradation by Oxygen Depletion
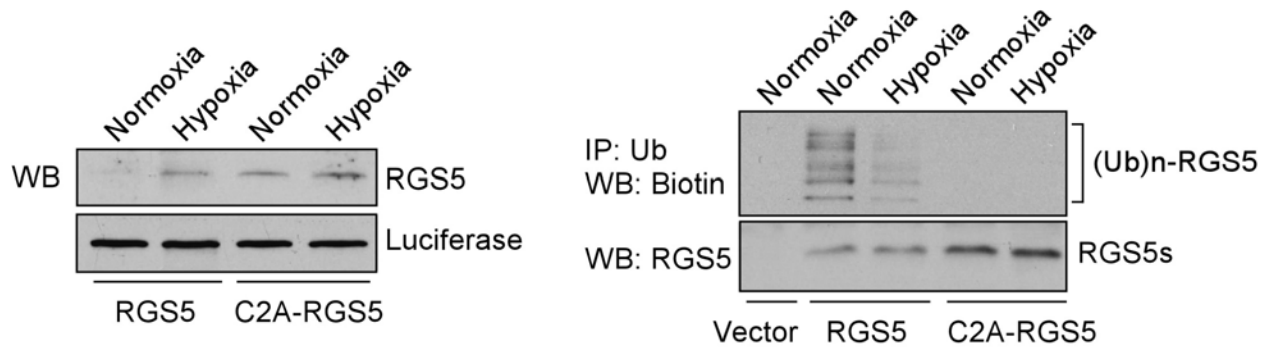
Figure 7. Proteolysis of RGS4 and RGS5 influenced by oxygen concentration. (Left panels) RGS5 and C2A-RGS5 were expressed in reticulocyte lysates under normoxic or hypoxic condition, followed by anti-RGS5 or co-expressed luciferase immunoblotting. (Right panels) RGS5 and C2A-RGS5 were expressed in reticulocyte lysates under normoxic or hypoxic condition, followed by anti-Ub immunoprecipitation and a subsequent anti-biotin Western blotting. Comparison of expression levels using anti-biotin Western blotting is shown on the bottom. Hypoxia inhibited ubiquitylation and degradation of RGS5, suggesting that oxygen may play an important role in RGS protein degradation.

Based on the observation that the molecular weight of N-terminal Cys_2 of a portion of RGS4 purified from mouse L cells has been increased by 48 Da, it was proposed that the N-terminal Cys_2 had been oxidized into Cys sulfinate ($CysO_2$) or cysteic acid ($CysO_3$) (Kwon et al. 2002). However, it remains unknown whether the 48 Da-increase is due to oxidation. Therefore, I examined whether O_2 depletion would perturb the proteolysis of RGS5 and, if so, whether the Cys_2 residue is required for O_2-dependent proteolysis. To this end, a novel method for measuring the effect of O_2 depletion on the proteolysis of newly synthesized proteins in reticulocyte lysates was developed (see Methods). The level of normally short-lived RGS5 was increased upon O_2 depletion (Fig. 7), indicating that O_2 may be an essential cofactor for the proteolysis of RGS5. In contrast, the level of the long-lived C2A-RGS5 mutant was not affected by O_2 depletion (Fig.7), indicating that Cys_2 is required for O_2-dependent proteolysis of RGS4, RGS5, and RGS16. To determine the effect of O_2 depletion on RGS5 ubiquitylation, RGS5 was expressed in the blot with HRP-streptavidin: the ubiquitylation of RGS5 was reduced upon O_2 depletion (Fig. 7). Previously, Cys_{12} was detected as alkylated Cys, whereas Cys_2 could not be identified, suggesting that Cys_2 of RGS4 is oxidized prior to alkylation (Kwon et al. 2002). Although the role of O_2 in Cys_2-dependent proteolysis of short-lived proteins (including RGS proteins) is to be further investigated under physiological conditions, these results together suggest that Cys_2 oxidation of RGS proteins may be an essential and limiting regulatory mechanism for *ATE1-*

21
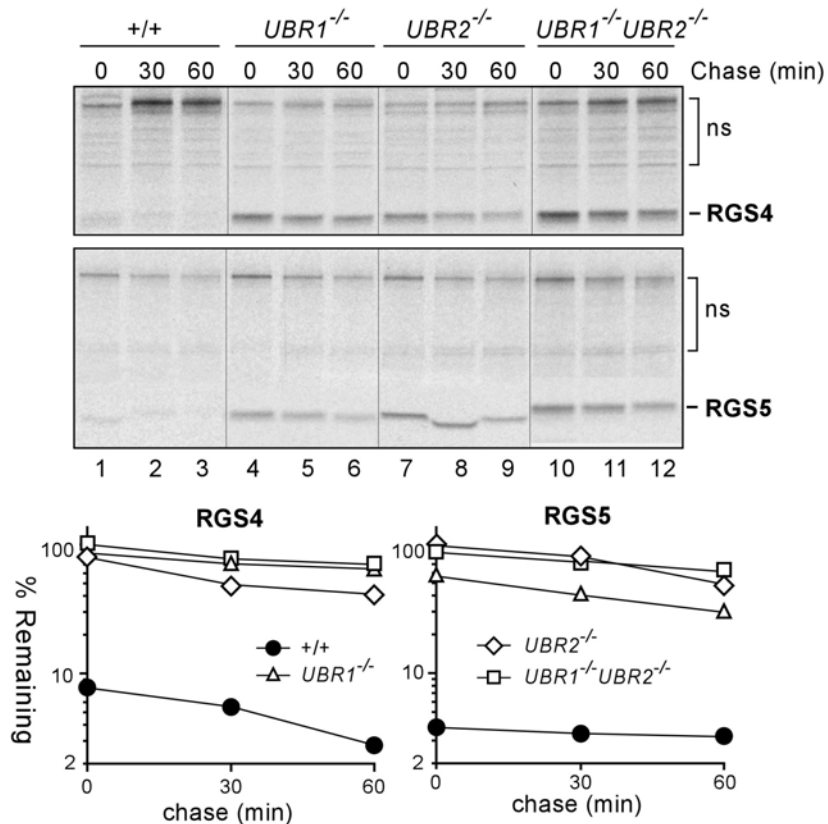
Figure 8. Proteolysis of RGS4 requires UBR1 and UBR2. Pulse chase analysis of RGS4 and RGS5 in wild type, $UBR1^{-/-}$, $UBR2^{-/-}$, and $UBR1^{-/-}UBR2^{-/-}$ cells. The transfected cells were labeled for 12 min with ^{35}S-Met/Cys, followed by anti-RGS4 or RGS5 immunoprecipitation and SDS-PAGE analysis. Quantitation of data in the left panels using PhosphorImager is shown in the bottom panels. RGS4 and RGS5 showed significantly longer half-lives in $UBR1^{-/-}$, $UBR2^{-/-}$, and $UBR1^{-/-}UBR2^{-/-}$ mouse embryonic fibroblasts, suggesting UBR1 and UBR2 are indeed E3 Ub ligases for RGS4 and RGS5 degradation. The difference between the single mutant cells and the double mutant cell in terms of stabilizing effects was negligible. Non-specific bands are denoted as ns.

dependent proteolysis.

2.4.4 Overlapping Role of UBR1 and UBR2 for RGS Proteolysis as E3s

The identity of E3s that are required for proteolysis of RGS4 and RGS5 were not clear. Since the Cys_2 residue of RGS4 and RGS5 is a determinant for ATE1-dependent arginylation (Figs. 8), N-terminal Arg is likely to be an N-degron for their ubiquitylation. It was previously observed that Ub ligases UBR1 and UBR2 directly bind to N-terminal Arg as well as other type 1 and type 2 N-degrons (of a model substrate) and it was proposed that UBR1 and UBR2 are functionally overlapping E3s for type 1 and type 2 N-degrons (Kwon et al. 2003). However, the physiological
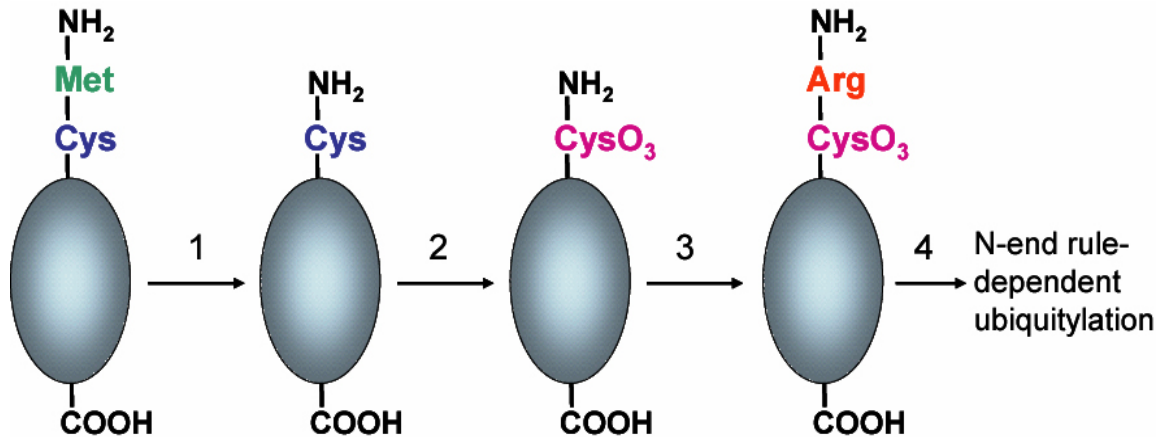
Figure 9. Summarization of RGS Proteolysis. 1. Proteolysis of these RGS proteins initiates from the removal of N-terminal Met by MetAPs, exposing Cys-2 at the N-terminus. 2. The exposed N-terminal Cys-2 appears to be oxidized into Cys-sulfinic acid ($CysO_2$ (H)) or Cys-sulfonic acid ($CysO_3$(H)), which requires NO as well as oxygen (O_2) or its derivatives. 3. Oxidized Cys-2 residue is conjugated with Arg by ATE1 R-transferase. 4. N-terminally arginylated RGS proteins are ubiquitylated by UBR1 and UBR2 for degradation, perhaps with the help by E2 enzymes HR6A and/or HR6B. The proteolysis of RGS proteins and cardiovascular homeostasis.

substrates of UBR1 and/or UBR2 remain unknown. To test whether UBR1 and UBR2 are indeed required for the proteolysis of RGS4 and RGS5, the *in vivo* half-lives of RGS4 and RGS5 in wild type, $UBR1^{-/-}$, $UBR2^{-/-}$, and $UBR1^{-/-}UBR2^{-/-}$ cells were examined. While less than 4% of RGS5 (compared with the level in $UBR1^{-/-}UBR2^{-/-}$ cells at the end of pulse) remained after the 60 min-chase in wild type cells (Fig. 8, lanes 1-3; 13D), 30%, 49%, and 61%, respectively, remained in $UBR1^{-/-}$, $UBR2^{-/-}$, and $UBR1^{-/-}UBR2^{-/-}$ cells under the same condition (Fig. 8, lanes 4-12). Similarly, the *in vivo* degradation of RGS4 was significantly perturbed in these *UBR* mutant cells (Fig. 8). The strong stabilization of RGS4 and RGS5 in $UBR1^{-/-}$ and $UBR2^{-/-}$ single knockout cells (Fig. 8, lanes 4-9) may be because RGS4 and RGS5 are ubiquitinated by a UBR1/UBR2 heterodimer.

Together, these findings establish RGS4 and RGS5 (and perhaps RGS16 as well) as the physiological substrates, the first to be identified, of UBR1 and UBR2, functionally overlapping E3s of the mammalian N-end rule pathway. These data indicate that efficient N-end rule-dependent proteolysis of RGS4, RGS5, and RGS16 requires N-terminal methionine excision by MetAPs, oxidation of N-terminal Cys, arginylation by ATE1 isoform-encoded Arg-transferses, coordinated recognition of both an N-terminal amino acid (pro-N-degron and N-degron) by UBR proteins (Fig. 9).
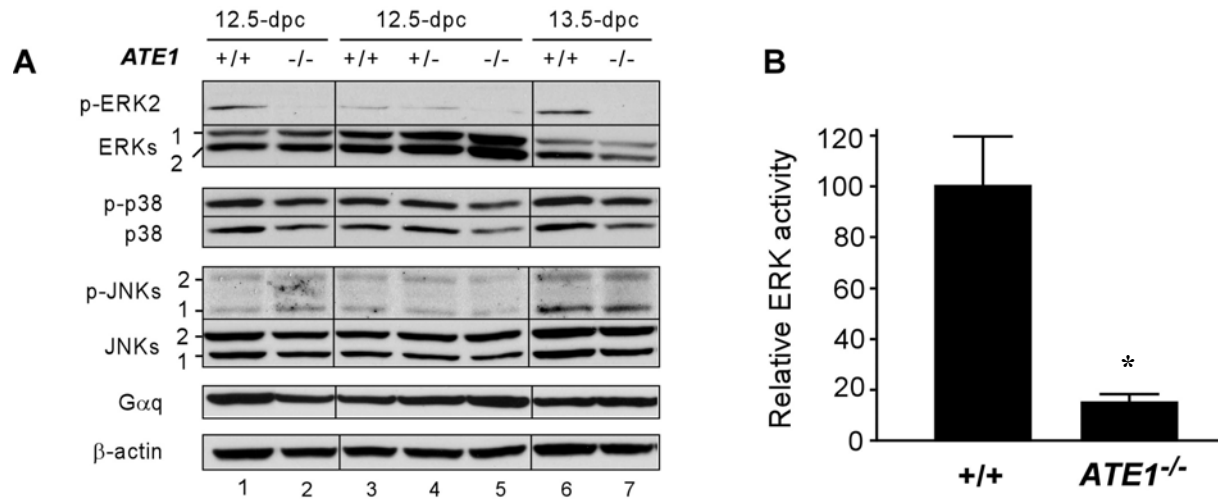
Figure 10. MAPK activities in *ATE1*^{-/-} Embryos. The 12.5 dpc and 13.5 dpc- wild type and *ATE1*^{-/-} embryonic extracts were subjected to anti-ERK1/2, p38, and JNK (phosphorylated and non-phosphorylated forms). As a control, the levels of Gαq and β-actin were examined. Two different litters were used for 12.5 dpc embryos. In both 12.5 dpc and 13.5 dpc, ERK2 activities were significantly reduced in *ATE1*^{-/-} embryos. *In vitro* ERK kinase activity assay using whole embryonic extract and synthetic ERK substrates also showed reduced ERK activity in ATE1-deficient embryos. Data represents mean ± s.e.m. of the relative ERK activity from three embryonic extracts. *: $p < 0.05$.

2.4.5   Impaired ERK Activity in ATE1-deficient Embryos and Cells

Above results suggest that ATE1-dependent N-terminal arginylation is essential for the proteolysis of RGS4 and RGS5 (and perhaps RGS16 as well). There is accumulating evidence that RGS4, RGS5 and RGS16 act as negative regulators of the Gq- and Gi-activated signaling pathways in the cardiovascular system and probably other biological processes as well. Consistent with the function of *ATE1* in RGS proteolysis, it was reported that *ATE1*^{-/-} embryos die due to various cardiovascular defects (Kwon et al. 2002). Gq and Gi activate a complex network of MAPKs: extracellular signal-regulated protein kinases (ERK1 and ERK2), c-Jun N-terminal kinases (JNKs), and p38 MAPKs. Therefore the activation of MAPKs in *ATE1*^{-/-} embryos was examined by using phospho-specific antibodies. The amounts of Gαq and inactive ERK1/ERK2, JNKs, p38 MAPKs were not affected in 12.5 dpc-*ATE1*^{-/-} embryos (Fig. 10). However, the active, phosphorylated form of ERK2, but not of JNKs and p38 MAPKs, was decreased in *ATE1*^{-/-} embryos, although phosphorylated ERK1 was not detected in embryonic extracts (Fig. 10). Consistent with this result, total kinase activities of ERK1 and ERK2 in
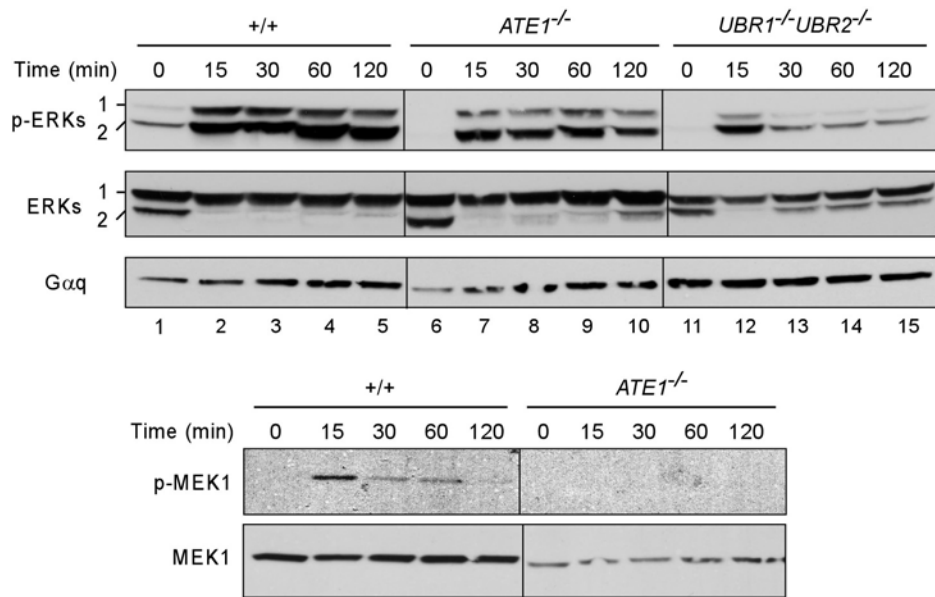
Figure 11. Serum-starved and serum-stimulated ERK1/2 MAPK activities in wild type, $ATE1^{-/-}$, and $UBR1^{-/-}UBR2^{-/-}$ mouse embryonic fibroblasts. (Upper) Cells were serum-starved for 24 h and subsequently stimulated with 20% FBS for the times indicated. Total cell extracts were subjected to immunoblotting with antibodies against Gαq and phosphorylated and unphosphorylated ERK1 and ERK2. (Lower) Similar experiment was performed for serum-starved and serum-stimulated MEK1 activity in wild type and $ATE1^{-/-}$ mouse embryonic fibroblasts. Activation of both ERK1/2 and MEK1 on serum stimulation was delayed in $ATE1^{-/-}$ mouse embryonic fibroblasts, compared with wild type. Interestingly, $UBR1^{-/-}UBR2^{-/-}$ mouse embryonic fibroblasts showed even more delayed activation, suggesting these E3 Ub ligases may have an ATE1-independent role in MAPK activities.

$ATE1^{-/-}$ embryonic extracts, as determined by the kinase assay with myelin basic protein as a substrate, was ~5 fold lower than in wild type cells (Fig. 10).

Next, the effect of serum starvation and stimulation on the activation of ERK1 and ERK2 in wild type, $ATE1^{-/-}$, and $UBR1^{-/-}UBR2^{-/-}$ cells were examined. The N-end rule-dependent ERK1 and ERK2 activation was prominent upon 24 hr-serum starvation when the active forms were barely detected in $ATE1^{-/-}$ and $UBR1^{-/-}UBR2^{-/-}$ cells (Fig. 11, lanes 6 and 11). Quantitation showed that the total amounts of active ERK1 and ERK2 upon serum stimulation were also lower in $ATE1^{-/-}$ and $UBR1^{-/-}UBR2^{-/-}$ mouse embryonic fibroblasts (Fig. 11). Notably, the function of ERK1 and ERK2 was more severely impaired in $UBR1^{-/-}UBR2^{-/-}$ mouse embryonic fibroblasts than in $ATE1^{-/-}$ mouse embryonic fibroblasts, suggesting that UBR1 and UBR2 may have an ATE1-independent role in the MAPK pathways. The upstream signal transducers that are involved in the ATE1-dependent activation of ERK1 and ERK2 were therefore examined. ERK1 and ERK2 can be activated by MEK1, a crucial player in cardiovascular signaling pathways.

25
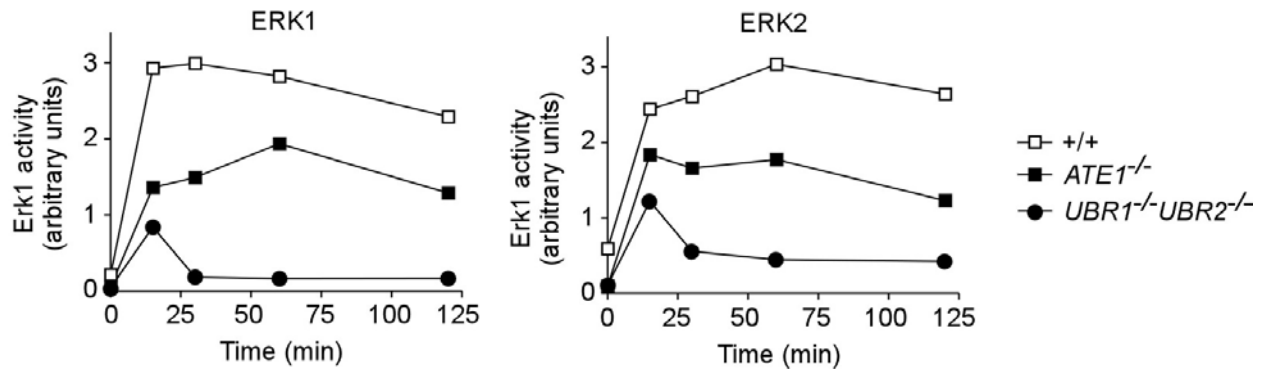
Figure 12. ERK and MEK activities after serum stimulation. Quantitation of the active forms of ERK1 and ERK2 in wild type embryonic extracts, ATE1-mutant, and UBR1UBR2-double mutant cells shown in the previous figure. Gαq was used for normalization. Activation of both ERK1/2 and MEK1 on serum stimulation was delayed in $ATE1^{-/-}$ mouse embryonic fibroblasts, compared with wild type. Interestingly, $UBR1^{-/-} UBR2^{-/-}$ mouse embryonic fibroblasts showed even more delayed activation, suggesting these E3 Ub ligases may have an ATE1-independent role in MAPK activities. Unlike ERK1, which showed maximum activity on 15 min after serum-stimulation, ERK2 showed relatively prolonged activity in wild type mouse embryonic fibroblasts.

$ATE1^{-/-}$ cells did not show detectable activation of MEK1 upon serum stimulation after 24 hr-serum starvation (Fig. 11), suggesting that the MEK1-ERK1/2 pathway is regulated by the ATE1-UBR1/UBR2 pathway.

The activated GPCR pathways, including the MAPK pathways, promote cell growth via transcriptional induction of downstream effectors. To test whether *ATE1* has a role in the induction of GPCR-regulated gene expression in normally growing mouse embryos, Microarray analysis of 96 GPCR-induced genes was employed using total RNAs from 12.5-dpc-wild type and $ATE1^{-/-}$ embryos (Fig. 13). The mRNA levels of several MAPK-activated downstream effectors, including Jun, Fos, Pdpk1, and cyclin D1, were ~2-fold down-regulated in 12.5-dpc $ATE1^{-/-}$ cells (data not shown), which was in part confirmed by Northern blot analysis (Fig. 14). Myocardial growth through stimulation of the G protein signaling is accompanied by activation of ventricular embryonic genes such as those for βMHC and skeletal α-actin. To examine the role of *ATE1* in myocardial growth, Northern blot analysis of these genes was performed using 12.5-dpc-wild type and $ATE1^{-/-}$ embryos and embryonic hearts. The mRNA level of βMHC, but not of MLC2, RGS4, or α-actin, was ~2-fold decreased in $ATE1^{-/-}$ embryos and embryonic hearts (Fig. 14). Taken together, these results (Fig. 14) suggest that altered expression of a rather broad spectrum of cardiovascular downstream effectors that are induced by the G protein pathways may collectively underlie the observed cardiovascular phenotypes of $ATE1^{-/-}$ embryos.

	WT	KO	
Eif4a2	19241.17	26315.91	136.8
Agt	27128.47	45073.73	166.1
Anf-ESTs	19912.44	47811.28	240.1
Cdkn1a	24533.88	39400.97	160.6
Gnrhr	22631.6	33499.18	148.0
Lhb	16498.36	25257.73	153.1
Oprk1	24598.58	30197.77	122.8
Ccl4	8267.456	11065.18	133.8

	WT	KO	
Agtrap	13518.02	7263.444	53.7
Ccnd1	39291.83	24519.92	62.4
Cmklr1	17679.18	11664.52	66.0
Egr1	14341.51	9549.656	66.6
Fgf2	12468.59	9012.367	72.3
Fos	13038.03	9983.044	76.6
Il1b	10719.44	8250.278	77.0
Il4	11834.99	8765.9	74.1
Il6	11920.31	9189.889	77.1
Jun	10874.44	8400.267	77.2
Pdpk1	57131.26	40799.64	71.4
Rho	12555.98	9189.1	73.2

Figure 13. GPCR signaling pathway-specific microarray. Total RNAs from 13.5 dpc- wild type and *ATE1*^{-/-} embryonic hearts were used for microarrays that are specific for the GPCR signaling pathway. Induced genes in ATE1 mutants were labeled with blue rectangles and suppressed genes with red. Northern blotting was performed to confirm these data (see Fig. 14).

2.5   DISCUSSION

There is an increasing need to identify systematically the entire set of ubiquitylation substrates, especially for the mammalian proteome to understand the molecular mechanisms of various ubiquitin functions. Although *S. cerevisiae* Ub conjugates have been successfully isolated using affinity purification of 6xHis-Ub-conjugates associated with mass spectrometry (Peng et al. 2003), given the enormous complexity of peptide mixtures to be processed for mass spectrometry, it is yet to be applied to the mammalian proteome that has a significantly higher

27
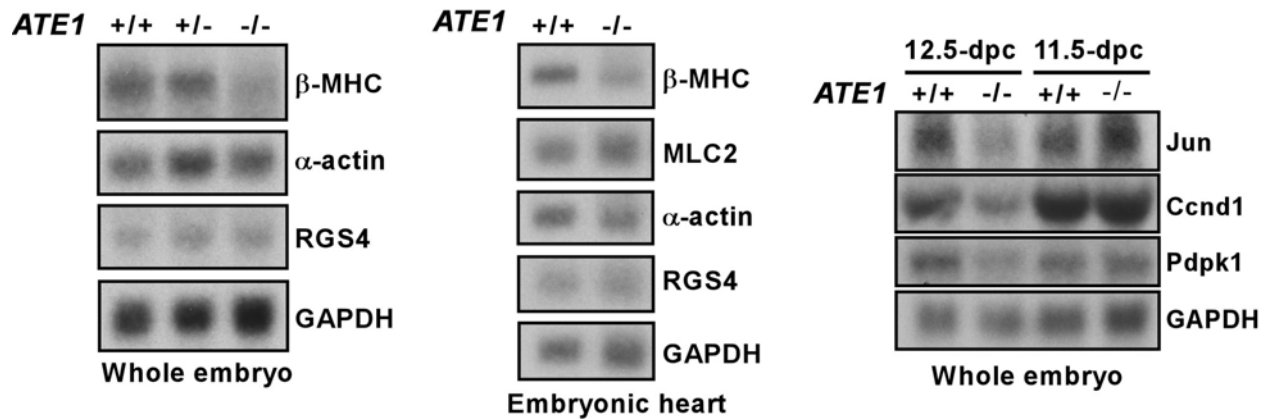
Figure 14. Analysis of the downstream effectors in $ATE1^{-/-}$ Embryos. Total RNAs from 12.5 dpc- wild type and $ATE1^{-/-}$ embryos (left panels) and embryonic hearts (middle panels) were subjected to Northern blotting to examine hypertrophic gene expression. (Right panel) Total RNAs from 11.5- and 12.5 dpc (days post-coitus)-wild type and $ATE1^{-/-}$ embryos were subjected to Northern blotting to confirm the initial microarray results.

complexity. Therefore, the genome-wide functional proteomic method described here provides for the first time a general tool to detect mammalian ubiquitylation substrates. The advantages of this method are that it: *1)* allows automatic analysis of the entire proteome in 1-2 days, *2)* is applicable for different species, *3)* allows identification of rare or rapidly degraded substrates, *4)* is applicable for conditional ubiquitylation by employing defined components (e.g., caspases or kinases) or extracts (e.g., UV irradiated HeLa cell extracts), and *5)* is applicable for a specific E3 system by employing purified E3 components or their inhibitors. The disadvantages of this method are that: *1)* the *in vitro* expression system may not optimally represent physiological conditions and thus may yield false positives, and *2)* the selection procedure is sensitive to the sorting method. The validity of this method was also confirmed by independent studies using other candidates such as aprataxin and MRPL1 (Fig. 15).

The current study and previous observations (Davydov and Varshavsky 2000; Kwon et al. 2002) together suggest a model, in which the MetAPs- O_2- ATE1-UBR1/UBR2 proteolytic system counter-regulates RGS4, RGS5, and RGS16, and thus functions as a positive regulatory mechanism of the G protein signaling pathway in the cardiovascular system as well as other biological processes. Given that Cys_2 is a degradation determinant of RGS4 and RGS5 and that Cys_2 of RGS4 has been retrieved as an N-terminally arginylated form, it was indicated that MetAPs are essential components for degradation of RGS4, RGS5, and RGS16 as well as potentially other short-lived proteins bearing Cys_2 as well. However, it is unclear whether N-

28
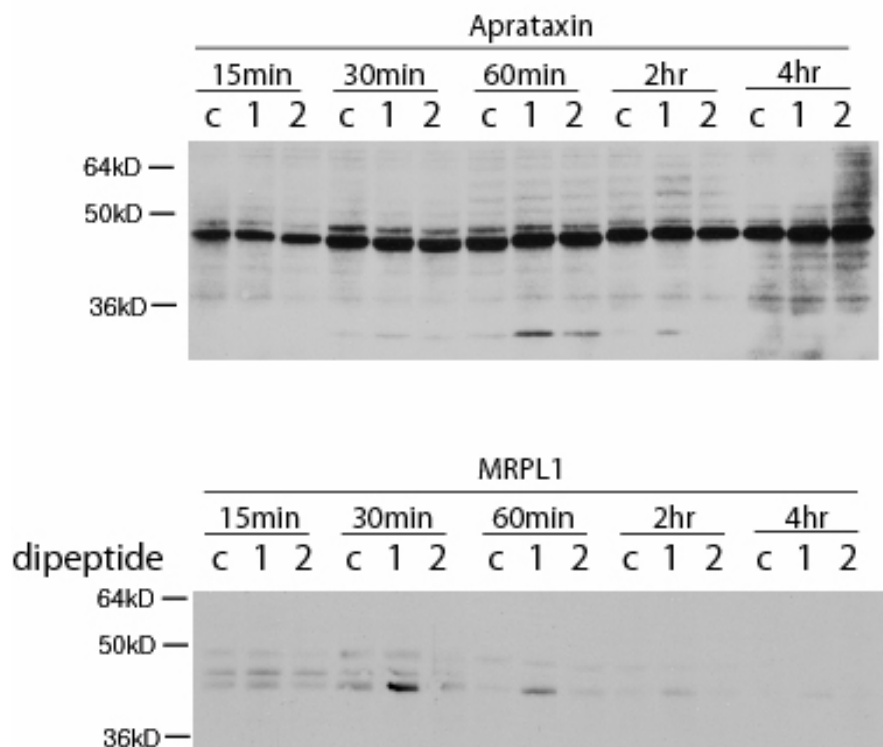
Figure 15. Validation of the screening using Aprataxin (upper) and MRPL1 (lower). Other hits from the functional proteomic screening, including aprataxin and MRPL1, were validated by small scale immunoblotting in the presence of dipeptides that are N-end rule inhibitors. Proteins were expressed in reticulocytes in different reaction times as experiment in RGS expression (see Methods). c: PBS, 1: Arg-Ala, 2: Trp-Ala. Both of aprataxin and MRPL1 act as type 1 substrate, stabilized by Arg-Ala dipeptides. The cleavage site, which can generate an N-degron, have been not characterized yet.

terminal Met cleavage by MetAPs is a licensing step for proteolysis. Notably, MetAP2 is a target of angiogenic inhibitors such as fumagillin and its related drugs (Sin et al. 1997). This finding, together with the previous reports that $ATE1^{-/-}$ embryos display defective angiogenesis (Kwon et al. 2002), suggests that RGS4, RGS5, and RGS16 may be the physiological targets of these anti-angiogenic drugs. In this model, the treatment of fumagillin may partially inhibit N-terminal Met cleavage of RGS4, RGS5, and RGS16, and thus their proteolysis as well, which in turn may suppress the cardiovascular GPCR signaling pathway, resulting in angiogenic inhibition in the clinical setting. RGS5 is indeed prominently expressed in vascular smooth muscle cells and pericytes (Cho et al. 2003) and has been implicated in capillary growth and angiogenesis (reviewed in Wieland & Mittmann, 2003 (Wieland and Mittmann 2003)). Given the findings that O_2 depletion perturbs the *in vitro* and *in vivo* proteolysis of RGS5 (Fig. 7) and that Cys-2 of arginylated RGS4 can be converted into $CysO_3$ in mammalian cells, the N-terminal Cys-2 may
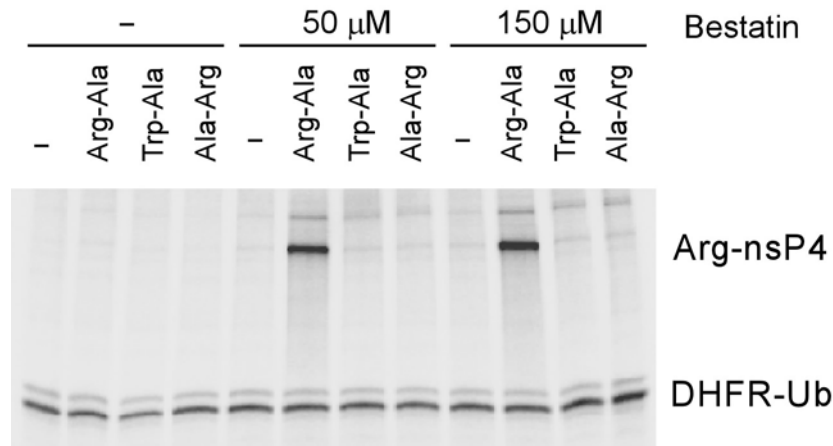
Figure 16. Stability of dipeptides in reticulocyte lysates. Without an endopeptidase inhibitor, bestatin, cognate dipeptides, i.e. Arg-Ala for type 1 model substrate, Arg-nsP4, exert no inhibitory effects on the degradation of N-end rule model substrates. Bestatin itself showed no effect on the stability of the model substrates.

act as a pro-N-degron through an unknown oxidation mechanism. During oxidation of Cys-2 to $CysO_3$, there may be a transiently oxidized form, $CysO_2$, whose structure is similar to Asp (Kwon et al. 2002). Therefore, it is conceivable that the oxidized Cys structurally mimics Asp, an ATE1 substrate, for recognition by ATE1 Arg-transferase. Therefore, the Cys-2 oxidation of RGS proteins may be a regulatory mechanism that is essential and limiting for Cys-2 arginylation. Taken together, the dissolved O_2 gas is proposed to act as a cofactor for the GPCR signaling by diffusing across the plasma membrane of the target cell and oxidizing RGS4, RGS5, and RGS16, and thereby provides a vital regulatory mechanism for the cardiovascular GPCR pathway (Fig. 17). If this were true, the (unknown) oxidase that mediates Cys-2 oxidation of RGS proteins may function as an O_2 sensor, like prolyl-4-hydroxylases that oxidize HIF1α in a normoxic condition (Ivan et al. 2001). These data also suggest that a broad range of proteins bearing N-terminal Cys may be regulated by the same N-terminal Cys oxidation, opening up a new field in studies of the role of protein oxidation in various biological processes.

The findings that the *in vivo* degradation of RGS4 and RGS5 requires *ATE1*-encoded R-transferases and that the N-terminal Cys_2 of RGS4 can be conjugated with Arg suggest that arginylation of the N-terminal Cys_2 of RGS4, RGS5, and RGS16 is essential and rate-limiting for subsequent ubiquitylation by E3s. The mammalian genome encodes ~350 Cys_2-bearing proteins. However, since the presence of Cys_2 is not sufficient for proteolysis, only a small subset of proteins bearing Cys_2 may be arginylated for proteolysis and possibly for non-

30

proteolytic processes as well. Together, this result suggests that the proteolysis of RGS4, RGS5, and RGS16 is tightly controlled by Cys_2 exposure, oxidation, and arginylation (for pro-proteolysis), and Cys_2 palmitoylation (for anti-proteolysis). Perhaps, these complicated Cy2 modifications function as a licensing mechanism prior to their irreversible degradation by the Ub machinery in response to various physiological states. Since *ATE1*-dependent arginylation requires Arg- tRNA^{Arg} which is an essential component for protein synthesis, ATE1 may act as a translation sensor for appropriate cell growth (e.g., cardiomyocytes and vascular smooth muscle cells).

The findings that *in vivo* degradation of RGS4 and RGS5 is perturbed in cells deficient in UBR1 and UBR2 and that UBR1 and UBR2 direct bind to N-terminal Arg suggest that Cys_2-arginylated RGS4, RGS5, and RGS16 are ubiquitinated by two functionally overlapping UBR1 and UBR2. Notably, RGS4 and RGS5 were less stabilized in *UBR1$^{-/-}$UBR2$^{-/-}$* cells than in *ATE1$^{-/-}$* cells, suggesting the presence of additional E3s for RGS4 and RGS5. Consistent with this result, it was reported that RGS4 is more severely stabilized in *UBR1$^{-/-}$UBR2$^{-/-}$UBR4^{RNAi}* cells than in *UBR1$^{-/-}$UBR2$^{-/-}$* cells (Tasaki et al. 2005). It is to be further investigated whether UBR4 and UBR5 participate in proteolysis of RGS4, RGS5, and RGS16. *UBR1$^{-/-}$* mice are alive but show mild alteration in fat metabolism and muscle protein degradation, while *UBR2$^{-/-}$* mice show male-specific infertility and female-specific lethality. Notably, *UBR1$^{-/-}$UBR2$^{-/-}$* embryos die at ~12.5-dpc (days post-coitus) associated with gross morphology indicative of cardiovascular defects at ~11.5 dpc (An et al. 2006). However, since *UBR1$^{-/-}$UBR2$^{-/-}$* embryos also develop defects in the central nervous system at ~10.5-dpc (An et al. 2006), it is to be investigated whether the apparent cardiovascular defects are primary or secondary. It is also to be seen whether the known physiological functions of UBR1 and UBR2 are related with abnormal proteolysis of RGS4, RGS5, and/or RGS16.

In conclusion, these results raise a model (Fig. 17), in which the controlled proteolysis of RGS4, RGS5, and RGS16 by the MetAPs-O_2-ATE1-UBR1/UBR2 pathway is important for appropriate cell growth in the hearts, blood vessels, and other organs as well. This was supported by other reports that: *1) ATE1$^{-/-}$* embryos are impaired in myocardial growth and vascular integrity/maturation, *2)* RGS4, RGS5, and RGS16 act as negative regulators of Gq and Gi pathways, *3)* RGS4 is required for normal myocardial function, *4)* the pathways composed of

31
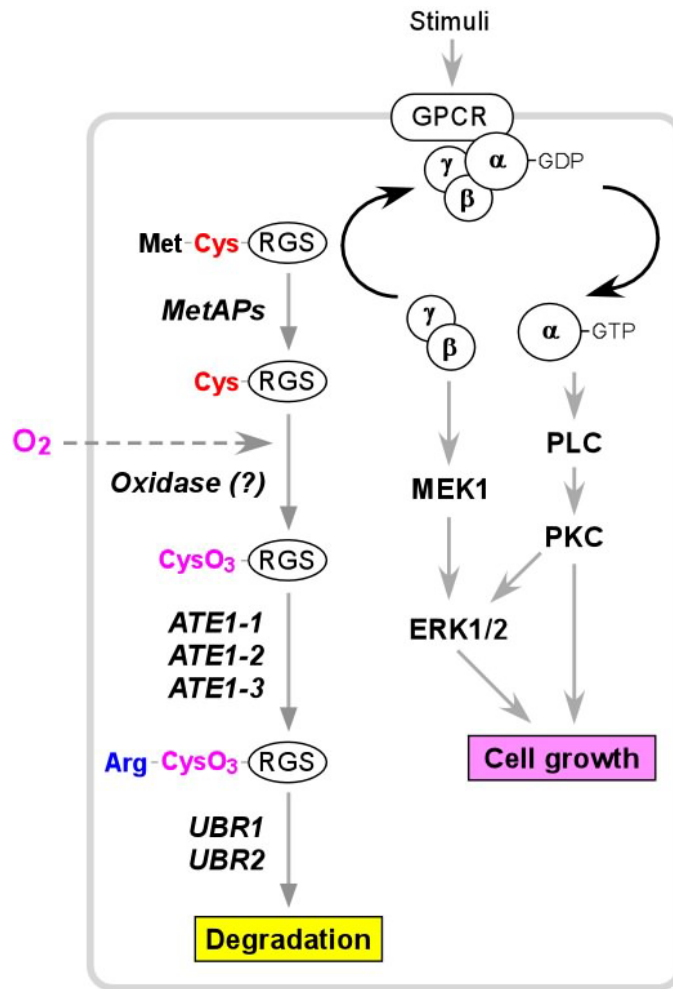
Figure 17. Model for the role of the N-end rule pathway in G protein signaling. The cellular concentrations of RGS4, RGS5 and RGS16 are tightly controlled by the N-end rule pathway. RGS4 and RGS5 have been implicated as negative regulators of Gq-dependent signaling in the hearts and blood vessels, respectively, while RGS16 has been shown to control the chemokine-stimulated signaling and migration of megakaryocytes. This results suggest that the regulated proteolysis of these RGS proteins by the ATE1 branch of the N-end rule pathway plays an important role in the control of cardiovascular signaling and homeostasis.

Gq, Gi, their agonists, and the downstream signal transducers such as PKC, MAPKs, and Ras are critical for cardiac function and in the pathogenesis of myocardial hypertrophy, and *5)* the expression pattern of ATE1 and these RGS proteins (Wieland and Mittmann 2003) are functionally correlate. To further support this model, I also demonstrated that *ATE1* knockout in embryos reduces the function of ERK1/2 MAPKs, signal transducers downstream of Gq and Gi, and the mRNA level of βMHC, a cardiac hypertrophy marker (Fig. 14). Notably, in contrast to ERK1/2 activities (Fig. 10), the mRNA level of βMHC was moderately decreased in *ATE1*^{-/-} embryos (Fig. 14). One possible explanation is that the mutant embryos may induce

compensatory reserve pathways to overcome the fatal consequences of functional loss. The mechanisms underlying the N-end rule-regulated GPCR pathway remain to be further dissected using specific organs (e.g., hearts) or cells (e.g., cardiomyocytes and endothelial cells), in the absence and presence of activation by various GPCR agonists, associated with conditional, tissue-specific knockout approach.

Cardiac hypertrophy is the major cause of various myocardial diseases. Due to the high mortality of cardiac hypertrophy that is frequently associated with hypertension, cardiac valvular disease, or ischemia(Dorn and Hahn 2004), the identification of its regulatory determinants is a major concern in the pharmaceutical field. In sum, although the clear connection between the N-end rule pathway, RGS proteins, and the cardiovascular GPCR pathway is to be further investigated, these results suggest that the regulated proteolysis of RGS4, RGS5, and RGS16 by the MetAPs-O_2-ATE1-UBR1/UBR2 proteolytic pathway may be important for the optimal function of the cardiovascular GPCR signaling pathway.

CHAPTER III

3.0 CHARACTERIZATION OF PROLIFERATION AND SIGNALING IN ATE1-DEFICIENT CARDIOMYOCYTES

3.1 OVERVIEW

It has been shown that ATE1-deficient mice die during embryogenesis associated with various defects in cardiac development. However, the underlying molecular mechanisms of these phenotypes remain unclear. In Chapter II, I have identified a set of regulators of G protein signaling pathway, RGS4, RGS5, and RGS16, as ATE1 substrates, and demonstrated that downstream components of G protein signaling were impaired in $ATE1^{-/-}$ embryos and cells. In this study, to understand the role of ATE1-mediated RGS proteolysis in cardiac development, I characterized $ATE1^{-/-}$ mice and embryonic cardiomyocytes with an emphasis on GPCR signaling pathway. I found that the cell-autonomous function of ATE1 regulates the proliferation of developing hearts and cardiomyocytes. ATE1 was prominently expressed in cardiomyocytes of the isolated embryonic heart cells, compared to non-cardiomyocytes. Consistent with the previous results, I found that the levels of endogenous RGS4 and RGS16 in $ATE1^{-/-}$ embryoninc hearts were significantly increased, suggesting that the concentration of these RGS proteins are controlled by ATE1 during normal cardiac development. The downstream activities of Gq- and Gi signaling pathways, which are known to be regulated by RGS proteins, were also reduced in $ATE1^{-/-}$ hearts. These results together indicate that the ATE1-RGS circuit acts as an important regulator of cardiomyocyte proliferation during cardiac development.

3.2   BACKGROUND

ATE1 is an evolutionarily conserved protein observed in all eukaryotes from fungi to animal (Hu et al. 2006). In prokaryotes, Leu/Phe-transferase, a functionally analogous enzyme to ATE1, transfers Leu or Phe to N-terminal Arg, or Lys, distinct from Asp, Glu, or oxidized Cys in eukaryotes, which are recognized by the ClpAP protease (Graciet et al. 2006). *S. cerevisiae* mutants lacking the ATE1-encoded Arg-transferase are viable and phenotypically normal (Balzi et al. 1990). However, ATE1-deficient mice died at the later stage of cardiac development (about at E14.5 to E15.5) associated with cardiovascular defects resembling human congenital heart disease (CHD) including ventricular hypoplasia, ventricular septal defect, and impaired angiogenesis (Kwon et al. 2002). This result suggests that ATE1-dependent proteolysis of unknown substrate(s) is a crucial regulatory mechanism for myocardial growth and blood vessel integrity/maturation. However, the underlying molecular mechanism to explain how knocking out *ATE1* gene in mice induces characteristic features of CHD has remained elusive although the details of heart formation in mouse embryos has been known for decades and many genes that control its developmental program has been identified, including GATA4, Nkx2.5, TBX5, and MEF2 (Fishman and Chien 1997; Srivastava and Olson 2000).

As described in chapter II, I found that RGS4, RGS5, and RGS16 are degraded through the ATE1-dependent N-end rule pathway and that knocking out *ATE1* gene in mice reduces the activities of downstream effectors of GPCR pathway and the expression of cardiac hypertrophy marker genes (see Chapter II) (Lee et al. 2005). Heterodimeric G proteins are signal transducers that connect the ligand-activated G protein-coupled receptors (GPCRs) to effectors for the intracellular signaling pathways (Neves et al. 2002), and RGS4, RGS5, and RGS16, are negative regulators of Gi- and Gq-mediated signaling pathway by accelerating (up to 10^3-fold) the rate of Gα-GTP hydrolysis, resulting in reassociation of the Gαβγ heterotrimer (Ross and Wilkie 2000; Hollinger and Hepler 2002). The RGS proteins and G protein signaling pathway have been known to have important roles in cardiac development and in the cardiac function under normal and pathological condition (Sierra et al. 2000; Riddle et al. 2005). Mammalian R4 RGS proteins are highly expressed in the cardiovascular system, including ventricle, atrium, and cardiomyocytes (Doupnik et al. 2001; Wieland and Mittmann 2003; Larminie et al. 2004). Moreover, transgenic mice overexpressing RGS4 in postnatal ventricular tissue developed left

ventricular dilatation, depressed systolic function, and higher postoperative mortality in response to pressure overload (Rogers et al. 1999; Rogers et al. 2001). RGS4 levels are elevated in cardiac hypertrophy and in failing human heart (Zhang et al. 1998; Owen et al. 2001), while RGS4 can impair G protein-mediated signaling in cardiomyocytes (Tamirisa et al. 1999).

Overexpression of Gq in cardiac myocytes increased heart weight and cardiomyocyte size associated with the expression of cardiac hypertrophic markers genes, such as β-myosin heavy chain (MHC) (D'Angelo et al. 1997; Adams et al. 1998; Mende et al. 1998). Conversely, mice lacking both Gαq and Gα11 die at E11.5 because of hypoplasia in the ventricular wall (Offermanns et al. 1998). Gq and Gi pathways are critical for proliferation and differentiation of myocardial cells under physiological and pathological conditions (Molkentin and Dorn 2001). Angiotensin II, phenylephrine, endothelin, and prostaglandin F2α that activate Gq- or Gi-coupled receptors all stimulated the hypertrophic response in cardiomyocytes (Adams et al. 1996). Gαq overexpression in cardiac tissue increased heart weight and cardiomyocyte size associated with impaired contractility and the expression of cardiac hypertrophic markers. Similarly, various studies using cardiomyocytes or transgenic/ knockout animals indicated that Gq- or Gi-activated effectors such as PKC, Ras, and MAPKs are critical for the regulation of myocardial cell growth (Molkentin and Dorn 2001). The present study indicates that defective G protein signaling underlies reduced proliferation of ATE1-deficient cardiomyocytes, which results in the cardiac phenotype of $ATE1^{-/-}$ embryos. Moreover, the function of ATE1, which is expressed in the cardiomyocyte, is found to be cell-autonomous and angiotensin II (AngII) is one of major proliferative stimuli, whose function is abrogated in $ATE1^{-/-}$ cardiomyocytes. These results, therefore, suggest a general physiological control mechanism of the ATE1-RGS-AngII circuit for heart development.

3.3   METHODS

Mice. All animal studies were in accordance with protocols approved by the Institutional Animal Care and Use Committee at University of Pittsburgh. The exon 1 to exon 3 of *ATE1* gene was disrupted in CJ7 embryonic stem cells (ES) as previously described (Kwon et al. 2002).

Embryos staged E10.5 to E17.5 were obtained from intercrosses of heterozygous mice in the 129SvEv/C57BL/6 (mixed) genetic background. The presence of a vaginal plug after overnight mating was regarded as E0.5. Genotyping of the yolk sac or tail DNA of each embryo was performed using standard polymerase chain reaction (PCR) with primers F1 (CCAGCTCATTCCTCCCACTCATGATC), R1 (GGTATTTGCTGCCGTCCTTTGGTGGTC), and R2 (CTGGAGACAAAGCCCCAGCCA-GAC), amplifying 570-bp and 430-bp fragments for the wild type allele and knockout allele, respectively. For *in vivo* proliferation assay, 5-bromo-2-deoxyuridine (BrdU, Sigma) was intraperitoneally injected into pregnant mice with E11.5, E12.5, or E13.5 embryos from ATE1 heterozygous mutant intercrosses at the dose of 150 mg/g body weight in 250 µL saline. After 2 hrs post-injection, embryos were isolated, fixed, and embedded into paraffin for sectioning.

Histology and LacZ staining. For histological analysis, whole embryos were dissected in ice-cold PBS and fixed overnight at 4 °C in 4 % paraformaldehyde (PFA, Fisher Scientific) in PBS. Samples were treated with 70 % ethanol, dehydrated, embedded in paraffin wax, and sectioned transversely or sagittaly at 7 µM, followed by staining with hematoxylin/eosin (H&E). For LacZ staining, embryos or tissues were fixed in 4% paraformaldehyde/PBS for 10 min, rinsed in PBS three times, and stained overnight at 37 °C in X-Gal solution (1.3 mg/mL potassium ferrocyanide, 1 mg/mL potassium ferricyanide, 0.3 % Triton X-100, 1 mM MgCl$_2$, 150 mM NaCl, and 1 mg/mL 4-choloro-5-bromo-3-indolyl-β-galactoside (X-Gal, Roche Applied Science) in PBS (pH 7.4)) followed by post-fixation. For LacZ staining of cultured primary heart cells, cells were fixed in 0.25 % gluta-aldehyde (Fisher Scientific) in PBS for 5 min, and stained in X-Gal solution for 1 hr, followed by immunostaining with mouse anti-sarcomeric α-actinin (Clone EA-53, Sigma) for identifying cardiomyocytes.

Primary cardiomyocytes and explanted heart. The primary cells from mouse embryonic heart were isolated as described with slight modification for obtaining more viable cells (Jung et al. 2005). Briefly, the dissected hearts at the stage of E13.5 were digested in Hank's Balanced Salt Solution (HBSS) containing 0.2 % collagenase II, 0.005 % trypsin, 0.1 % chicken serum for 15 min at 37 °C. Enzymes were deactivated by addition of horse serum (HS), and the cells were precipitated by mild centrifugation and plated in DMEM supplemented with 10 % fetal bovine

serum (FBS). Twenty-four hrs after plating, the medium was replaced by serum-free DMEM supplemented with 10 µg/mL insulin, 5.5 µg/mL transferrin, 5 µg/mL selenium, and 110 µg/mL pyruvate (Sigma) or with 10% HS and 5% FBS. Approximately 50 % of the cells were identified as cardiomyocytes by immunostaining with anti-sarcomeric α-actinin or anti-troponin I (Santa Cruz Biotechnology). For cell proliferation assay, cells were incubated with 10 µM of BrdU for 16 hrs. For heart organ culture, E13.5 embryonic hearts including outflow regions were removed and cultured in DMEM containing 5 % FBS, penicillin and streptomycin and media was changed serum-free DMEM with supplements. The explanted hearts continued beating during the incubation of 40 µM BrdU for 24 hrs in the presence or absence of GPCR agonists. Proliferation of the hearts was examined by immunohistochemistry against BrdU after paraffin sections were prepared.

Immunotechniques. For immunoblotting analysis, whole embryos, embryonic hearts, or embryonic brain at the stage of E13.5 or E14.5 were isolated in ice-cold PBS and homogenized in lysis buffer (20 mM Hepes, pH 7.5, 150 mM KCl, 10 % glycerol, 0.1 mM EDTA) containing protease inhibitor cocktail, sodium orthovanadate, and sodium fluoride (Sigma). A soluble fraction was separated by a two-step centrifugation (9,000 g and 100,000 g). Total protein extract from a heart (~20 µg), one tenth of extracts from a brain (~30 µg), or 50 µg of total protein from whole embryos were subjected to electrophoresis, blotted to polyvinylidene fluoride (PVDF) membrane, and probed with anti-RGS4, anti-RGS5, or anti-RGS16 antibody (generous gifts from Dr. Susanne M. Mumby (Krumins et al. 2004), Dr. Kayoko Moroi (Zhou et al. 2001), and Dr. Ching-Kang Chen (Derrien et al. 2003; Hiol et al. 2003), respectively) followed by reprobing with anti-actin antibody (Sigma). The signals were visualized by Supersignal West Pico Chemiluninescent Substrate (Pierce).

To detect *in vivo* BrdU incorporation, sections were antigen-retrieved by heating in 10mM sodium citrate (pH 6.0) in a microwave oven for 10 min, permeabilized with 0.2 % Triton X-100 for 10 min, and incubated with rat anti-BrdU antibody (Serotec, Oxford, UK) diluted 1:50 in PBST with 2 % goat serum, followed by anti-rat IgG-Alexa555 antibody (Invitrogen). Cells were counterstained with 4'6'-diamidino-2-phenylindole (DAPI, Vector Laboratories) to visualize the nuclei. Control staining was performed using embryos into which BrdU was not injected. For phosphorhistone staining, the sections were incubated with anti-phosphohistone H3

antibody (Upstate) (1:100 dilution), followed by anti-rabbit IgG-FITC (Jackson Immunoresearch). Each antibody was applied for 1 hr at room temperature in 1 % goat serum/PBST and secondary antibody was diluted 1 to 200.

For detection of BrdU incorporation in the primary cardiomyocytes, cells were fixed in 4 % PFA for 25 min at 4 °C and for 5 min at room temperature, permeabilized in 0.2 % Triton X-100 for 10 min, denatured with 2N HCl, and neutralized with 0.1 M sodium borate. Then, cells were co-immunostained with rat anti-BrdU antibody and rabbit anti-troponin I antibody, followed by secondary antibody incubation (anti rat-IgG-Alexa 555 and anti-rabbit IgG-FITC, respectively) and counterstaining with DAPI. For phosphorhiston H3, atrial natriuretic protein (ANP) and Flag detection in cardiomyocytes, staining was performed as BrdU staining without acid treatment and neutralization.

For RGS4 immunostaining of paraffin sections, samples were blocked in 10% heat inactivated goat serum in PBST, incubated with rabbit anti-RGS4 antibody (1:50 dilution), following quenching the endogenous peroxide activity with 3 % H_2O_2 in MeOH for 30 min. Biotinylated goat anti-rabbit IgG and diaminobenzidine were used for the signal development. Control sections and embryos were incubated with pre-immune anti-sera instead of anti-RGS4 antibody. Whole-mount immunohistochemical staining of embryos for RGS4 was performed as described (Kwon et al. 2003). The antibody could not be used for location of endogenous RGS4 in subcellular level.

Hypertrophy. Cardiomyocyte size was determined by measuring the surface area of sarcomeric α-actinin-positive cells in cultured primary cardiomyocyte. Planimetry was performed using ImageJ software version 1.34s (NIH) (Rasband 1997-2006) and outcome arbitrary unit was used. Although cell surface area does not constitute an accurate measurement of cell size, this parameter was generally used to estimate cardiomyocyte hypertrophy (Fredj et al. 2005). Immunohistochemical analysis was performed to detect hypertrophic marker genes, such as ANP with coimmunostaining for cardiomyocyte marker protein, e.g. sarcomeric α-actinin. For [^{3}H] leucine incorporation assay, cultured cardiomyocytes in serum-containing medium were incubated with 5.0 μCi/mL of [^{3}H] leucine (Amersham Bioscience) for 24 hrs. The radioactivity incorporated into the trichloroacetic acid-precipitatable material was determined. To analyze mRNA expression of heart genes, semiquantitative reverse transcription-PCR was performed on

1 μg of total RNA from embryonic hearts for 25 cycles.

GPCR Effectors and GPCR Agonists. Activities of ERK, CaMKII, PKA, and PKC in the embryonic hearts were determined using kinase assay kits from Upstate Biotechnology with myelin basic protein, a substrate peptide (KKALRRQETVDAL), kemptide, and a substrate peptide (QKRPSQRSKYL) as substrates respectively. Inositol phosphate formation by PLC was assayed using [^{3}H] phosphatidylinositol bisphosphate (PIP$_2$) as substrate as described earlier (Pandey et al. 2002). To activate (phosphorylate) kinases, DMEM complemented with 20% FBS was added to primary cardiomyocytes or immortalized mouse embryonic fibroblasts cultured in serum-free medium and cells were subject to immunoblotting as described above.

After genotyping, cultured primary cells and explanted hearts were stimulated every 24 hrs with 200 μM phenylephrine (PE), 2 μM Angiotensin II (AngII), 100 nM prostaglandin F2α (PGF2α), 50 ng/mL basic fibroblast growth factor (FGFb), or 4 μM isopreterenol (ISO) in serum-free culture media for two days. Cells were also incubated with 10 μM of BrdU 16 hrs before fixing and proliferation of cardiomyocytes was examined by immunohistochemistry against BrdU as described above.

Adenovirus Construction and Infection. All recombinant adenoviruses were constructed by employing the Cre-lox recombination system as described (Hardy et al. 1997; Song and Lee 2005). Briefly, N-terminally Flag tagged mouse ATE1-1, ATE1-2, or ATE1 -3 genes were isolated by PCR using pcDNA3-ATE1-1 to -3 as templates and inserted into BamHI/XhoI-cut pAdlox shuttle vector to generate pAdlox-ATE1-1 to -3 shuttle vectors, respectively. The selective cell line CRE8 has β-actin-based expression cassette driving a Cre recombinase gene with an NH$_2$-terminal nuclear localization signal stably integrated into 293 cells. For the production of adenovirus, 2 μg of *sfi*I-degested shuttle vector was co-transfected into CRE8 cells with 2 μg of *sfi*I-degested Ψ5 viral genomic using LipofectAMINE (Invitrogen). The recombinant adenoviruses were generated by intermolecular homologous recombination between the shuttle vector and Ψ5 viral DNA. Plaques were harvested, analyzed, and purified. The insertion of each component to adenovirus was confirmed by Western blot analysis after the infection of corresponding recombinant adenovirus into HeLa S3 cells or DU-145 cells.

40

| | Genotype | | |
stages	wild type	Heterozygous mutant	Homozygous mutant
10.5-dpc	12	21	14
11.5-dpc	31	63	25
12.5-dpc	29	52	24 (2 inviable)
13.5-dpc	71	133	77 (14 inviable)
14.5-dpc	50	78	45 (12 inviable)
15.5-dpc	17	32	9 (9 inviable)
16.5-dpc	10	18	5 (5 inviable)
17.5-dpc	4	6	1 (1 inviable)
post-natal	223	404	0

Table 4. Genotype Table from ATE1 Heterozygous Intercross. *ATE1*^{-/-} embryos died during E12.5 and E14.5 and no live embryos from E15.5 was obtained.

Primary cardiomyocytes cultures were infected with adenoviral constructs at a multiplicity of infection (MOI) of 10 diluted in serum-free DMEM with supplementation for 3 hrs. Efficiency of transgene expression of an isoform of ATE1 assessed by coimmunostaining with anti-Flag antibody and anti-troponin I antibody is constantly > 95 % up to 48 hr post-infection. Adenoviral expression in cardiomyocytes cultures did not influence cell viability.

Statistical Analysis. For experiment using embryonic hearts, at least three different litters (10 sections each) were analyzed. For cardiomyocyte analyses *in vitro*, more than 5,000 cells for each experimental group were counted. Samples were counted twice, and there was less than 3% variability per sample. For enzymatic activity assay, three hearts for each genotype were used and it was duplicated. The images were analyzed using ImageJ software, version 1.34s (Rasband 1997-2006) (NIH) to count BrdU positive cells and to measure the area of cardiomyocytes. Data are presented as mean ± sd and statistical analysis was performed by unpaired student's *t*-test or ANOVA. A value of $P < 0.1$ was accepted as statistically significant.
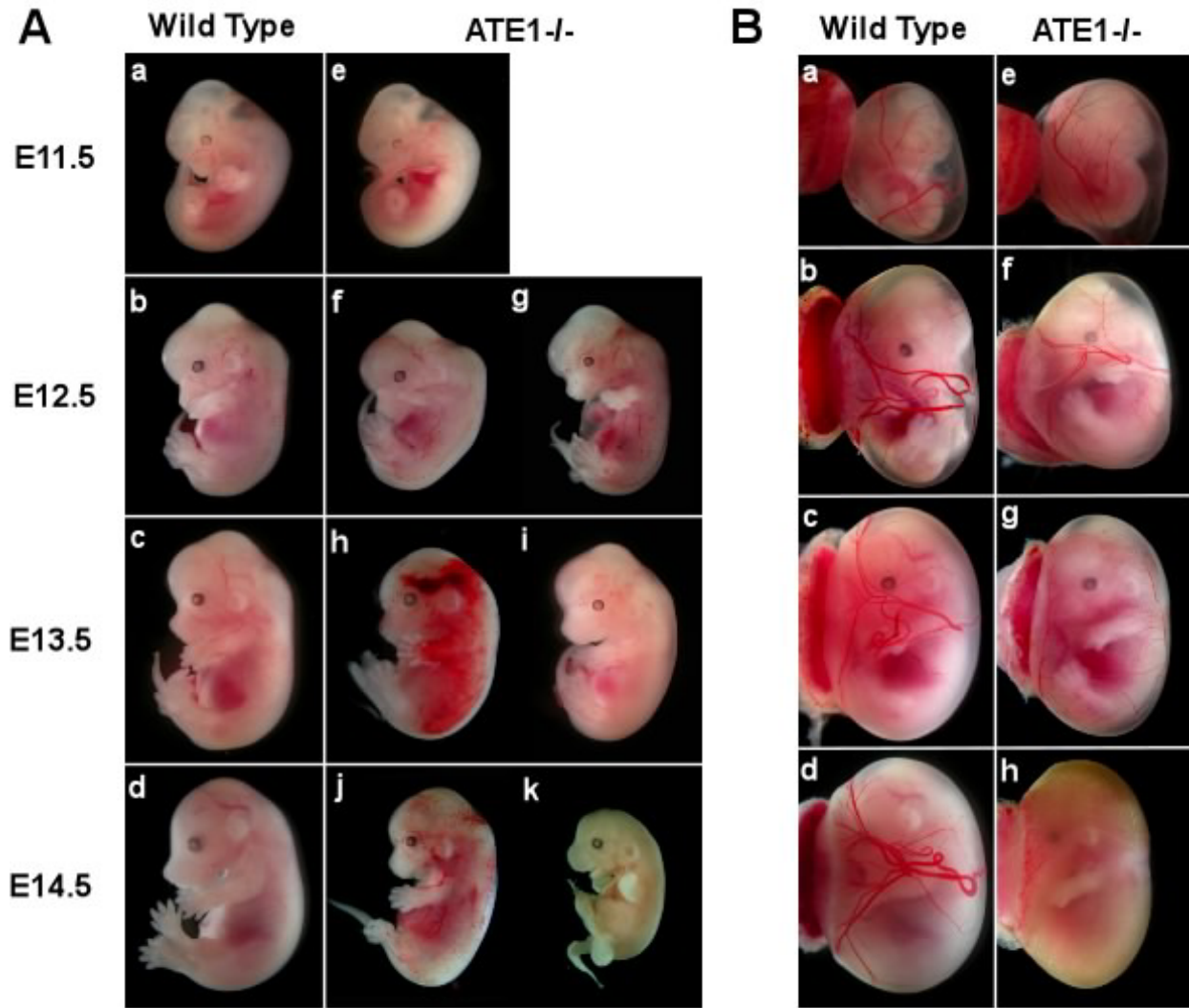
Figure 18. Analysis of gross morphology of ATE1-deficient embryos and yolk sacs. (A) Comparison of wild type and ATE1 $^{-/-}$ embryos in different stages. (B) Comparison of yolk sacs. Before E11.5, there is no difference in gross morphology between the genotypes. However, the growth retardation and other cardiovascular defects became apparent as midgestation stages are higher. Although clear developmental defects were observed after E13.5, histological analysis revealed that the defects started from E12.5.

3.4   RESULTS

3.4.1   Characterization of ATE1-deficient Mice

Genotyping of litters retrieved from heterozygous intercross revealed no homozygous mutants after E15.5 and of 627 newborn pups (Table 4). This result showed that the deletion of ATE1

Figure 19. Notable phenotypes of 12.5-dpc *ATE1*$^{-/-}$ embryos. (A) Closer look of 12.5 dpc-*ATE1*$^{-/-}$ embryonic heart. Hemorrhages in the atrial chambers were frequently observed. (B) Hemorrhages in brain ventricles. This phenotype is believed to be related with the circulation defects in ATE1$^{-/-}$ embryos. (C) E16.5 embryo litters with two dead embryos, which were identified to be ATE1 homozygous mutants after genotyping. Homozygous mutants showed no distinguishable phenotypes from wild types.

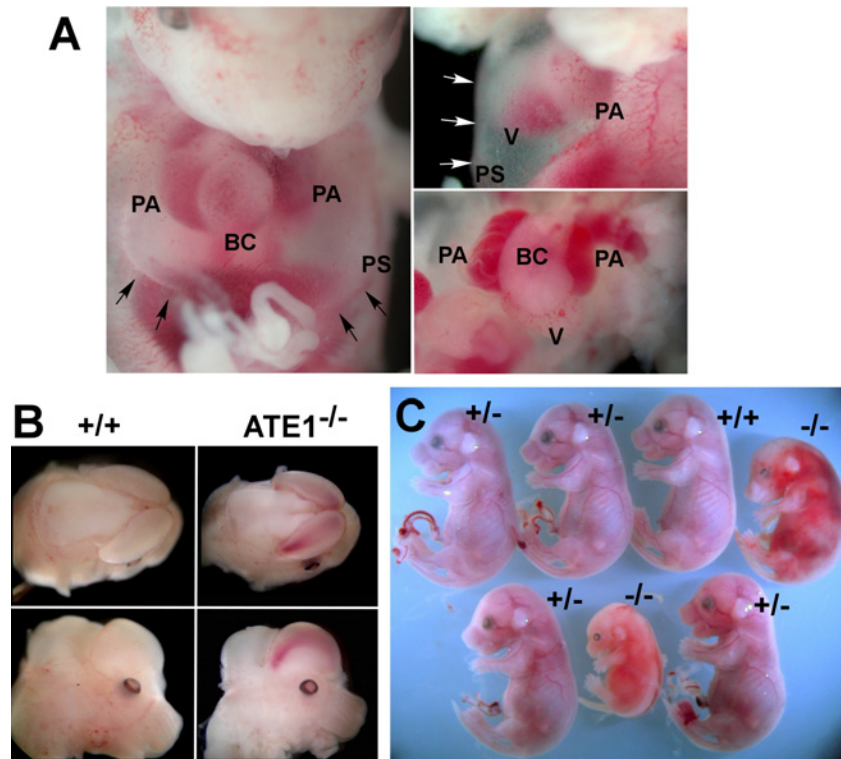gene caused midgestation lethality. To ascertain the timing and nature of the embryonic lethality of *ATE1*$^{-/-}$ mice, the morphology of more than 1,000 embryos produced from timed intercrosses between *ATE1*$^{+/-}$ in B6/129S mixed background at various stages from E10.5 to E17.5 was dissected (Fig. 18A). *ATE1*$^{-/-}$ embryos at the stages up to E11.5 were recovered with the expected number and outwardly normal although subtle morphological or physiological abnormalities could not be ruled out (Fig. 18A-a, and e). In contrast, E12.5 *ATE1*$^{-/-}$ embryos were distinguishable on gross inspection from their wild type or heterozygous mutant littermates (Fig. 18A-b, f, and g), although E12.5 *ATE1*$^{-/-}$ embryos were recovered approximately in Mendelian ratios. Their growths were clearly retarded (~65 % to 90 % of wild type littermates) although somite numbers of homozygous embryos showed no apparent difference from wild type or heterozygous littermates. Some of them developed local effusion in the midbrain, hearts (or primitive atrium), and/or swollen pericardiac sac (Fig. 19A). About half of them also exhibited
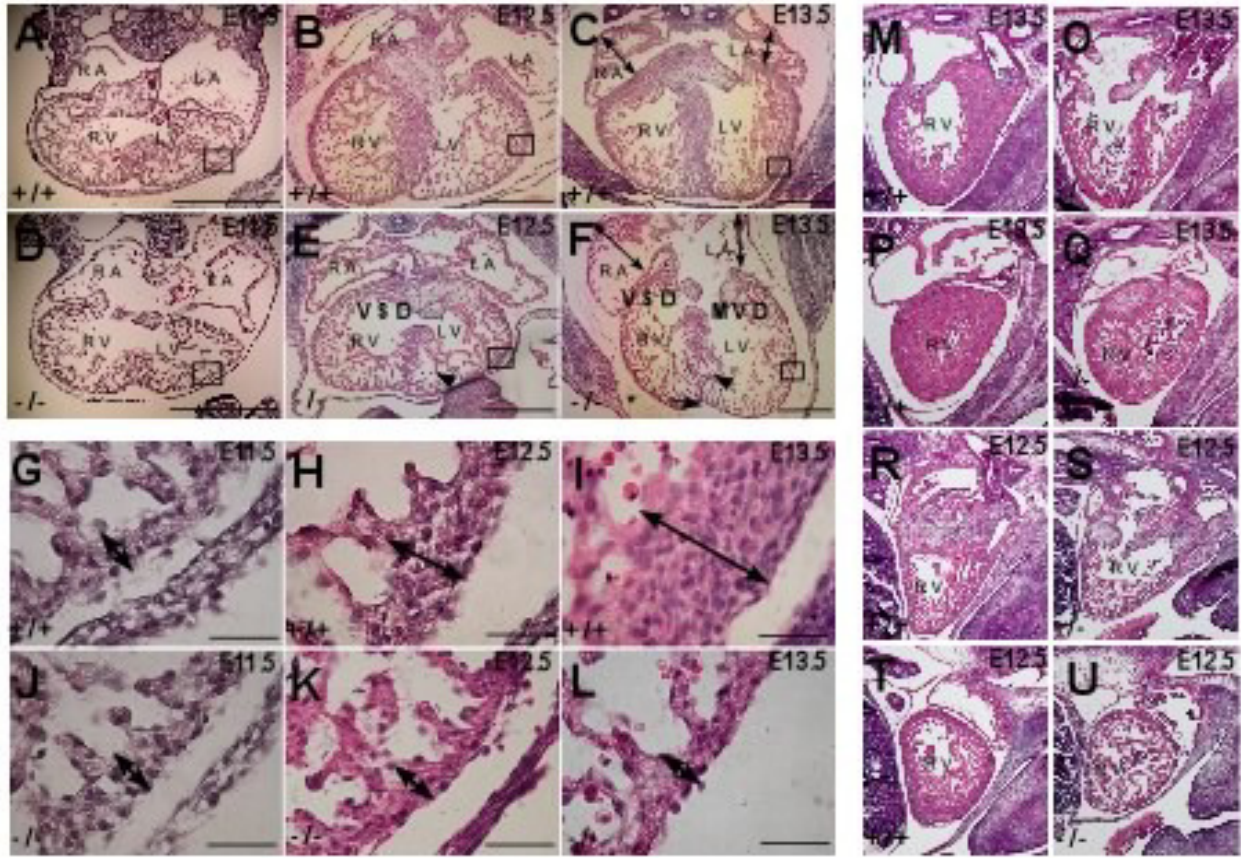
Figure 20. Histological analysis of ATE1-deficient embryonic hearts. (A-F) H/E staining of wild type (A-C) and ATE1$^{-/-}$ (D-F) embryonic hearts in different stages; E11.5 (A, B, G, J), E12.5 (B, E, H, K, R-U), and E13.5 (C, F, I, L-Q). (G-L) Magnified image of ventricular wall area from A-F. (M-U) Sagittal section of embryonic hearts. Left panels: wild type, right panels: mutant. After E12.5, *ATE1*$^{-/-}$ embryonic hearts persistently revealed the abnormal heart morphology, thin and scarce trabecular cells, and thinner ventricular wall in mutant embryos. The thickness of the compact zone was significantly reduced in mutant (2 to 3 myocardial cells compared to ~5 myocardial cells in controls) and this difference was more evident at E13.5, where the development of compact zone was arrested at E12.5 while wild type embryonic hearts were ~ 10-cell-thick, suggesting that proliferation and/or maturation of cardiac myocytes might be defective in *ATE1*$^{-/-}$ ventricular wall.

an edematic accumulation of fluid under the dermal layer of the brain and the skin, an indicator of suppressed cardiac function. About 18 % of E13.5 *ATE1*$^{-/-}$ mutants were found dead and development of surviving mutants appeared to be arrested in sizes at ~E12.5 and exhibited blood leakage into the pericardial cavity and the brain which indicates interauterine heart failure (Fig. 18A-c, and h). Some of mutant mice were anemic in the extremities, suggesting hemodynamic insufficiency Another defect frequently noticed in E13.5 *ATE1*$^{-/-}$ embryos was hemorrhage in the lateral ventricles, which is common in preterm and low birth weight infants and probably arose secondarily from the cardiac defects (Fig. 19B) (Cherian et al. 2004). More than 26 % of E14.5
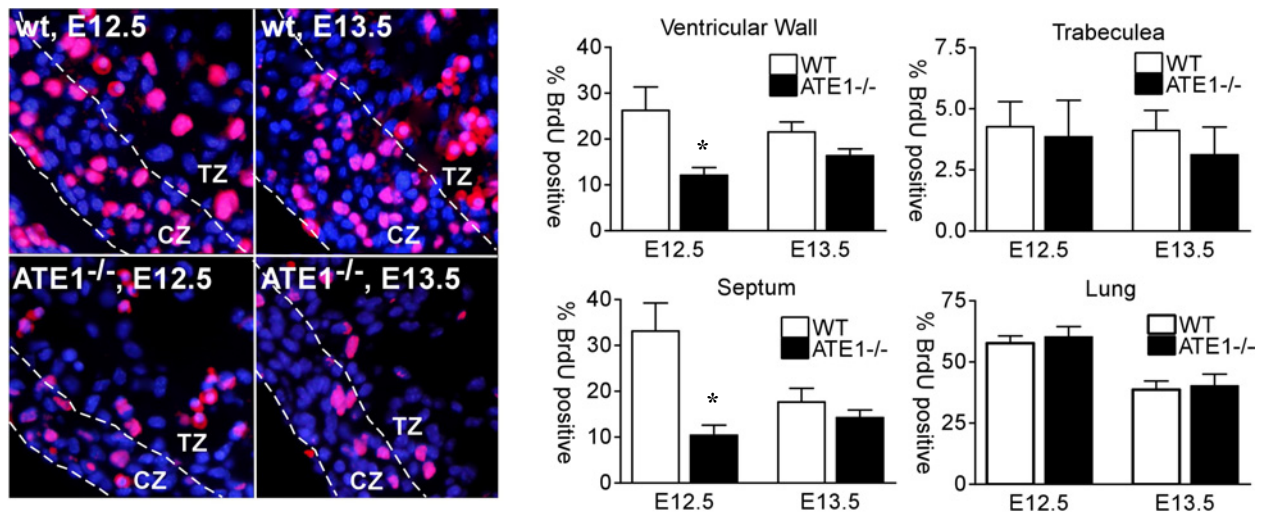
Figure 21. Reduced DNA synthesis of $ATE1^{-/-}$ embryonic hearts. Immunostaining of BrdU-positive embryonic hearts at 12.5-dpc and 13.5-dpc. Compact zone and trabeculae zone were visually separated with dotted lines. Ventricular wall areas were magnified. BrdU index in a specific area were quantified. BrdU index in the lung were used as control to show cardiac specific defects in proliferation. Data represents mean ± s.e.m. from three non-litter embryos (See details in Methods). *: $p < 0.05$.

$ATE1^{-/-}$ mutants were found dead and surviving embryos showed significant widespread hemorrhages (Fig. 18A-d, j, and k). No live $ATE1^{-/-}$ embryos were recovered after E15.5 and often they were found resorbed (Fig. 19C). ATE1$^{+/-}$ heterozygotes did not show any discernable phenotypic abnormalities and no gross abnormality of other major organ was observed. Along with developmental defects in $ATE1^{-/-}$ embryos, their yolk sacs with intact ectoplacental cones revealed poorly developed blood vessels and inefficient circulation (Fig. 18B). Analysis of E11.5 and earlier embryos revealed no distinguishable difference between $ATE1^{-/-}$ and control embryos, both displaying hierarchically organized vessel architecture with vielline vessels, suggesting effective initial erythropoiesis. However, at E12.5, ~75 % of mutant embryos exhibited less-branched and thinner vitelline vessels, and irregular plexus of enlarged capillaries (Fig. 18B-b and f). Transparent and pale yolk sacs were also observed in more than half of mutants at this stage. In $ATE1^{-/-}$ embryos, the vitelline vessels started to rapidly degenerate during E12.5 to E13.5, probably because of cardiac insufficiency from defects in $ATE1^{-/-}$ embryonic hearts and subsequent deterioration of blood vessels. At the E14.5 stage, 45 % of mutant yolk sac showed no vascular structures and some of them became yellowish (Fig. 18B-d and h). These results indicate that the lethality from disruption of ATE1 gene starts from E13.5 although there might be cardiovascular abnormality as early as E11.5.
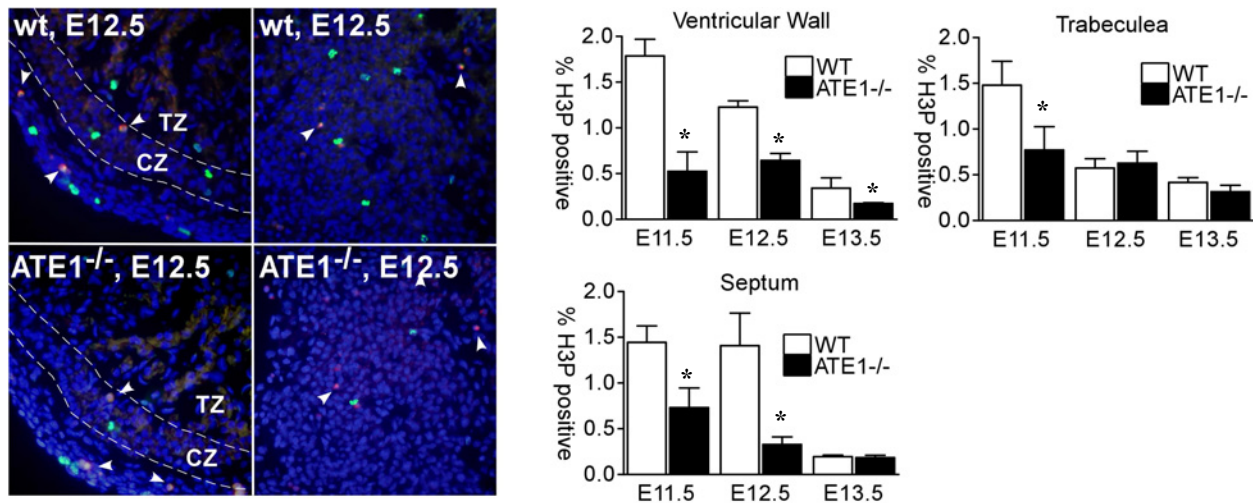
45

Figure 22. Reduced mitosis of *ATE1*^{-/-} embryonic hearts. Immunostaining of phosphor-Histone H3 (mitosis marker) embryonic hearts at 12.5-dpc. Compact zone and trabeculea zone were visually separated with dotted lines. Magnified ventricular wall areas (Left panels) and interventricular septum (right panel) were shown. Percentage of H3P-positive nuclei in a specific area were quantified. Data represent mean ± s.e.m. from three non-litter embryos. *: $p < 0.05$.

3.4.2 Cardiac Abnormality of *ATE1*^{-/-} Mice

Because of obvious cardiovascular demise, histology of embryonic hearts from E10.5 to E14.5 by hematoxylin and eosin (H&E) was examined (Fig. 20). Serial histological sections from up to E11.5 embryos exhibited that looping and septation of the heart tubes were normally developed, making wild type and ATE1 mutant indistinguishable and suggesting normal epithelial-to-mesenchymal transition (Fig. 20A, D). One day later, however, at E12.5, they persistently revealed the abnormal heart morphology, thin and scarce trabecular cells, and thinner ventricular wall in mutant embryos (Fig. 20B, E). The thickness of the compact zone was significantly reduced in mutant (2 to 3 myocardial cells compared to ~5 myocardial cells in controls) and this difference was more evident at E13.5, where the development of compact zone was arrested at E12.5 while wild type embryonic hearts were ~ 10-cells-thick, suggesting that proliferation and/or maturation of cardiac myocytes might be defective in *ATE1*^{-/-} ventricular wall (Fig. 20C, F). Moreover, mocytes from mutant embryos appeared more separated from each other and less arrayed than wild type controls, but no significant reduction of the cytoplamic volume was observed in the ATE1 mutant cardiomyocytes at the cellular level. These phenotypes are biventricular. Intriguingly, the thickened compact layer becomes the major contractile force in

46
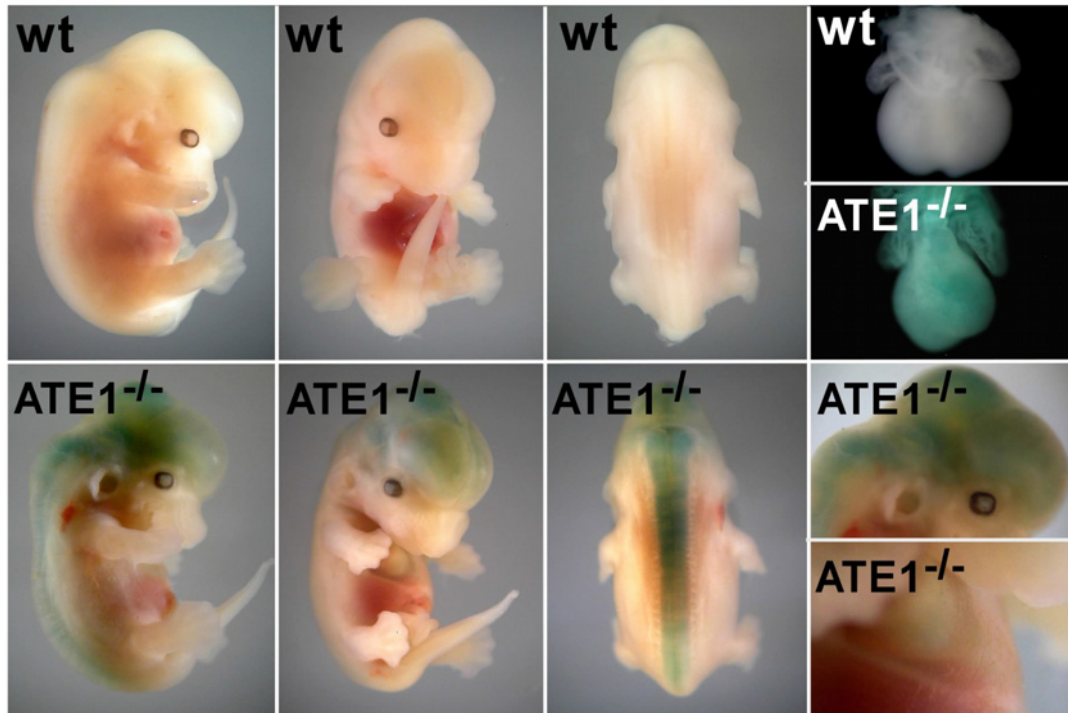
Figure 23. Expression of ATE1 in embryos. Whole mount X-gal staining of wild type (indicated) and *ATE1*$^{-/-}$ embryos at 12.5-dpc (days post-coitus). Prominent expression was detected in the brain, the neural tube and the heart.

embryos during E12.5 and this may explain this observation that embryonic lethality occurs after E12.5 rather than earlier stages.

The ventricular wall is composed of replicating cardiomyocytes, which starts to expand at around E11.5 with the ventricular chamber wall thickening with advanced stages, whereas the forming trabeculae consists of less proliferating cardiomyocytes. Although the control hearts at E13.5 had abundant and thick trabeculae, the mutant ATE1 had thinner and less-abundant trabeculations. Additionally, abnormally dilated atrial chambers were frequently observed in ATE1-mutants. There was an abnormally deep interventricular sulcus in ATE1-mutant embryos, which may be implicated with the abnormal morphogenesis of interventricular septum. Interventricular septa began to form normally both in wild type and *ATE1*$^{-/-}$ mutants and undistinguiable until E11.5. In contrast, at E12.5, mutants exhibited disorganized interventricular septum with holes and slower development that that of wild type from E12.5. The membrane portion of the ventricular septum (pars membranacea) of *ATE1*$^{-/-}$ embryos failed to fuse, resulting in ventricular septal defects (VSD) which was observed with full penetration. Some of *ATE1*$^{-/-}$ embryonic hearts revealed underdeveloped of dysplastic mitral valve and persistent truncus

47

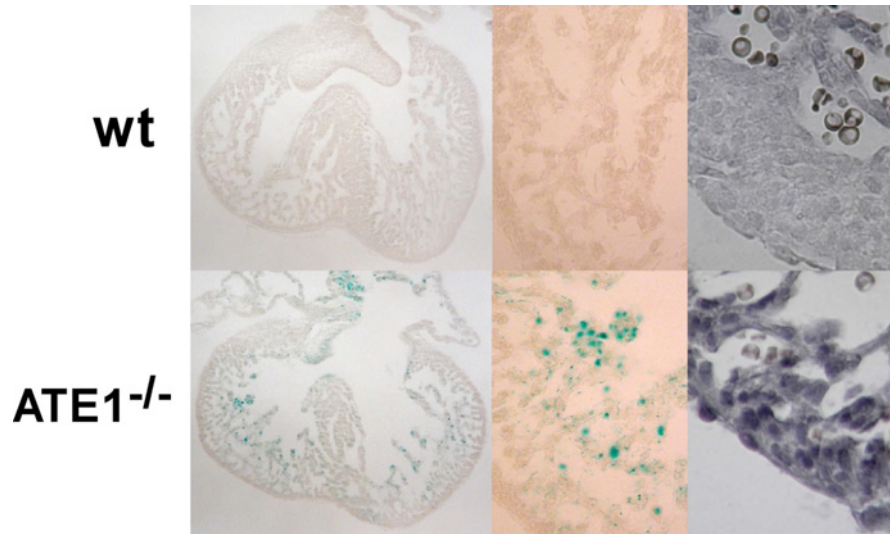**Figure 24.** Expression of ATE1 in the embryonic hearts. Xgal staining (left and middle panels) and immunohistochemistry for β-galactosidase was performed with paraffin sectioned 13.5-dpc embryonic hearts. LacZ signals were observed mainly in trabeculea, ventricular walls, and interventricular septum.

arteriosus. The severity of cardiac and valvular defects of ATE1 mutants varied between embryos, possibly reflecting the mixed genetic background. The sizes of lumens of ventricles appeared to be normal or slightly reduced in mutant embryos. In summary, these finding indicate that the severe heart abnormality such as the hypoplastic ventricular chamber and the poorly formed interventricular septum in *ATE1*$^{-/-}$ embryos accounts for a failure of the circulatory system and ultimately in fetal death.

3.4.3   Reduced Proliferation of *ATE1*$^{-/-}$ Embryonic Hearts

To determine whether the aforementioned hypoplastic phenotypes were a result of decreased proliferation, increased cell death, or both, the rates of cell proliferation in *ATE1*$^{-/-}$ hearts were first examined by measuring BrdU incorporation into newly synthesized DNA in different developmental stages (Fig. 21). At E12.5, the proliferation rates were 26.3 ± 5.1 % and 33.1 ± 6.1 % in wild type ventricular wall and intraventricular septum, respectively, while *ATE1*$^{-/-}$ mutants had significantly reduced BrdU index, 12.1 ± 1.7 % and 10.4 ± 2.2 %, respectively. At E13.5, the proliferation rates of wild types were 21.6 ± 2.2 % in ventricular wall and 17.6 ± 3.0 % in septum and, at the same stage, mutants showed 16.4 ± 1.5 % and 14.3 ± 1.7 %, respectively. These data indicate that abrogation of ATE1 causes decreased DNA synthesis in the
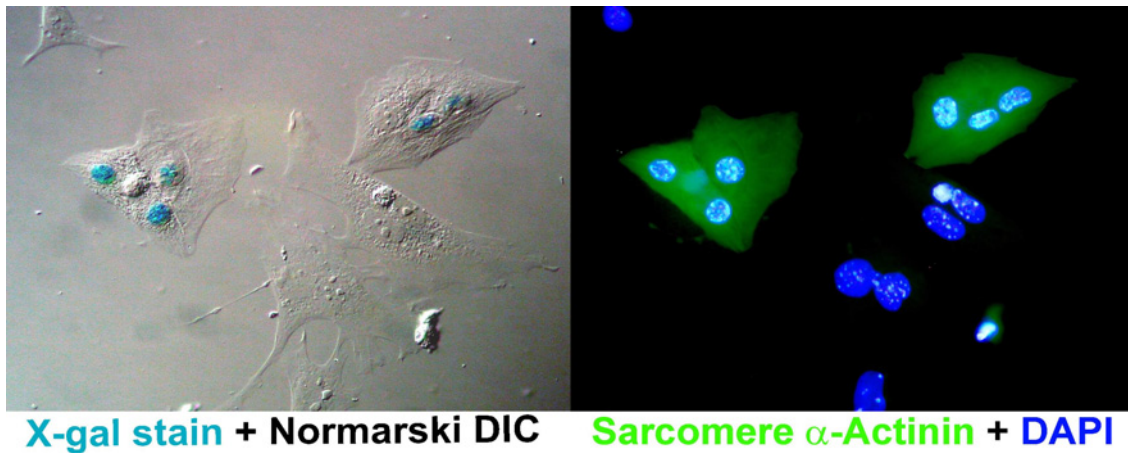
Figure 25. Expression of ATE1 in cardiomyocytes. X-gal staining of primarily cultures heart cells from 13.5-dpc embryos followed by α-actinin immunostaining, a marker for cardiomyocytes. DIC images (left panel) and immunofluorescence image (right panel) shown. Nucleus-specific LacZ signals were observed in the cardiomyocyte-specific manner.

heart. While the proliferation of the ventricular wall and the septum which forms by cardiomyocytes were markedly reduced, the trabecular layer appeared to be less affected. There were no significant differences of BrdU index between wild type and mutants in trabeculae (4.3 ± 1.0 % and 3.9 ± 1.5 %, respectively, at E12.5, and 4.1 ± 0.8 % and 3.1 ± 1.1 %, respectively, at E13.5) at both stages. The reduced proliferation appeared to be specific to the hearts, rather than global cell growth retardation, since proliferation of other organs, such as brain and lung in ATE1-mutant embryos (57.6 ± 5.2 % and 60.2 ± 7.4 %, respectively, at E12.5, and 38.6 ± 6.2 % and 40.2 ± 8.3 %, respectively, at E13.5) is indistinguishable from that in wild type controls. The discrepancy between trabeculae phenotype in ATE1 mutant and no BrdU difference may be from that trabecular layer proliferation occurs at earlier stages (E10.5-E11.5) than the compact zone and, at E12.5, the forming trabeculae consists of less proliferating cardiomyocytes (Sucov et al. 1994; Sedmera and Thomas 1996).

In addition to the BrdU assay, the mitotic index was measured by immunostaining against phosphor-histone H3 (H3P), a mitosis marker, from E11.5 to E13.5. As shown in Figure 22, more H3P-positive cells are observed at the earlier stages and there were markedly reduced numbers of relative H3P-positive cells in the heart of null mice when compared to wild type littermates, especially in the compact layer and ventricular septum. Mitotic index was peak at E11.5. In ventricular wall, wild type showed 1.79 ± 0.18 %, 1.23 ± 0.07 %, and 0.24 ± 0.11 % of mitotic index at E11.5, E12.5 and E13.5, respectively. $ATE1^{-/-}$ mutants had significantly reduced
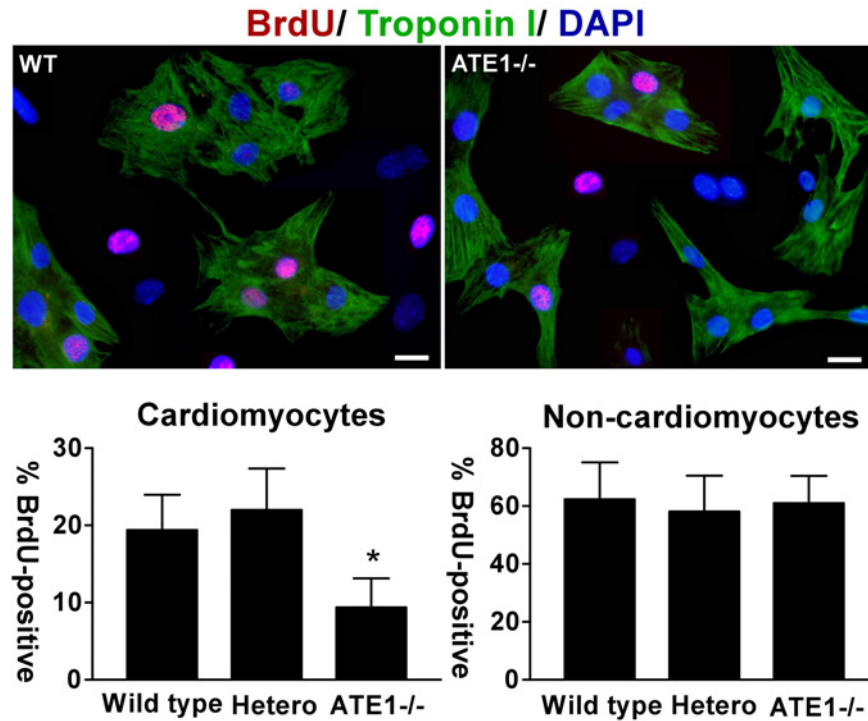
Figure 26. DNA synthesis defects in ATE1-deficient cardiomyocytes. (Upper panels) BrdU incorporation assay using primarily isolated wild type and *ATE1*^{-/-} mouse embryonic cardiomyocytes. (Lower panels) Quantificaiton of BrdU index from immunostaining. Cell proliferation indices were not altered in ATE1-deficient cardiac fibroblasts compared to wild type and heterozygous and homozygous mutants. Data represents mean ± s.e.m. from three independent experiments.

mitotic index compared to wild type, which are 0.52 ± 0.21 %, 0.64 ± 0.08 %, and 0.17 ± 0.01 %, respectively, in ventricular wall, although, at this stage, no lethality or change in gross morphology is seen. In the septum, the mitotic index was significantly reduced at E11.5 (1.44 ± 0.18 % in wild type and 0.73 ± 0.21 % in mutants) and E12.5 (1.41 ± 0.35 % in wild type and 0.33 ± 0.08 % in mutants), although there was no significant difference at E13.5 (0.19 ± 0.02 % in wild type and 0.18 ± 0.03 % in mutants). In trabeculea, E11.5 embryos showed significant difference (1.48 ± 0.26 % in wild type and 0.77 ± 0.26 % in mutants).

The results stated above were consistent with the previous report that the peak of mitotic index in compact layer and in trabecular layer is earlier than E11.5 (Toyoda et al. 2003). Cardiac myocytes lose their proliferative capacity right after birth in mice or about at E17.5 in rat (Wang et al. 1996). Cell death was examined by TUNEL assay to understand whether increased apoptosis plays a role in the decreased proliferation in the mutant hearts from E11.5 to E14.5. Only a few cardiac cells were stained during the stages prior to global necrosis of mutant embryos, indicating no significant cell death by apoptosis, and no indication was observed that

50
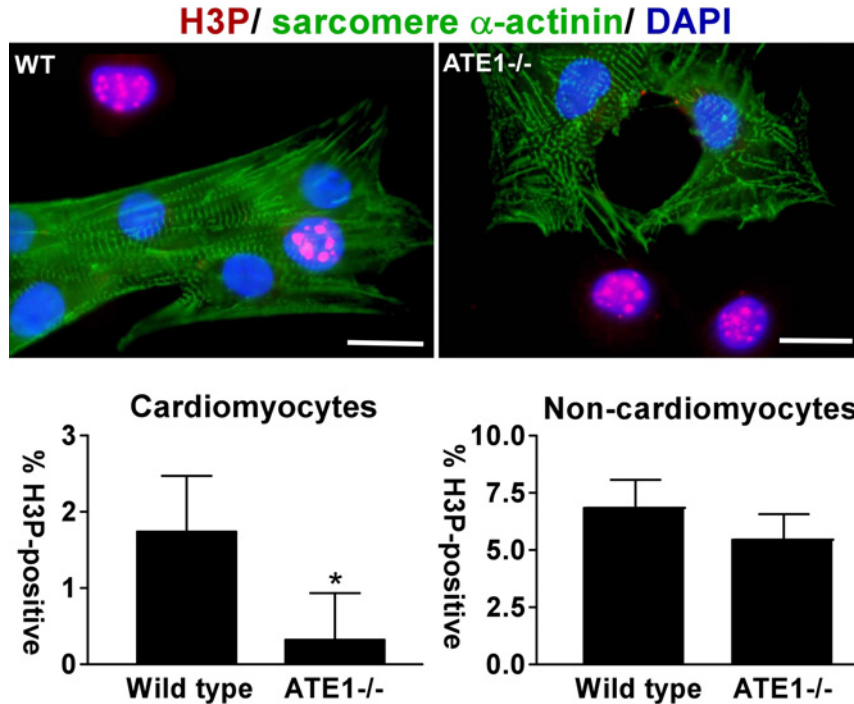
Figure 27. Mitosis defects in ATE1-deficient cardiomyocytes. Immunostaining against phosphor-Histone H3 (mitosis marker) using primarily isolated wild type and *ATE1*^{-/-} mouse embryonic cardiomyocytes and its quantification. Similar to BrdU index, cell proliferation indices were not altered in ATE1-deficient cardiac fibroblasts compared to wild type and homozygous mutants. Data represents mean ± s.e.m. from three independent experiments.

elevated cell death contributes to this phenotype (data not shown). Together, these data

suggested that impaired proliferation of ATE1-deficient heart, with onset at E11.5, accounts for

the defective cardiac morphogenesis and, ultimately, for fetal death.

3.4.4   Expression of LacZ from the ATE1 Allele in Cardiomyocytes

The expression of LacZ reporter integrated into the targeted ATE1 allele was prominently

detected in the brain, neural tube, and the heart as monitored by β-galactosidase activity (Fig.

23), which is consistent with ATE1 mRNA expression detected in wild type embryos by in situ

hybridization (Kwon et al. 2002). The expression of ATE1 in histological sections was also

examined (Fig. 24). The β-gal signals were located in the nucleus due to the nuclear localization

signal placed at the 5' terminus of the LacZ sequence. Strong signals in the nucleus were

observed in trabeculae, in atrio-ventricular bulbar cushion, and both in right and left ventricular

walls. However, the signal was decreased after E12.5. Expression in the atrium was relatively

Figure 28. Hypertrophy in ATE1-deficient Cardiomyocytes. (A) Immunostaining against ANP, a hypertrophy marker. Its peri-nucleic expression was observed in both wild type (a, b) and $ATE1^{-/-}$ (c, d) primary cardiomyocytes.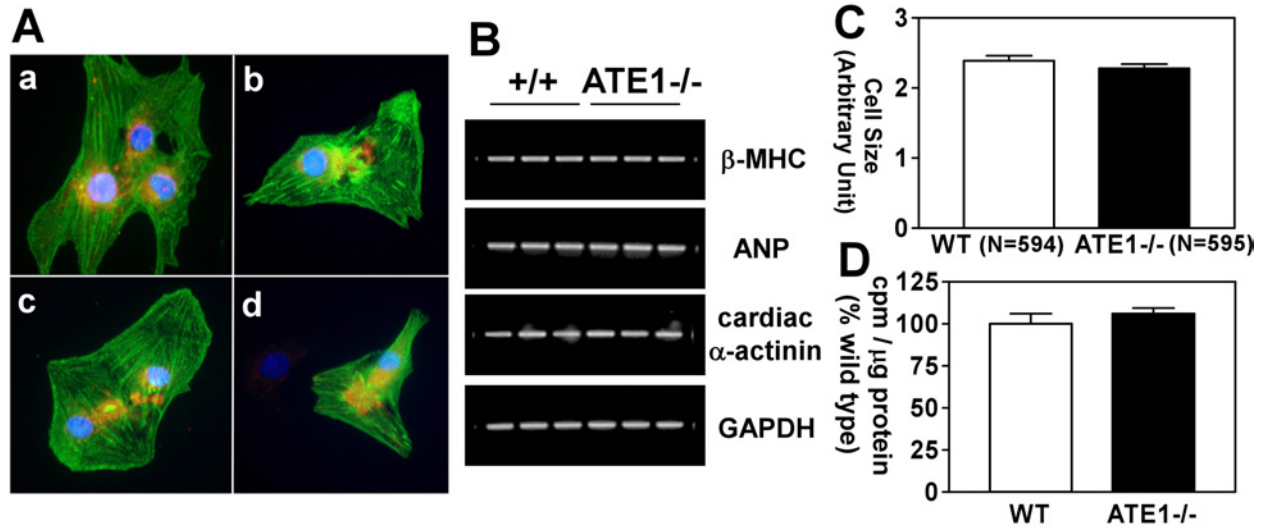 (B) mRNA expression of hypertrophic genes were examnined by RT-PCR with GAPDH control. (C) Size analysis and leucine incorporation assay. No detectable difference in terms of hypertrophism between these two genotypes was seen, suggesting hypoplasia not hypertrophy in ATE1-deficient cardiomyocytes might be responsible the phenotype of $ATE1^{-/-}$ embryos. Data represent mean ± s.e.m. from three independent measurements of cardiomyocyte size and cpm. No significant difference was observed between the genotypes.

weak. Although ATE1 expression was observed from all over the compact zones of the developing heart, cell type specificity of ATE1 expression has not been determined. The expression of LacZ in the developing heart was also confirmed by immunohistochemistry by using anti-β-galactosidase antibody. To dissect the expression pattern of ATE1 in the heart, LacZ staining was performed on primarily cultured heart cells isolated from $ATE1^{-/-}$ mutant hearts (Fig. 25). LacZ staining followed by immunostaining with sarcomeric α-actinin antibody readily revealed that ATE1 expression was mainly observed in cardiomyocyte population, where hypoplasia defect was found in the developing $ATE1^{-/-}$ heart while not (or less) in cardiac fibroblasts which can also be identified by their characteristic morphology and bigger nucleus size. The results suggest an autonomous stimulatory role of ATE1 on the proliferation of cardiomyocytes. Abnormal proliferation of cardiomyocytes in ATE1 mutant was also observed as described below.

3.4.5 ATE1 as Cell Autonomous Proliferation Regulator of Cardiomyocytes

The thinner ventricular wall layers and the decreased proliferation of $ATE1^{-/-}$ hearts as well as restricted expression of ATE1 in the cardiomyocytes suggested less proliferative cardiomyocytes in the developing heart. Moreover, it remained to be demonstrated whether ATE1 functions in the cardiomyocytes, not from adjacent components of the hearts, to initiate proliferation. In order to determine the level of proliferation in $ATE1^{-/-}$ cardiomyocytes, BrdU incorporation assay was performed using primary cardiomyocytes cultured from embryonic hearts (Fig. 26A, B). Coimmunostaining with anti-cardiac troponin I antibody and with anti-BrdU antibody distinguished proliferating cardiomyocytes from noncardiomyocytes. Moreover, the primary culture system minimized the multiple growth signals originating from adjacent cell lineages of the developing heart or from the whole body. In serum-containing media, the BrdU labeling index in ATE1 mutant cardiomyocytes (9.4% ± 3.6%) was significantly lower than heterozygous mutant (22.0% ± 5.4%) or wild type (19.4% ± 4.6%), indicating that cell growth is defective in mutants. Cardiomyocytes have been known to undergo cell division until postnatal day 3 although the rate decreases after E11.5 (Wang et al. 1996). To examine whether cell proliferation of cardiac fibroblasts was also affected in ATE1 mutants, the cell proliferation index of primary cardiac fibroblasts was assessed. The non-cardiomyocyte population that was not stained by cardiac troponin I antibodies was regarded as cardiac fibroblasts although other cell populations such as endothelial cells and smooth muscle cells may exist as a minor population. As shown in Fig. 26, cell proliferation indices were not altered in ATE1-deficient cardiac fibroblasts (60.9% ± 2.4%) as compared to wild type (62.3% ± 3.2%) and heterozygous mutants (58.1% ± 3.4%). Therefore, cell proliferation of cardiomyocytes, but not cardiac fibroblasts was down-regulated in ATE1 mutant hearts when cells were cultured.

To determine if ATE1 also regulates mitosis in primary cardiomyocytes, the mitotic index by immunostaining phospho-histone H3 (H3P), a marker for mitotic cells, was evaluated (Fig. 27C, D). Most mitotic cells both in wild type and ATE1 mutants were at prophase or prometaphase. Knocking out $ATE1$ gene significantly decreased the number of H3P-positive cells by 78.2% in cardiomyocytes (1.73% ± 0.33% wild type and 0.33% ± 0.32% ATE1 mutant). However, noncardiomyocyte cells from $ATE1^{-/-}$ had comparable mitotic indices to those observed from the wild type (6.85% ± 1.23% wild type and 5.47% ± 1.2% ATE1 mutant). Collectively, these data strongly indicate that the cardiac phenotype of ATE1-deficient mice during embryogenesis is mainly due to a proliferative deficiency, i.e. decreased DNA synthesis
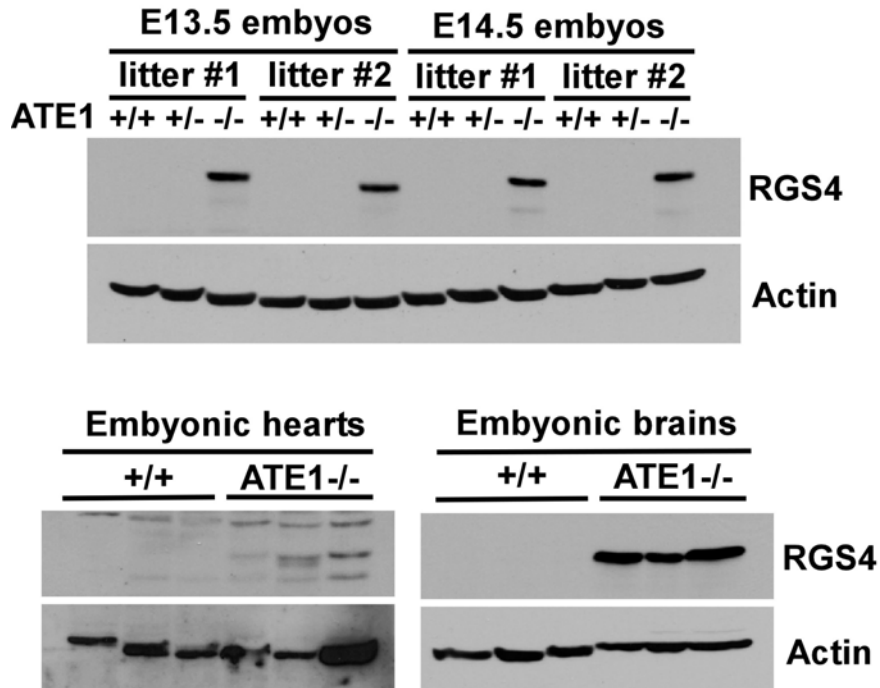
Figure 29. Level of RGS4 protein in *ATE1*^{-/-} embryos. Immunoblot using whole embryonic extract (upper panel), embryonic heart extract (lower panel, left), or embryonic brain extract (lower panel, right) to detect and compare endogenous levels of RGS4 in wild type and *ATE1*^{-/-} embryos. RGS4 was not detected in wild type embryos and organs while prominent expression was observed in ATE1-deficient samples. Anti-RGS4 antibody is a kind gift from Dr. Mumby.

associated with perturbed mitotic activities of cardiomyocytes. Moreover, these *in vitro* data indicate that the function of ATE1 is intrinsic to cardiomyocytes in a cell autonomous manner.

3.4.6   Hypertrophy in ATE1-deficient Cardiomyocytes

Embryonic cardiomyocytes have two complementary characteristics; hyperplastic (cell division) and hypertrophic (cell enlargement) until they are terminally differentiated. I examined whether ablation of ATE1 affects hypertrophic behavior in primary cardiomyocytes by measuring cell size, protein content increase ([^{3}H] leucine uptake), and hypertrophy marker gene expression through RT-PCR and immunostaining against ANP in the primary cardiomyocytes culture system under physiological conditions (with serum). As shown in Figure 28, ANP, a representing hallmark of hypertrophic genetic reprogramming in cardiomyocytes and a prognostic indicator of clinical severity of hypertrophy, was immunostained, revealing a perinulear staining pattern in cardiomyocytes (Liu and Olson 2002). However, significant difference was not detected in

Figure 30. Expression of RGS4 mRNA in *ATE1*^{-/-} embryos. Quantitative PCR to compare mRNA levels of RGS proteins which revealed no significant difference between the mut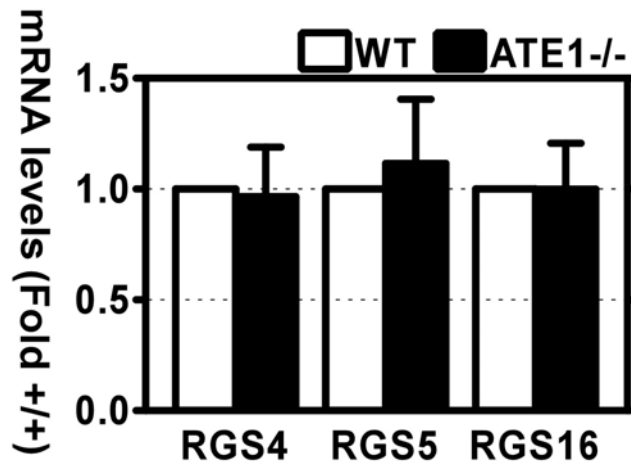ants and controls indicating that down-regulation of RGS proteins occurs posttranscriptionally. Data represent mean ± s.e.m. from three independent measurements of mRNA level. No significant difference was observed between the genotypes.

expression level and pattern between both genotypes. During this experiment, more differentiated cardiomyocytes, which are multinucleated, coexisted (~55% of all cardiomyocytes) with mitotically active mononucleated cardiomyocytes both in wild type and in the ATE1 mutant, which indicates thatDNA synthesis continued although cell division ceased. Organization of sarcomere was also examined by immunofluorescence microscopy, but myofilament organization exhibited no significant difference between both genotypes. The mRNA level of β-MHC, cardiac α-actnin, ANP was determined by semi-quantitative RT-PCR using GAPDH as a control and observed not significantly changed in *ATE1*^{-/-} embryonic hearts. Measurement of cell size with NIH ImageJ software revealed that the cell surface area of ATE1 mutant cardiomyocytes was comparable to that of wild type. Moreover, the hypertrophism was measured by [^{3}H] leucine incorporation using primary culture system. However, no detectable difference between these two genotypes was seen. Although many *in vivo* studies using rat cardiomyocytes indicate that chronic stimulation of Gq-coupled receptors is sufficient to induce cardiomyocyte hypertrophy(Dorn and Hahn 2004), their contribution in mouse embryonic cardiomyocytes remain elusive. This result suggested that lack of ATE1 does not appear to affect the transition to hypertrophy of cardiomyocytes and that embryonic mouse cardiomyocytes undergo "autonomous hypertrophy" as shown in neonatal mouse cardiomyocytes (Deng et al. 2000). Therefore, hypoplasia not hypertrophy in ATE1-deficient cardiomyocytes might be
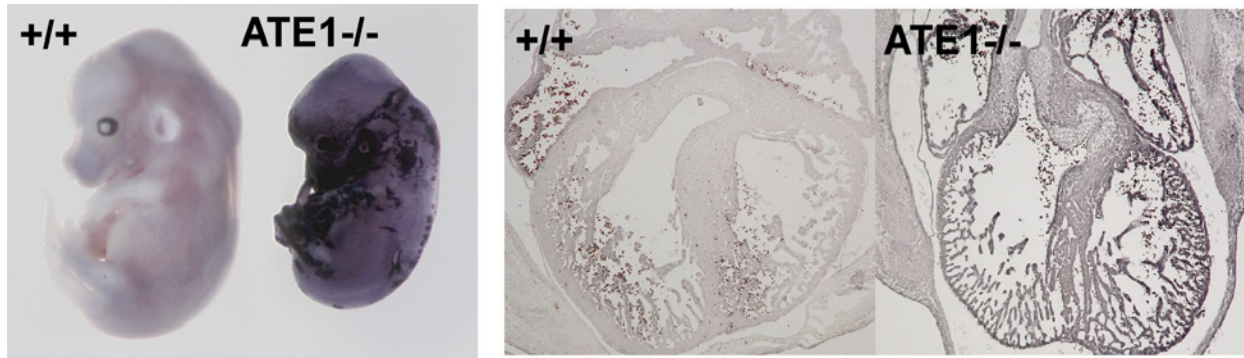
Figure 31. Immunostaining of RGS4 protein in *ATE1*$^{-/-}$ embryos. Whole mount immunostaining (left panel) using anti-RGS4 antibody and Immunostaining of embryonic hearts (right panel) using 13.5-dpc wild type and ATE1 mutants. ATE1 mutant embryonic hearts showed defective morphogenesis including sparse trabeculea, thin myocardium, and holes in interventricular septum. Consistent with immunoblot data, RGS4 expression was prominent only in ATE1-mutant embryos and embryonic hearts.

responsible the phenotype of *ATE1*$^{-/-}$ embryos.

3.4.7   RGS proteins and G protein Signaling in *ATE1*$^{-/-}$ Cardiomyocytes

In Chapter II, I identified a set of RGS proteins (RGS4, RGS5, and RGS16) as the first *in vivo* substrates of mouse ATE1 (Lee et al. 2005). However, the information was mainly obtained by *in vitro* translated RGS proteins and overexpressed RGS proteins in ATE1-deficient mouse embryonic fibroblast cells because of the lack of a good antibody which could detect endogenous protein levels and the low natural abundance of the proteins despite the relative abundance of their mRNA. Previously, Dr. Mumby's group (Krumins et al. 2004) and Dr. Druey's group (Derrien et al. 2003) developed monoclonal antibodies with appropriate specificity and sufficient sensitivity to detect endogenous RGS4 and RGS16, respectively, and, in the present study, their endogenous levels were examined in the ATE1 mutant. Figures 29 shows a Western blot performed on extracts of whole E13.5 embryos and embryonic tissues, e.g. brain and heart using the antibodies. Strikingly, a substantial level of RGS4 in *ATE1*$^{-/-}$ embryos and embryonic hearts and brain was observed, while there is no detectable RGS4 in littermate controls. RGS16 level was lower than RGS4, but revealed that RGS16 was also stabilized in *ATE1*$^{-/-}$ embryos. The amount of RGS4 was higher in the brain than the heart. Quantitative RT-PCR analysis with total RNA prepared from E13.5 embryonic hearts revealed no significant difference between the mutants and controls which indicates that down-regulation of RGS proteins occurs
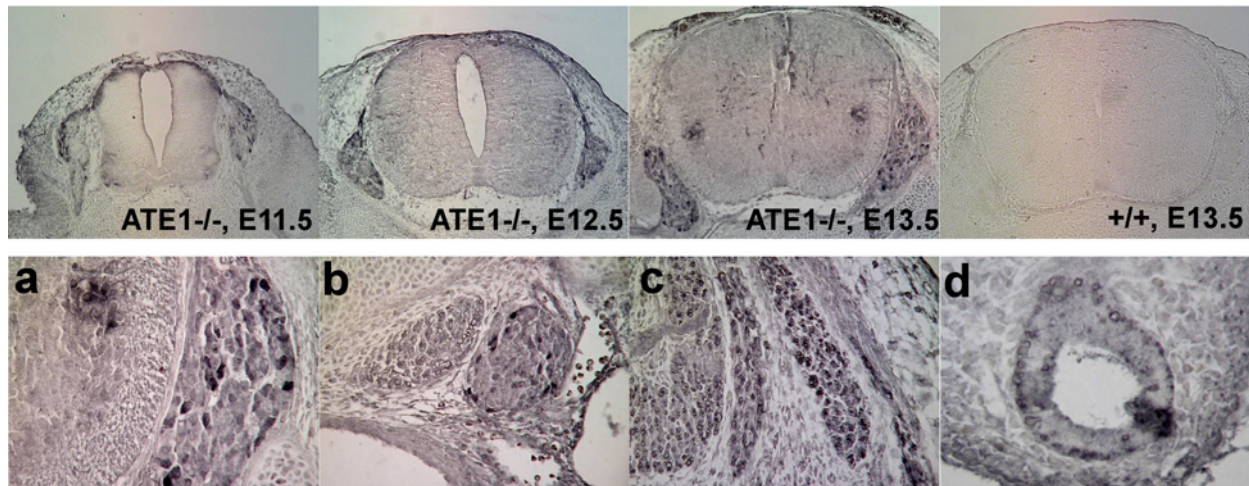
Figure 32. Expression pattern of RGS4 protein in $ATE1^{-/-}$ embryos. Immunostaining of different stages of $ATE1^{-/-}$ embryos using the same antibody. Magnified neural tube areas (upper panels) and other neural crest cell destination areas (lower panels). RGS4-positive cells appeared along the pathway of neural crest cell migration, including dorsal root ganglia, sympathetic ganglia, muscle linage, and developing alveolus.

posttranscriptionally (Fig. 30). Consistent with immunoblot results, the high level of expression, probably because of stabilization of otherwise unstable RGS4 protein, was also observed in ATE1-deficient embryos and embryonic hearts when immunostained with anti-RGS4 antibody (Fig. 31). Moreover, immunostaining revealed RGS4-positive cells along the pathway of neural crest cell migration, including dorsal root ganglia, sympathetic ganglia, muscle linage, and developing alveolus (Fig. 32). The migration of RGS4-positive cells started as early as E11.5 when the neural folds had remained open, and begin cranially and then gradually extend caudally (Fig. 32).

In light of the role of RGS proteins as negative regulators in Gq- and Gi-mediated signaling and the referential expression of ATE1 in cardiomyocytes, I asked whether GPCR signaling pathway in the ATE1-mutant heart might be defective because of stabilized RGS protein. To explore this possibility, the downstream kinases of the GPCR signaling pathway in the embryonic hearts were measured by *in vitro* kinase activity assay. The activated α subunit of Gq directly stimulates phospholiphase (PLC) leading to hydrolysis of phosphoatihylinositol bisphosphate (PIP2) into IP3, which induces Ca^{++} release from endoplasmic reticulum, and diacylglycerol, which regulates the activities of protein kinase C (PKC) and MAPKs. All these proteins involve the Gq-signaling pathway have been known to play key roles in regulating cardiomyocyte growth (Adams and Brown 2001). Previously, the activity of ERK1 and ERK2, a
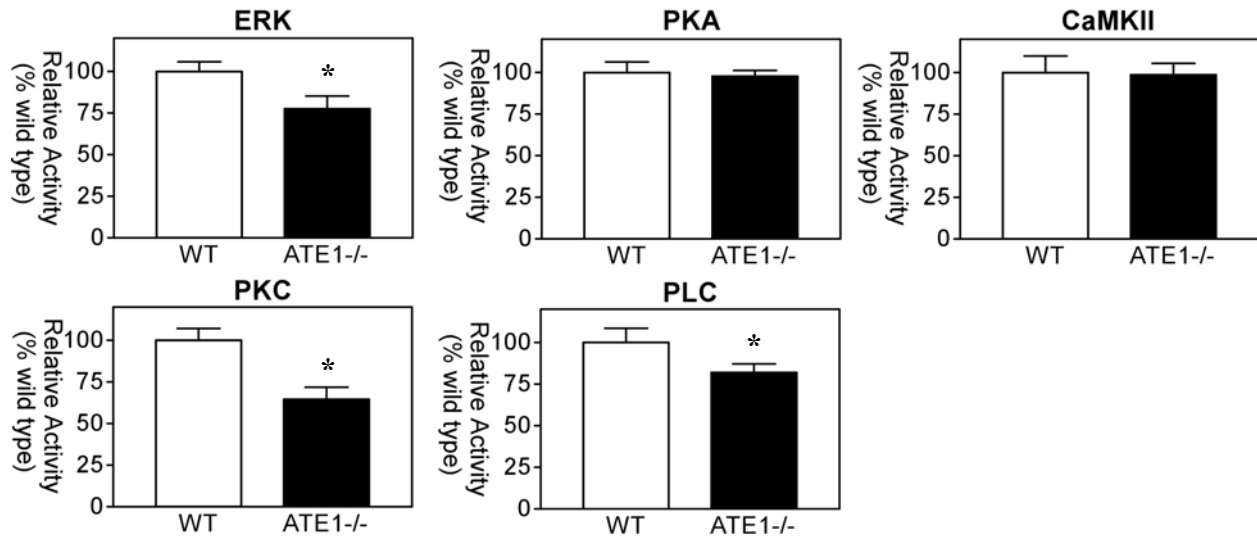
57

Figure 33. Activities of effectors of G protein signaling in $ATE1^{-/-}$ embryos. Activities of GPCR downstream effectors were measured using embryonic heart extracts from wild type and $ATE1^{-/-}$. Following substrates were used for each kinase, MBP for ERK, Kemptide for PKC, PIP2 for PLC, and other synthetic peptides for CaMKII and PKA. Data represent mean ± s.e.m. from independent measurements of the kinase activities using embryonic heart extract from three non-litter embryos. *: $p < 0.05$.

downstream effector of Gq- and Gi signaling pathway, was reported to be impaired in whole embryo. From embryonic heart extracts, total kinase activity of ERKs, which was determined by the kinase assay with myelin basic protein as a substrate, was 77.86% lower in $ATE1^{-/-}$ than in wild type embryonic hearts (Fig. 33). There was no significant difference in PKA and CaMKII activities between these genotypes. PKC and PLC activities also decreased significantly in ATE1 mutants (64.52% and 82.99%, respectively), while CaMKII and PKA activities showed comparable level as controls (Fig. 33). No change of PKA and CaMKII in the ATE1 mutant may reflect the weak relation of ATE1/RGS protein to Gs-cAMP signaling pathway. These data suggest that ATE1 specifically affects Gq and Gi signaling pathway probably through the RGS protein.

To determine the effect of ATE1 on signaling in cardiomyocytes, the responsiveness kinase activities on serum stimulation was examined in primarily cultured wild type and $ATE1^{-/-}$ mouse embryonic cardiomyocytes, especially for the activation of ERK1/ERK2, a crucial player in cardiovascular signaling pathways (See Background in Chapter II), and its upstream kinase, MEK1. Primary cardiomyocytes were harvested at multiple time points after serum stimulation, and activities were measured by immunoblotting and quantitative analysis with antibodies
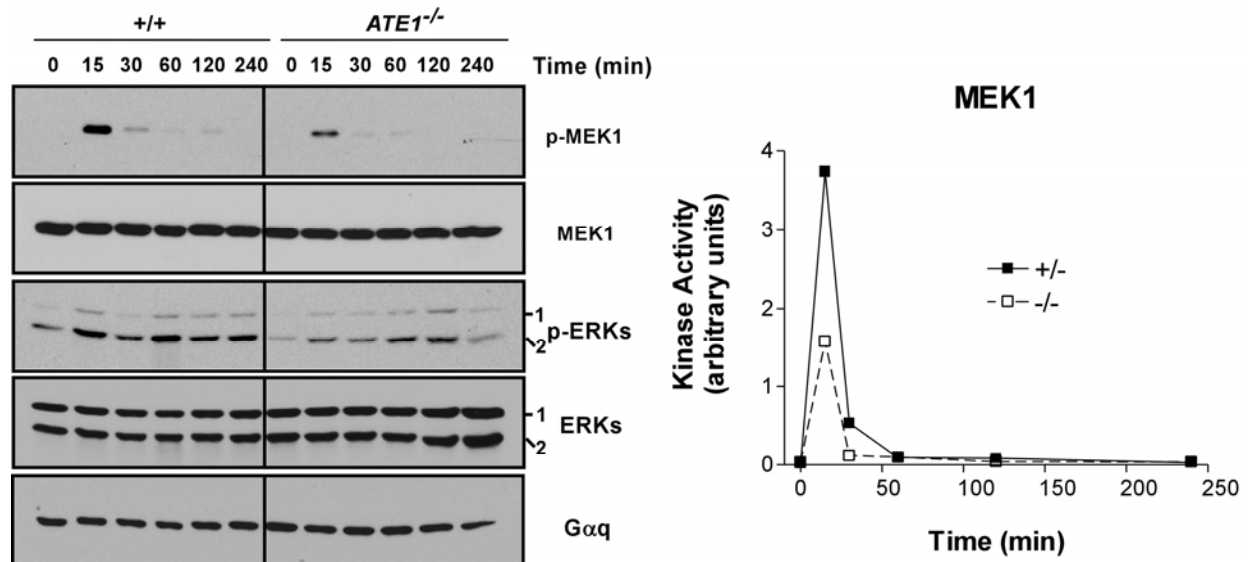
Figure 34. Serum-starved and serum-stimulated ERK1/2 and MEK1 activities in wild type, and *ATE1*^{-/-} embryonic cardiomyocytes. Primarily cultured mouse embryonic cardiomyocytes were serum-starved for 24 h and subsequently stimulated with 20% FBS for the times indicated. Total cell extracts were subjected to immunoblotting with antibodies against Gαq and phosphorylated and unphosphorylated ERK1/ERK2 and MEK1. Quantitation of the active forms of MEK1 shown in the right graphs.

specific for activated kinases. The increased activities by serum stimulation followed by serum starvation were observed as early as 15 min. However, significantly decreased level of active forms MEK1 and ERK1/2 were detected in *ATE1*^{-/-} cardiomyocytes compared to control (Fig. 34), suggesting that the MEK1-ERK1/2 pathway is regulated by the ATE1-RGS pathway. Taken together, these findings, consistent with the previous reports describing that overexpression of RGS proteins inhibits G protein signaling in cultured cardiomyocytes (Tamirisa et al. 1999), suggest that Gq signaling may decrease in ATE1-deficient cells by stabilization of negative regulators of the pathway, namely the RGS proteins.

3.4.8 Defective AngII-mediated Proliferation in *ATE1*^{-/-} Cardiomyocytes

Based on the results that proliferation of *ATE1*^{-/-} cardiomyocytes was reduced and RGS-regulated Gq- and Gi-signaling pathway was defective, it is reasonable to hypothesize that there are mitogenic signals mediated by GPCR in cardiomyocytes. To further examine the role of ATE1, Gq agonists on proliferation of cultured primary cardiomyocytes were evaluated (Fig. 35). There was no significant difference of cell proliferation between wild type and ATE1 mutant
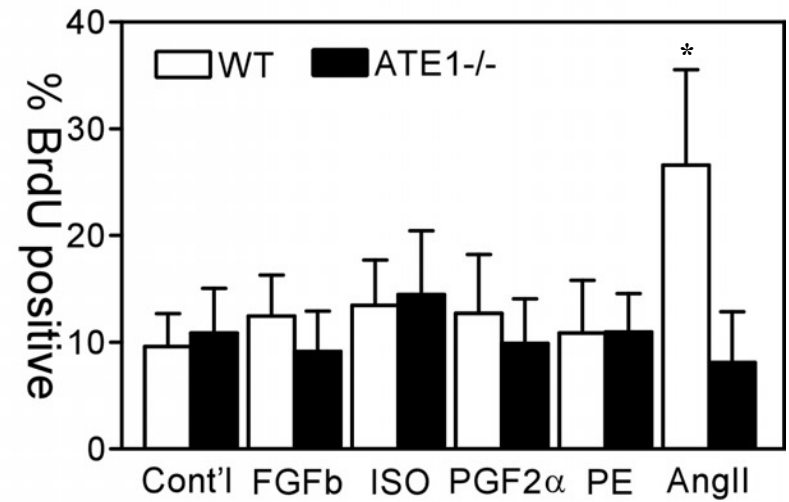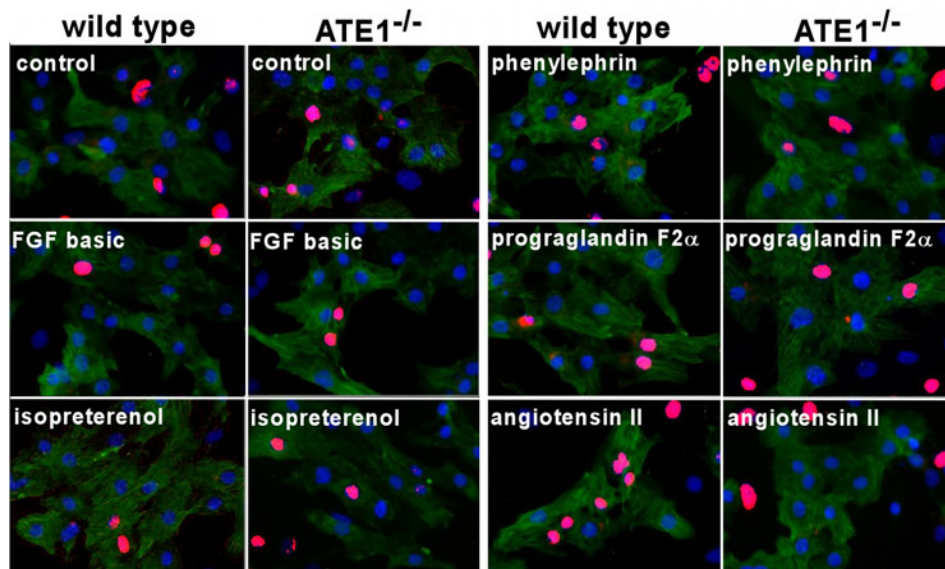
Figure 35. Defects in AngII-mediated proliferation in *ATE1*^{-/-} cardiomyocytes. (Left panels) BrdU incorporation assay using primary cardiomyocytes in the presence of different agonists. (Right panel) Quantification of the BrdU index. Agonists targeting different downstream effectors (ISO, Gs; PE, Gq; PGF2α, Gq; AngII, Gq-coupled AT$_2$; FGFb, control, not GPCR agonist) were used. In *ATE1*^{-/-} cardiomyocytes, AngII did not induce cell proliferation which was seen in wild type cardiomyocytes. Data represent mean ± s.e.m. from three independent measurements of cardiomyocyte proliferation rates. *: $p < 0.05$.
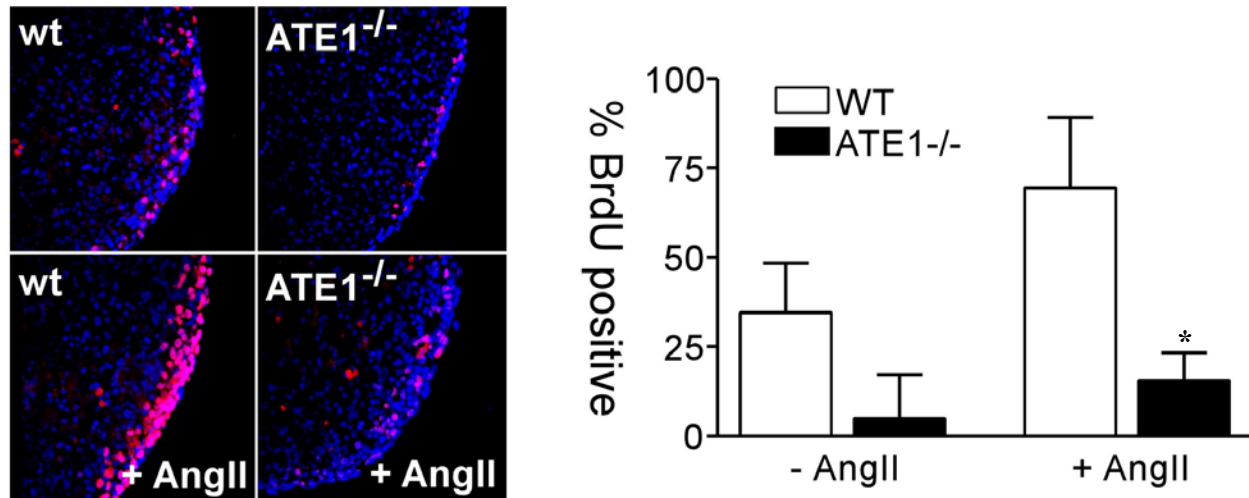
Figure 36. Defects in AngII-mediated proliferation in *ATE1*$^{-/-}$ embryonic hearts. BrdU incorporation assay using explanted hearts in the presence of AngII (left) and its quantification (right panel). Consistent with the results from cultured cardiomyocytes, explanted hearts showed reduced proliferation in the presence of AngII in *ATE1*$^{-/-}$ embryonic hearts. Data represent mean ± s.e.m. from three independent experiments (See details in Methods. *: $p < 0.05$.).

cardiomyocytes when treated with basic FGF, a ligand whose receptors are not directly coupled with G protein, which is consistent with a previous report that FGFb did not alter BrdU incorporation of mouse cardiomyocytes in the absence of serum (Lepic et al. 2006). However, ATE1 significantly enhanced levels of BrdU incorporation in wild type cardiomyocytes, while ATE1 mutant showed no difference. AngII has been known to induce cardiac hypertrophy though AT_1 receptor (Thomas et al. 2002), which is coupled with Gq- and Gi proteins, activating primarily the MAPK signaling pathway via PLC and PKC activation (Izumi et al. 2000). Moreover, AngII stimulates protein synthesis both in cultured rat cardiomyocytes and in the isolated whole hearts (Schunkert et al. 1995; Sundgren et al. 2003). Phenylephrine (PE) and prostaglandin F2α (PGF2α) also signals through Gq and Gi-coupled α-adrenergic receptors and prostaglandin receptors, respectively. However, no proliferative effect was observed from the agonists. Although they activate the same G proteins, the proliferative phenotype differed, which may be the result of receptors coupling to more than one G protein and initiating several signaling pathways. Isoprotenerol (ISO) stimulates Gs-coupled β-adrenergic receptors. It is known to have little effect on the hypertrophic response to pressure overload (Akhter et al. 1998) and also exhibited no effect on the proliferation of *ATE1*$^{-/-}$ cardiomyocytes.

The proliferation of whole hearts was also examined to further confirm a cell-

autonomous effect of AngII (Fig. 36). Embryonic hearts were excised from E13.5 embryos and the beating hearts were subsequently cultured in the presence or absence of AngII with BrdU. The BrdU-positive cells were observed mainly in the ventricular wall area. Consistent with the results using cultured cardiomyocytes, explanted hearts showed reduced proliferation in the presence of AngII, in $ATE1^{-/-}$ embryonic hearts (wilt type 69.4% and mutant 15.5%) although the proliferation rates were greater in the presence of AngII than in the absence of AngII both in wild types and mutants. MAPK signaling, which was defective in ATE1-deficient embryonic hearts and cardiomyocytes, has been known as a major mediator of AngII-induced cardiomyocyte growth (Thomas et al. 2002). These data strongly suggest that the AngII-mediated signaling pathway, which is controlled by ATE1-RGS circuit, is implicated in normal development of the heart.

3.5   DISCUSSION

The heart is the first organ to form in the embryo, whose function is essential to embryonic survival, even in early midgestation, and whose abnormality during morphogenesis results in congenital heart disease (Olson and Schneider 2003). Although it was reported that deficiency of ATE1 results in congenital heart disease-like abnormality in mice (Kwon et al. 2002), the role of ATE1 at the molecular level has remained unknown. In this study, I attempted to determine the function of ATE1 in cardiac development. The results suggest that there is an active pathway regulating cardiomyocytes proliferation that is controlled by ATE1. ATE1-deficient mice die during E12.5- to E14.5 asscociated with defects in cardiac development. I observed not only various morphological abnormality and significantly reduced proliferation in developing $ATE1^{-/-}$ hearts and cultured embryonic cardiomyocytes. ATE1 was prominently expressed in cardiomyocytes of cultured heart cells. Increased number of cardiomyocytes is responsible for the enlargement of hearts during embryogenesis until they lose their proliferative capacity right after birth in mice or at about E17.5 in rat (Wang et al. 1996). During E11.5 and E14.5, cardiomyocytes rapidly proliferate leading to expansion of the ventricular wall and cardiomyocytes take 70 % to 80 % of the mass of the adult heart. The diminishing ability of the cardiomyocytes proliferation at the latest stage has been attributed to a block in the cell cycle

62

either in the G0 or G1 phases (Brooks et al. 1998). It was observed previously that post-transcriptional down-regulation of the amount of D-type cyclins, which is crucial for G1-S phase transition, in $UBR1^{-/-}UBR2^{-/-}$ embryos compared to littermate controls (An et al. 2006). Although we could not provide conclusive evidence here, it is possible that the G1 arresting may cause reduced proliferation of ATE1-deficient cardiomyocytes.

I also identified that the levels of endogenous RGS4 and RGS16 in $ATE1^{-/-}$ embryoninc hearts were significantly increased and the downstream activities of Gq- and Gi signaling pathways, which are regulated by RGS proteins, were also reduced in $ATE1^{-/-}$ hearts. Gq expresses in cardiomyocytes as well as non-cardiomyocytes in the developing heart (Offermanns et al. 1998). Although GPCR can interact with most or all members of their preferred G protein family, specific downstream pathways from Gq-coupled receptors may be able to distinguish among different members and have different roles to regulate heart development. Angiotensin II transgenic mice showed midgestation lethality with grossly enlarged atria (Hein et al. 1995), but α-adrenergic receptor transgenic mice showed no changes in ventricular morphology (Milano et al. 1994). Ang II-induced AT1 receptor activation via Gq or Gi on the rennin-angiotensin system stimulates PLC, and activates IP3/Ca^{2+} signaling, PKC, and MAPKs. Moreover, Ang II mediates the production of reactive oxygen species under physiological condition and pathological states (Hunyady and Catt 2006), raising a possibility that the role of oxygen in RGS4, RGS5, and RGS16 degradation can be expanded (Hu et al. 2005; Lee et al. 2005). At least 13 different members of the RGS family, including RGS4, RGS5, and RGS16, are expressed in mammalian cardiomyocytes and cardiac tissues which have GAP activity toward the Gαq and Gαi family G proteins (Wieland and Mittmann 2003). Interestingly, a recent paper described that RGS2 regulates the intracellular signaling of AngII and AT1 receptor desensitization in a negative feedback manner on aldosterone synthesis, which is one of critical factors in the development of Ang II-induced cardiovascular damage (Struthers and MacDonald 2004; Romero et al. 2006). However, their exact roles in the developing hearts and in the adult hearts in the normal and diseased states have remained poorly defined. Interestingly, knockout mice lacking both Gαq and Gα$_{11}$ die at E11.5 because of hypoplasia in the ventricular wall (Offermanns et al. 1998). Consistent with these reports, RGS4 overexpression in the ventricular myocytes blunted the stimulated PLC activity (Mittmann et al. 2002) and MAPK activity (Rogers et al. 2001).

However, overexpression of Gαq in mouse hearts or in cultured cells also showed activated PLC and increased cell growth (LaMorte et al. 1994; D'Angelo et al. 1997).

The pattern of sarcomeric protein gene expression is tightly regulated in a tissue- and developmental stage-specific manner, To evaluate the roles of genes regulating cardiac morphogenesis in ATE1-mutant hearts, the levels of GATA4, Nkx2.5, MEF2C, dHAND, eHAND, αMHC, βMHC, cardiac α-actinin, and ANP, were examined by using quantitative RT-PCR. However, no significant differences in the level of the genes were observed in $ATE1^{-/-}$ and wild type controls (data not shown). Given the complexity of the heart development and crosstalk among G protein signaling pathways, another approach such as genome-wide screening with Ang II treatment may clarify genes regulated by the ATE1-RGS-GPCR circuit. To date, most study for cardiomyocytes phenotypes and signaling have used neonatal rat cardiomyocytes, while there are only few studies using embryonic mouse cardiomyocytes, and they exhibited remarkably different characteristics (Deng et al. 2000). Identification of the factors controlling mouse cardiomyocytes proliferation and development is of great importance. Based on the results that proliferation of $ATE1^{-/-}$ cardiomyocytes was defective in RGS-regulated Gq- and Gi-signaling pathway, we examined various mitogenic Gq agonists and β-adrenergic receptor agonist on wild type and ATE1-deficient embryonic cardiomyocytes. Among Gq agonists, only Ang II increased the proliferation of wild type cardiomyocytes. However, in $ATE1^{-/-}$ cardiomyocytes, that effect was not observed. Moreover, there is no significant morphological difference between the genotypes after the treatment of agonists. BrdU index from primary cardiomyocytes cultured in serum-free condition showed no significant difference, suggesting that proper cardiomyocyte proliferation requires stimulation by specific Gq agonist including Ang II.

I also examined the possibility that hypertrophism may be involved in the phenotypes of $ATE1^{-/-}$ mice. However, cardiomyocyte size and hypertrophic gene expression in the mutant were comparable with wild type. This result suggested that lack of ATE1 does not appear to affect the transition to hypertrophy of cardiomyocytes. Although many *in vivo* studies using rat cardiomyocytes indicate that chronic stimulation of Gq-coupled receptors is sufficient to induce cardiomyocyte hypertrophy, their contribution in mouse embryonic cardiomyocytes remain elusive. Recently, it was reported that embryonic mouse cardiomyocytes undergo "autonomous hypertrophy" regardless of extracellular stimulation (Deng et al. 2000). Therefore, hypoplasia

not hypertrophy in ATE1-deficient cardiomyocytes might be responsible the phenotype of $ATE1^{-/-}$ embryos.

The increased RGS4 level in $ATE1^{-/-}$ embryos allowed us to detect its expression pattern in different stages of embryogenesis. Immunostaining revealed that its expression was significantly overlapped with the destination of neural crest cell migration, including dorsal root ganglia, sympathetic ganglia, muscle lineage, and developing alveolus, and the RGS4-positive cells migrated cranially at E11.5 when the neural folds had remained not closed and gradually extended caudally at the later stages. Although Gq signaling has also been known to be implicated in the migration of neural crest cells, $ATE1^{-/-}$ embryos showed no defects in migration. However, the outflow defects and valve defects in $ATE1^{-/-}$ embryos, including persistent truncus arteriosus and ventricular septal defects (Kwon et al. 2002), may be related with the function of neural crest cells or neural crest-differentiated cells, since neural crest cells migrate into the cardiac outflow tract and cardiac valves contributing to formation of the ductus arteriosus and septation of the truncus arteriosus into the aortic and pulmonary trunks (Clark et al. 2006). This result demonstrates that ATE1-deficient mice can be one model system for the study of short-lived proteins such as RGS4.

In summary, this study identified a cell-autonomous function of ATE1 in cardiac development. $ATE1^{-/-}$ embryonic hearts and cardiomyocytes showed impaired proliferation. ATE1 was prominently expressed in cardiomyocytes of developing hearts. Moreover, downstream activity of Gq- and Gi signaling pathways, regulated by RGS proteins, was decreased in $ATE1^{-/-}$ embryonic heart and cardiomyocyte. Endogenous levels of RGS4 and RGS16 were significantly increased in $ATE1^{-/-}$ embryos. Since proliferation of cardiomyocytes terminates completely shortly after birth (Wang et al. 1996), cardiac muscle loss in adults is a leading cause of the morbidity and mortality in the industrialized world. These results, suggesting a general physiological control mechanism of ATE1-RGS-GPCR signaling circuit for heart development, may raise a possibility that the manipulation of ATE1 expression can reinduce cardiomyocytes proliferation in adult mammals.

CHAPTER IV

4.0   DEVELOPMENT OF HETEROVALENT INHIBITORS TARGETING N-RECOGNINS

4.1   OVERVIEW

Multivalent binding allows high selectivity and affinity in ligand-protein interaction. The N-end rule pathway is a Ub-dependent proteolytic system, where specific E3s called N-recognins initiate ubiquitylation through recognition of type 1 and type 2 destabilizing N-terminal residues of substrates. To explore a model of heterovalent interaction, RF-C11, whose two heterovalent ligands were designed to cooperatively target two cognate sites of N-recognins, has been developed. Heterovalent RF-C11 selectively inhibited the ubiquitylation and degradation of both type 1 and type 2 N-end rule substrates, with higher efficacy than homovalent compounds with two homovalent ligands. It directly interacted with UBR1 fragment containing the UBR box motif and pulled-down endogenous UBR proteins from rat testis extracts. The treatment of RF-C11 impaired both proliferation and hypertrophy in cardiomyocytes, unveiling a previously unknown function of the pathway in cardiac proliferation and signaling. These results provide a molecular basis of designing multivalent inhibitors for specific intracellular pathways and identify the most potent inhibitor of the N-end rule pathway.

4.2   BACKGROUND

Nature employs multivalent interactions for selectivity and avidity of protein/protein or protein/ligand interaction, which are beneficial both thermodynamically (enhanced binding affinity) and kinetically (lessened rate of dissociation), and various synthetic multivalent
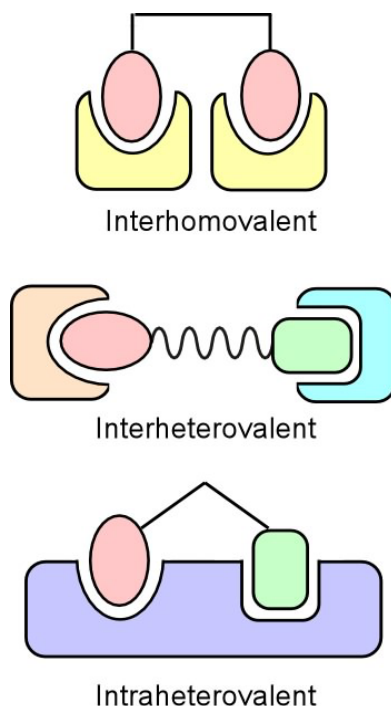
Figure 37. Models of interhomovalent, interheterovalent, and intraheterovalent interactions. Interhomovalent ligands bind to multiple identical receptors while interheterovalent inhibitors to multiple non-identical proteins. Intraheterovalent inhibitors interact with multiple binding sites in a single protein. Most current multivalent inhibitors employ interhomovalency-based interaction, targeting surface of bacteria, viruses, or cells. On the other hand, rapamycin from *Streptomyces hygroscopicus* is interheterovalent in that two heterovalent ligands target cognate binding sites of two different intracellular proteins (Sabatini et al. 1994).

molecules have been developed to exploit this type of interactions (Fig. 37) (Gestwicki et al. 2000; Choi 2004). However, the majority of the multivalent inhibitors target multiple, identical pairs of receptors on the cell surface, which form "interhomovalent" interactions to increase their recognition ability (Matrosovich 1989; Carrithers and Lerner 1996; Rao et al. 1998; Bertozzi and Kiessling 2001). For "heterovalent" inhibitors, which, to my knowledge, has not been explored extensively, bifunctional small molecules binding with only two distinct cytoplasmic targets were reported, e.g. chemical inducer of dimerization CID (Crabtree and Schreiber 1996) and synthetic bivalent peptides targeting two regions of a single protein, e.g. bivalirudin (Warkentin and Koster 2005). The present work explored the possibility that a small molecule-based "intraheterovalent" inhibitor, which retains two different ligands, can have increased efficacy and specificity through cooperative and simultaneous binding to the two independent, mutually nonexclusive sites of an enzyme or a heterobivalent receptor (Fig. 38).

In the light of the major challenges of identifying small, organic compound that inhibit protein-protein interactions, which are typically mediated through the flat, large, and flexible
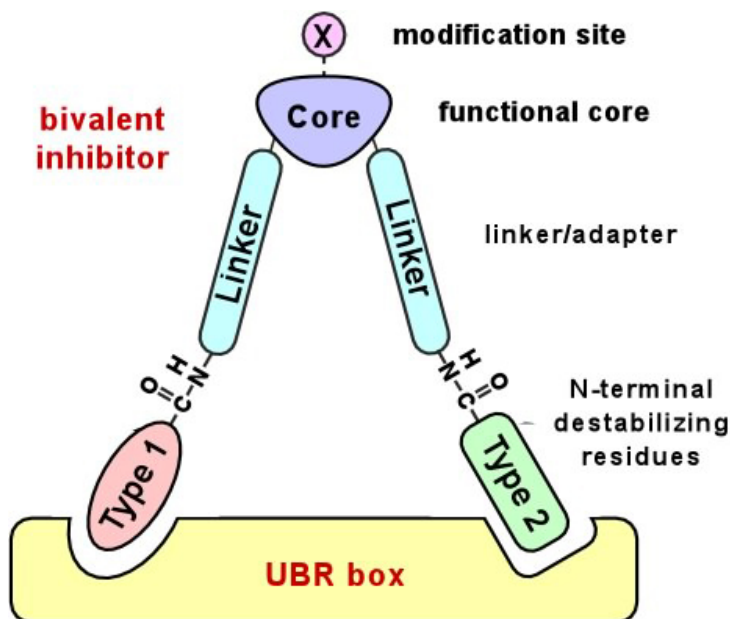
67

Figure 38. Structure of bivalent inhibitor. (A) Conceptual model for rationally designed bivalent inhibitors. It has mainly five building blocks; a core with multiple functional groups, two different "N-terminal" destabilizing residues, two appropriate linker/spacer. For the first generation of the bivalent inhibitor, RF-C11, Arg and Phe are "N-terminally" conjugated to a Lys core through C11 hydroxycarbon chains. Controls of RF-C11 differ only in the "N-terminal" residues. Biotinylated versions of the bivalent inhibitors were also synthesized and showed no loss of inhibitory activity.

protein interface, tethering weak monovalent inhibitors can be a good strategy to circumvent this problem. Moreover, unlike targeting cell surface receptors, cell-permeable multivalent inhibitors are not affected by the density of target proteins, do not causing receptor clustering, and are able to control signaling pathway within the cell. The N-end rule pathway is especially suited for this study because of the structural proximity between two substrate binding pockets in a single E3 Ub ligase enzyme, the independent binding properties of two binding modes, and a well-characterized binding mechanism that can be used to facilitate extender design (Varshavsky 1996; Kwon et al. 2001; Kwon et al. 2002; Kwon et al. 2003; An et al. 2006). Dipeptides bearing type 1 or type 2 N-degrons have been widely used in cell-free settings as competitive inhibitors of the N-end rule pathway. However, dipeptides are at best weak inhibitors *in vitro* and furthermore do not work in mammalian cells. Here the rational, mechanism-based design and *de novo* synthesis of a new class of N-end rule inhibitors are described (Fig. 38). The first generation of bivalent inhibitors, RF-C11, has two destabilizing N-terminal residues (e.g. Arg and Phe) connected through a Lys residue with hydrocarbon chain linker. The hypothesis is that the affinity between an inhibitor and a target protein can be enhanced by bivalent interaction (by

two ligands of a single inhibitor) compared to monovalent interaction (by two ligands in two independent inhibitors). RF-C11 showed inhibitory activity on the N-end rule pathway both *in vitro* and *in vivo*, much more effectively than dipeptide inhibitors, validating the concept of multivalent interaction. Moreover, the intraheterovalent inhibitor, RF-C11, cooperatively binds the UBR box motif and endogenous UBR proteins. I also demonstrated that RF-C11 can inhibit the degradation of RGS4, a physiological substrate of the N-end rule pathway (Hu et al. 2005; Lee et al. 2005), *in vivo* and exert anti-hypertrophic effects on primary cardiomyocytes, which mimics the effects of RGS4 overexpression (Zhang et al. 1998; Owen et al. 2001). Thus, these results contribute to designing small molecule inhibitors with multiple ligands in a single molecule and to understanding biochemical mechanisms and physiological functions of the N-end rule pathway.

4.3   METHODS

Synthesis of Inhibitors. The synthesis and characterization of RF-C11 is described in Appendix A and B. Controls of RF-C11 and biotinylated versions of bivalent inhibitors were synthesized using the similar scheme with modifications. Notably, the intermediate compounds of RF-C11 and controls were connected by conventional protocols of amide bond formation using EDC with high yield (See details in Appendix A and B). For biotin-labeled inhibitors, ethylenediamine-coupled biotin (**8**) was initially conjugated with N(ε)-Z-Lysine(-OMe)C11-NH$_2$ **6** prior to further reactions. The purity and identity of the intermediates and the final products were verified by TLC, analytical HPLC, ^{1}H NMR, and mass spectroscopy. Dipeptides, MG132, and bestatin were purchased (Sigma-Aldrich, St. Louis, MO).

In Vitro **Degradation and Ubiquitylation Assay.** Time- and concentration-dependent *in vitro* degradation and ubiquitylation assays were done as described in Chapter II (Levy et al. 1996; Lee et al. 2005) . Briefly, biotinylated lysine-tRNA complex (Transcend tRNA, Promega) was added into a reaction mixture for random labeling of expressed proteins and biotinylated proteins were detected against horseradish peroxidase (HRP)-conjugated streptavidin (Pierce). *In*

vitro ubiquitylation of RGS proteins was similarly determined except that the reaction was done in the presence of MG132, followed by anti-Ub immunoprecipitation / streptavidin immunoblotting. Anti-Ub antibody (Biomol International) recognizes both mono- and multi-ubiquitinated proteins but not free Ub. IC_{50} was regressed from sigmoidal dose-response model using GraphPad Prism 4.0 version 4.0 (GraphPad). IC_{50} was determined by using sigmoidal dose-response model based on the amounts of X-nsP4, relative to the amounts of DHFR-Ub at the same time points and normalized to the amount of the same substrate treated with RF-C11 for 60 min.

Direct Interaction Assay. For direct interaction assay, UBR1 fragment was synthesized by using the rapid-translation system (RTS) based on wheat germ lysate (Roche Applied Science) according to the manufacturer's instructions. The fragment was confirmed to be able to bind both type 1 and type 2 N-terminal destabilizing residues. RF-C11b or GV-C11b was incubated in Hisx6-UBR box-1 immobilized on Ni^{++}-coated microwells and its interaction was determined by streptavidin-infrared (IR) 800CW signal (LI-COR Biosciences). Reciprocal experiments were performed by adding Hisx6-UBR fragment-flag with immobilized biotinylated RF-C11 on streptavidin-coated microwells, followed by anti-Flag-IR incubation.

To confirm that endogenous UBR proteins bound to RF-C11, the biotin moiety of RF-C11b and GV-C11b was initially crosslinked to UltraLink Immobilized NeutrAvidin Protein Plus beads (Pierce). Rat testes were homogenized in buffer A (20 mM HEPES, pH 7.9, 75 mM KCl, 10 % Glycerol, 0.1 mM EDTA) containing protease inhibitors (Sigma) and diluted to 2 mg/ml in buffer B (20 mM HEPES, pH 7.9, 200 mM KCl, 10 % Glycerol, 0.05 % Tween-20), followed by incubation with RF-C11b or GV-C11b conjugated to beads. Precipitated proteins were resolved with 6% SDS/PAGE. Dipeptides (2 mM final concentration) were added to some reactions. Precipitated proteins were subjected to immunoblotting for UBR1 (Kwon et al. 2001) or UBR5 (Tasaki et al. 2005).

***In Vivo* Application and Primary Cardiomyocytes.** For *in vivo* degradation assay, two plasmids expressing RGS4 and the control β-galactosidase, respectively, were cotransfected into mouse embryonic fibroblasts. About 24 h after transfection, cells were treated for 3 h with RF-C11 or other compounds, followed by immunoblotting. For pulse chase analysis, mouse

embryonic fibroblasts were transiently transfected with pcDNA3-RGS4 plasmid and pCMV-luciferase plasmid. After 24 hr post-transfection, mouse embryonic fibroblasts were labeled with [^{35}S]methionine/cysteine for 10 min, followed by chase for 0, 30 min, and 60 min in the presence of cycloheximide. Extracts were prepared and immunoprecipitated with anti-RGS4 and V5 (for luc) antibodies, and SDS-PAGE, autoradiography, and quantification were sequentially performed.

The primary cells from mouse embryonic heart were isolated as described with slight modification for obtaining more viable cells (Jung et al. 2005). Twenty-four hrs after plating, the medium was replaced by serum-free DMEM supplemented with 10 μg/mL insulin, 5.5 μg/mL transferrin, 5 μg/mL selenium, and 110 μg/mL pyruvate (Sigma-Aldrich) in the presence or absence of the bivalent inhibitors with 5-bromo-2-deoxyuridine (BrdU, Sigma-Aldrich). After fixation in 5% paraformaldehyde, cells were coimmunostained with rat anti-BrdU antibody (Serotec, Oxford, UK) and rabbit anti-troponin I antibody (Santa Cruz Biotechnology), followed by secondary antibody incubation (anti rat-IgG-Alexa 555 and anti-rabbit IgG-FITC, respectively) and counterstaining with DAPI.

The effect of the bivalent inhibitors on MEC viability was determined by the MTT (3-(4,5-dimethylthiazolyl-2)-2,5-diphenyltetrazolium bromide; Promega) colorimetric dye reduction method. Cardiomyocyte size was determined by measuring the surface area of troponin I-positive cells in cultured primary cardiomyocyte. Planimetry was performed using ImageJ software version 1.34s (NIH) (Rasband 1997-2006) and outcome arbitrary unit was used. Although cell surface area does not constitute the accurate measurement of cell size, this parameter was generally used to estimate cardiomyocyte hypertrophy (Fredj et al. 2005). Immunohistochemical analysis was performed to detect hypertrophic marker, such as ANP with coimmunostaining for a cardiomyocyte marker protein, sarcomeric α-actinin.

4.4   RESULTS

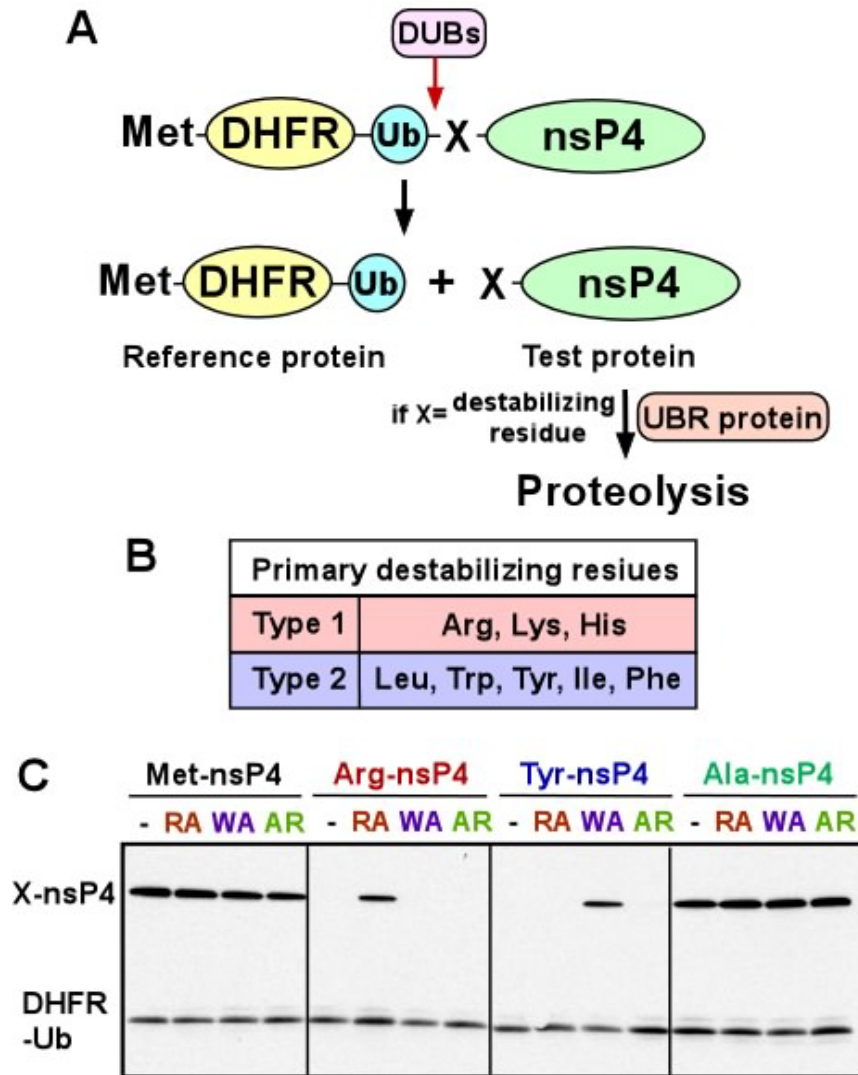### 4.4.1   *In vitro* Model System of the N-end Rule Pathway

Figure 39. *In vitro* model system for the N-end rule pathway. (A) Generation of the model substrates in reticulocytes using modified ubiquitin/protein/reference (UPR) technique (Bachmair et al. 1986). Abundant deubiquitylation enzymes (DUB) in the lysates cleave the amide bond of the last amino acid in ubiquitin almost at the co-translational stage, generating stable reference protein (DHFR-Ub) and test protein (X-nsP4). (B) Two types of the primary destabilizing N-terminal residues. UBR proteins are responsible for the recognition and ubiquitylation of the proteins bearing one of these amino acids, making them short-lived. (C) Type-specific inhibition of model substrate degradation by cognate dipeptides. Otherwise unstable Arg-nsP4 and Tyr-nsP4 were stabilized in the presence of 2 mM of Arg-Ala and Trp-Ala, respectively, while non-N-degron-bearing proteins, such as Met-nsP4 and Ala-nsP4 have long half-lives.

Small-molecule inhibitors of the N-end rule pathway were tested by using *in vitro* model substrates, which were generated through cleavage of a tripartitie fusion protein, $^{f}DHFR^{h}$-Ub^{R48} -X-nsP4^{f} fusions, in rabbit reticulocytes (Fig. 39A)(Levy et al. 1996). For a reference protein, DHFR-Ub fragment was stably detected. Half-lives of X-nsP4s were closely related with the identity of X, the N-terminal amino acid. Destabilizing N-terminal amino acids, or an N-degron,

which can be categorized into type 1 and type 2 (Fig. 39B), are recognized and ubiquitylated by a family of E3 Ub ligases named UBR protein (Tasaki et al. 2005). Therefore, the model substrates bearing type 1 and type 2 N-degron, such as Arg-nsP4 and Tyr-nsP4, respectively, were short-lived in normal condition, while proteins bearing non-N-degron, such as Met-nsP4 and Ala-nsP4, were robustly expressed as reference (Fig. 39C). Interaction between N-degrons and UBR proteins is stereo-selective, and single amino acids do not directly affect the degradation of N-end rule substrates although there is a possibility that they may influence non-canonical function of the proteins. Stereo-selectivity of UBR protein implies a contradictory, less important role of α-amine of N-degron at the recognition event and putative basic amino acid(s) near UBR box.

Cognate dipeptides function as competitive inhibitors of the N-end rule pathway. Type 1 dipeptides, such as Arg-Ala and Lys-Ala, inhibited type 1 model substrates degradation (Fig. 39C). Type 2 dipeptides, such as Trp-Ala and Phe-Ala, exerted inhibitory activity toward type 2 substrates, while control dipeptides did not affect substrate stability. Their significantly high specificity, for examples, 2 mM of Arg-Ala did not disturb degradation of type 2 substrates (Tyr-nsP4) and vice versa, suggested that UBR protein has two distinctive binding pockets consisted of UBR box motif and this architecture was taken advantage to explore the possibility of bivalency in the present study. Low efficiency of dipeptide inhibitors and their intrinsic limitation to *in vivo* application also made us develop distinguishable inhibitors despite the benefits from dipeptides (See Background). It was suggested that appropriate small molecules tethering type 1 and type 2 N-terminal destabilizing residues might increase their avidity for UBR box binding sites with higher selectivity. We tested this hypothesis using this model system. Of note, along with bivalent inhibitors, novel N-end rule inhibitors, including Tat-derived polyarginines, were also identified to be effective during an orthogonal study.

4.4.2   Design and Synthesis of Bivalent Inhibitors

The conceptual model of the bivalent inhibitor for the N-end rule pathway exploits two different "N-terminal" destabilizing residues (type 1 and type 2) which are connected to a core molecule with multiple functional groups through appropriate linker/spacer (Fig. 38). Non-functional modification(s) can be introduced at the core molecule depending on the purpose. Linkages

73
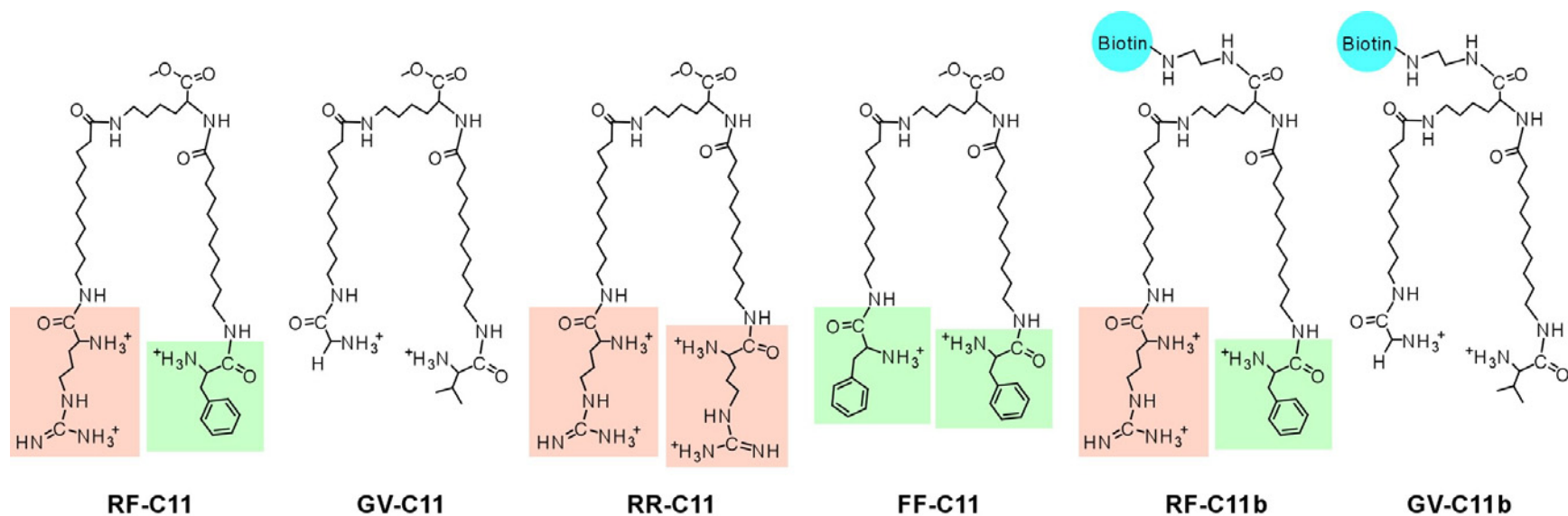
Figure 40. Chemical structures of RF-C11 and related compounds. N-terminal Arg and Phe are indicated by orange and green backgrounds, respectively. Core Lys moiety and biotin modification are indicated by blue and red background, respectively. C11 hydrocarbon chain was used as linker/adapter. Initially carboxylic group of core Lys was esterified to curb further reaction and later biotin moiety was conjugated (RF-C11b and GV-C11b) for direct binding assay. All the building blocks were connected through amide bonds.

Figure 41. Docking Model of the bivalent inhibitor into UBR box-like Protein. (A) Juxtaposition of ground-state RF-C11 and UBR box-like domain, both have a similar size of about 45 angstrom. (B) Putative binding model of RF-C11 into UBR box. Hydrophobic domains inside pocket interact with Type 2 N-terminal destabilizing residue, Phe.

interconnecting the building blocks can be also variable except two parallel amide bonds between N-degrons and linkers.
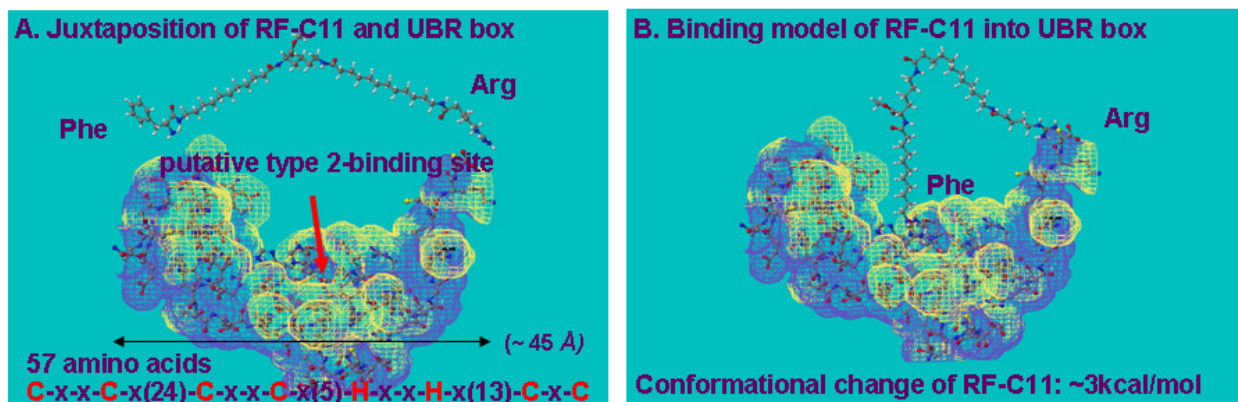
The prototype of the bivalent inhibitor, RF-C11, is based on a Lys platform whose trifunctional groups can afford broad applications (Fig. 40). The detailed synthesis of bivalent inhibitors is described in Organic Synthesis. Two linkers, C11 hydrocarbon chains attached to a carboxyl end of two "N-terminal" amino acids, Arg (type 1 N-degron) and Phe (type 2 N-degron), were connected through ε-amine and α-amine of the core Lys, respectively. All the scaffolds were connected via amine linkages for more stability and readiness of synthesis. Lipid-like structure using hydrophobic linker having the high degree of flexibility was inspired by the cell-permeable characteristics of transfection reagents for *in vivo* and animal model applications (Findeis 2001). Other linkers, such as polyethyleneglycol and polylysine, are being tested for more favorable pharmacological features. The chain length was determined by the structure of a UBR box homologue, mouse zinc finger protein 665 (Segal et al. 2006), whose size corresponded to the distance between the phenyl group and the guanidium group of RF-C11 (~45Å) at the ground state. Crystal structure of the active site indicates relatively spacious binding pocket and conserved hydrophobic residues, including Phe, Leu/Ile, and Tyr, in the inner part of the pocket, which can contribute to both hydrophobic and π–π interactions with type 2 N-degrons (Fig. 41).

Controls of RF-C11 differ only in the "N-terminal" residues. Substitution of Arg and Phe, which are destabilizing amino acids or N-degron, into non-N-degron, Gly and Val, respectively,

75

generated GV-C11, a structural negative control, whose synthesis scheme was comparable of that of RF-C11. RR-C11 (two "N-terminal" arginines) and FF-C11 were synthesized as monovalent controls of bivalent RF-C11. The reactive, free carboxylic acid end of the Lys moiety is esterified to curb any further reaction. Biotinylated versions of bivalent inhibitors including RF-C11b and GV-C11b were used for further characterization including interaction assay, pull-down assay, and localization assay. RF-C11 is highly water-soluble and assumed to have emulsion property in aqueous solution. The compounds were characterized by ^{1}H NMR, HPLC, and mass spectral data. Z-potential analysis revealed neutral, heterogeneous particle of the final chemicals in aqueous solution. Optimization of the synthesis methods provided good total yield at near 2.5 %.

4.4.3　*In vitro* Activity of the Bivalent Inhibitors

First, RF-C11 was rigorously evaluated as *in vitro* inhibitors of type 1 and type 2 N-end rule pathways by the *in vitro* model substrates; Arg-nsP4 for type 1 and Trp-nsP4 for type 2 both which are short-lived in reticulocyte lysates and their degradation was perturbed by MG132, a proteasome inhibitor (Fig. 42). With concentration- and time-course experiments, the activities of RF-C11 with the structural control, GV-C11, dipeptides, Arg-Ala and/or Trp (Phe)-Ala, and monovalent controls, RR-C11 and/or FF-C11, were compared. In type 1 model substrate, RF-C11 inhibited its degradation at the concentration of 10 μM at 40 min, while type 1 dipeptide inhibitor, Arg-Ala showed a similar effect at 250 μM concentration. Inhibitors such as Trp-Ala and FF-C11, which have type 2 destabilizing residue(s), had no effect on Arg-nsP4 degradation. Notably, RR-C11 showed intermediate effectiveness of RF-C11 and Arg-Ala dipeptides. The superior potency of RF-C11 compared with RR-C11 substantiated the concept of bivalent effects. Inhibitory activities of a mixture of two dipeptides (Arg-Ala plus Phe-Ala) or monovalent controls (RR-C11 plus FF-C11) were comparable to that of single dipeptides (Arg-Ala) or RR-C11 alone, respectively, suggesting no significant allosteric inhibition and further supporting cooperative effect of bivalent inhibitors. In type 2 model substrates, RF-C11 consistently showed higher efficiency than controls. Other N-end rule substrates, including the C-terminal fragment of cleaved CDC6 was tested and found that RF-C11, not GV-C11, inhibited

76

Figure 42. *In vitro* inhibition of Arg-nsP4 degradation by the bivalent inhibitors. Type 1 substrate Arg-nsP4 degradation in the presence of different inhibitors. The model substrates were expressed in reticulocytes in the presence of different inhibitors or controls, and their degradations were analyzed in time- and concentration-dependent manner using Western blotting. GV-C11 is a structural control of RF-C11, and RR-C11 and FF-C11 are heterovalent controls of the bivalent RF-C11.
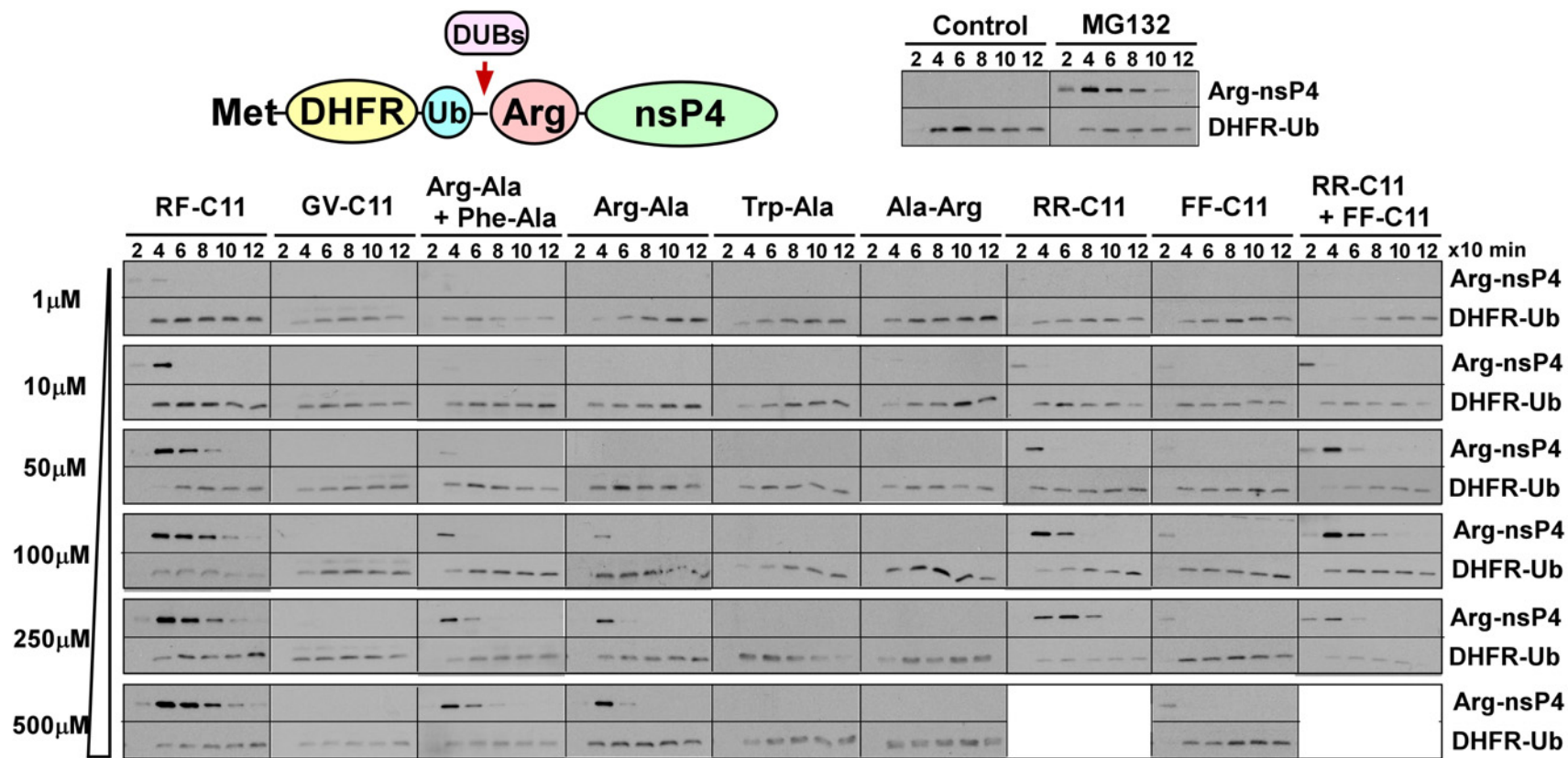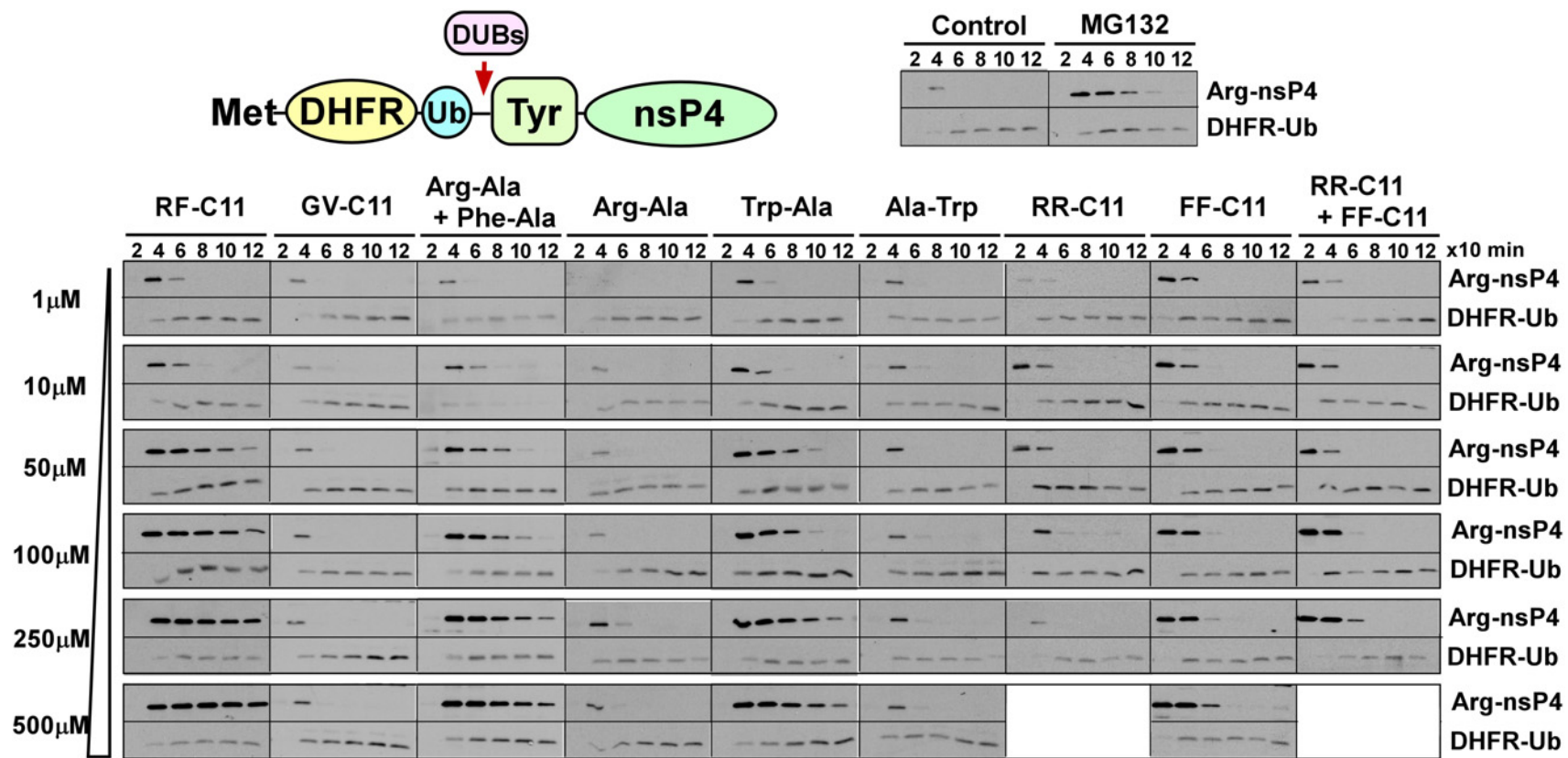
Figure 43. *In vitro* inhibition of Tyr-nsP4 degradation by the bivalent inhibitors. Type 2 substrate Tyr-nsP4 degradation in the presence of different inhibitors using similar methods in Fig. 42.
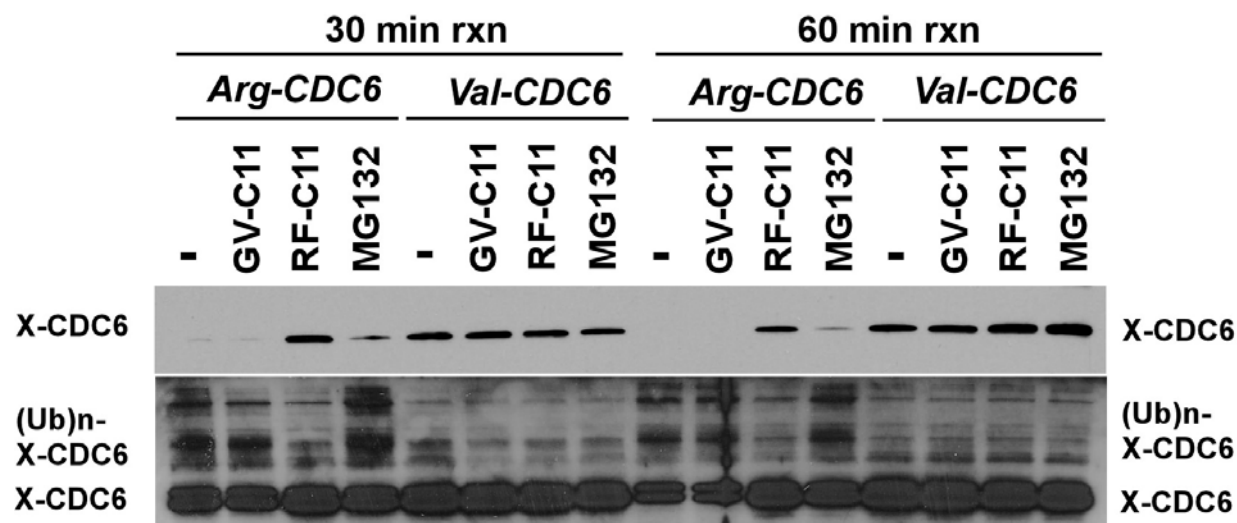
Figure 44. *In vitro* inhibition of Arg-CDC6 degradation by the bivalent inhibitors. A possible physiological substrate of the N-end rule pathway, CDC6 C-terminal fragments, Arg-CDC6 and Val-CDC6 (stabilized control) were expressed in reticulocytes in the presence of different inhibitors. Their degradations were analyzed in time- and concentration-dependent manner using Western blotting. GV-C11 is a structural control of RF-C11. While, Val-CDC6 is long-lived, Arg-nsP4 has short-half life, and RF-C11 stabilized the otherwise unstable Arg-CDC6 more than MG132.

its ubiqutylation efficiently. Together, these results suggested that RF-C11 is the first N-end rule inhibitor which can block both type 1 and type 2 pathways with higher efficiency compared with traditional dipeptide inhibitors. Moreover, the higher efficiency of the RF-C11 over homovalent controls highlights the advantages of bivalent interaction.

Single amino acids, such as Arg and Phe, did not affect the efficiency of RF-C11. GV-C11, a simple substitution of the N-degron from RF-C11, had no inhibitory effect on both type 1 and type 2 N-end rule substrates up to 2 mM concentration, supporting negligible non-specific effect. However, given the fact that small molecule inhibitors often target multiple intracellular enzymes(Huskens 2006), the effect of RF-C11 on stabilization of other ubiquitin substrates which are not mediated by the N-end rule pathway, such as full-length CDC6 (APC complex substrates) and p53 (Mdm2 substrates) were also examined. I found that there is no effect of RF-C11 on other substrtes of the ubiquitin pathway or the proteasome (Fig. 46). Interestingly, C-terminal fragment of CDC6 generated by caspase was stabilized by RF-C11, suggesting that novel N-end rule pathway substrates can be identified by screening of RF-C11. Kinetics of type 2 model substrate expression and degradation are different from that of type 1 under the same condition. This observation can be explained by that rates of translation or deubiquitylation, which happens cotranslationally (Baker et al. 1992; Papa and Hochstrasser 1993), may be slower
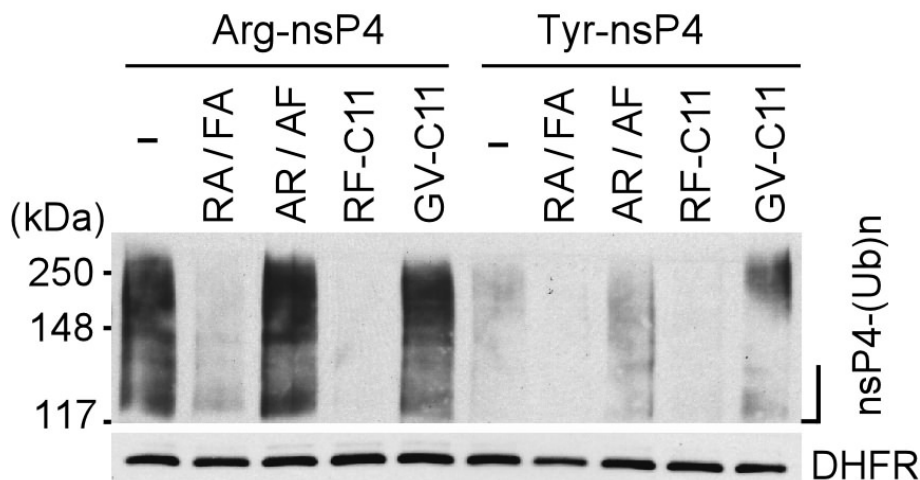
Figure 45. *In vitro* ubiquitylation of model substrates in RF-C11. Effect of RF-C11 on model substrate ubiquitylation. X-nsP4 proteins were expressed in reticulocyte lysates in the presence of MG132 (5 µM) and other compounds (50 µM) as indicated. RA, Arg-Ala; FA, Phe-Ala; AR, Ala-Arg; AF, Ala-Phe. After 20 min, their ubiquitylation was analyzed using anti-Ub immunoprecipitation and subsequent anti-biotin Western blotting (top panel), while their expression levels were determined using immunoblotting for the DHFR-Ub reference (bottom panels).

in type 2 model substrates than in type 1. It was partially proved by the degree of ubiquitylation in Fig.44. Interestingly, the N-terminal methionine excision (NME), one N-degron generating mechanism, is also a cotranslational process (Meinnel et al. 2006). The most simple, intuitive possibility is that the intrinsic stabilities of Arg-Ala and Trp-Ala in the reticulocyte lysates might be different. It seems not to be the case because dipeptides are highly unstable in reticulocytes (Fig. 43). However, it is possible that the UBR box conformational/functional changes may be accompanied by different substrate binding.

4.4.4 *In vitro* Assays Using the Bivalent Inhibitors

The degree of the *in vitro* efficiency of N-end rule inhibition of RF-C11 versus dipeptides was semi-quantitatively assessed by measuring the percentage of the amount of the remaining model substrates compared to the DHFR-Ub reference (Fig. 45). RF-C11 inhibited the degradation of model substrates concentration-dependently with at least ten-fold increased half-maximal inhibitory concentration (IC_{50}) value compared to dipeptide inhibitors. On the type 1 model substrate, quantification of the *in vitro* activity of RF-C11 showed 15.5 µM of IC_{50} value while Arg-Ala and Lys-Ala dipeptides inhibitors showed 283 µM and 148 µM. Type 2 inhibitors also
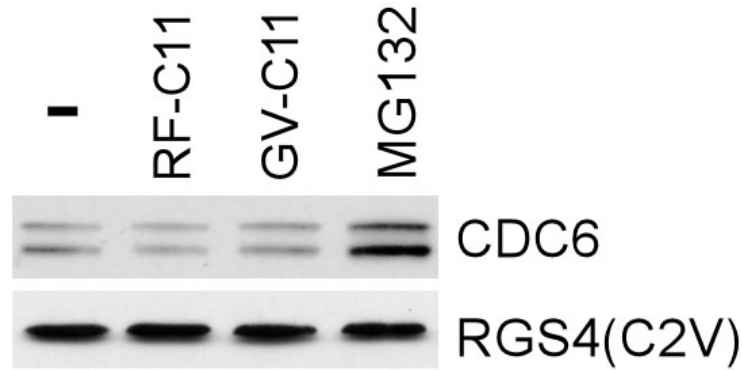
Figure 46. *In vitro* degradation of CDC6 in RF-C11. Effect of RF-C11 on non-N-end rule substrate CDC6. CDC6 is a substrate of APC complex and was stabilized by MG132 but not affected by RF-C11, suggesting RF-C11's specificity on the N-end rule pathway. y A long-lived RGS4(C2V)(Lee et al. 2005) mutant was used as a control.

exhibited dose-dependent effectiveness. RF-C11 (2.74 µM) were 10 to 30-fold more potent than type 2 dipeptides inhibitors such as Trp-Ala (21.39 µM) and Phe-Ala (72.37 µM). These observations were similar to those calculated from a simplified model for bivalent inhibition (Gargano et al. 2001). Based on the model, theoretically calculated binding enhancement of RF-C11 on a per ligand relative to the monomer should be approximately 100-fold, and these results exhibited that it was 10 to 30-fold ($\beta \geq 10$, Fig. 56). Moreover, from this study, although type 1 and type 2 interactions may be individual, dependent events, there is no significant affinity change ($\alpha \approx 1$) as expected in individual, independent binding events ($K_1 = K_1'$, $K_2 = K_2'$. Fig. 56).

Consistent with the effect of RF-C11 on substrate degradation, the N-end rule model substrates were rapidly ubiquitylated under normal conditions, but their ubiquitylation was inhibited by the Arg-Ala / Phe-Ala mixture or RF-C11 (Fig. 47). RF-C11 showed a higher degree of inhibition of ubiquitylation at the same concentration of dipeptides, suggesting direct and specific targeting of UBR proteins. Inhibition of proteolysis of the N-end rule substrates was diminished in time-dependent manner due to instability of the inhibitors, which can slowly be cleaved by endogenous endopeptidases, and decreased rates of *in vitro* translation kinetics (Fig. 47). However, RF-C11 showed more prolonged activity than dipeptides activity as either type 1 or type 2 substrates. The more effective and prolonged activity of RF-C11 might be partially contributed to its metabolic stability. In contrast to dipeptides which cannot exert their inhibitory activities in the absence of bestatin (Botbol and Scornik 1983), an endopeptidase inhibitor, RF-C11 exhibited similar efficiency regardless of the addition of bestatin, suggesting its invulnerability on endopeptidase cleavage (Fig. 47).

81
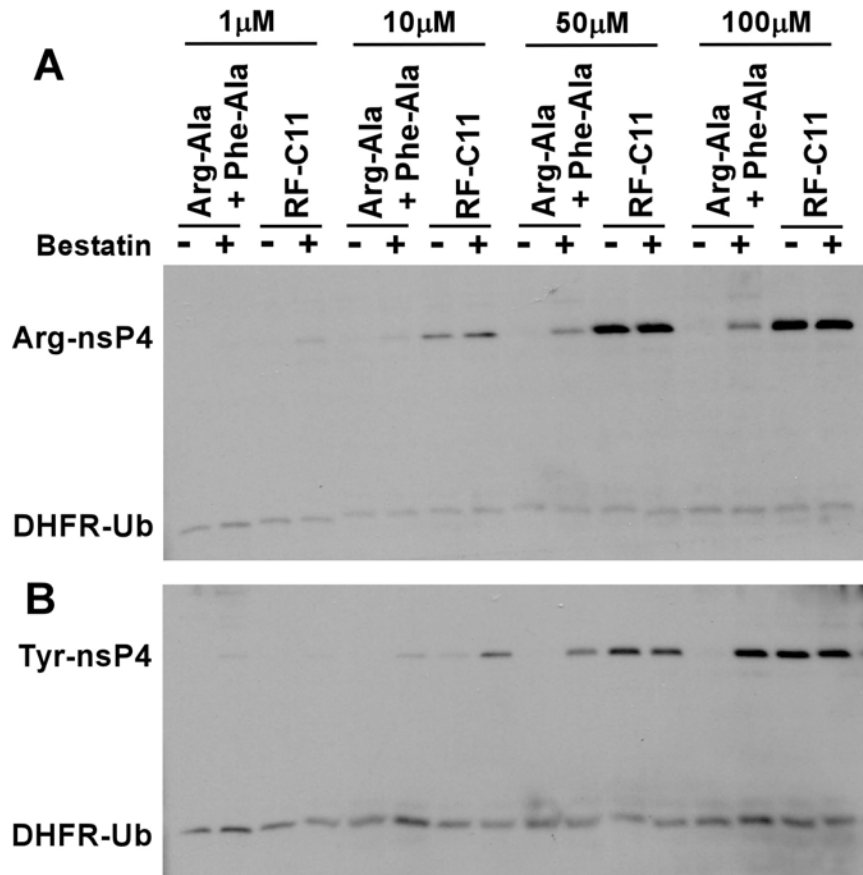
Figure 47. Metabolic stability of the inhibitors by endopeptidase. In contrast to RF-C11, dipeptides showed no effect without bestatin.

4.4.5 Direct Interaction between RF-C11 and UBR proteins

Although RF-C11 inhibited the N-end rule pathway and did not affect the proteolysis of non-N-end rule pathway substrates and proteasome activity, there is no conclusive evidence that RF-C11 directly binds to the UBR proteins. This question was addressed by employing biotinylated derivatives of bivalent inhibitors for newly developed ELISA-like binding assay and pull-down assay. As reasonably expected, biotinylated RF-C11 achieved a similar efficacy as RF-C11, while biotinylated GV-C11 exerted no effect (Fig. 49A). For the binding assay, target protein, UBR1(1-453), which contains the initial 453 amino acids of UBR1 protein. It is the smallest fragment of UBR box motif and was proved to be sufficient to bind to both type 1 and type 2 N-degron (Takafumi Tasaki, Kwon Lab). His_6-UBR1(1-453)-Flag with Hisx6 and/or flag epitopes was *in vitro* generated by Rapid Translation System using wheat germ lysates (Fig. 49B) and

Figure 48. Comparison between inhibitory effects of RF-C11 and controls. Comparison inhibitory effects of RF-C11, RR-C11, and dipeptides (Arg-Ala and Lys-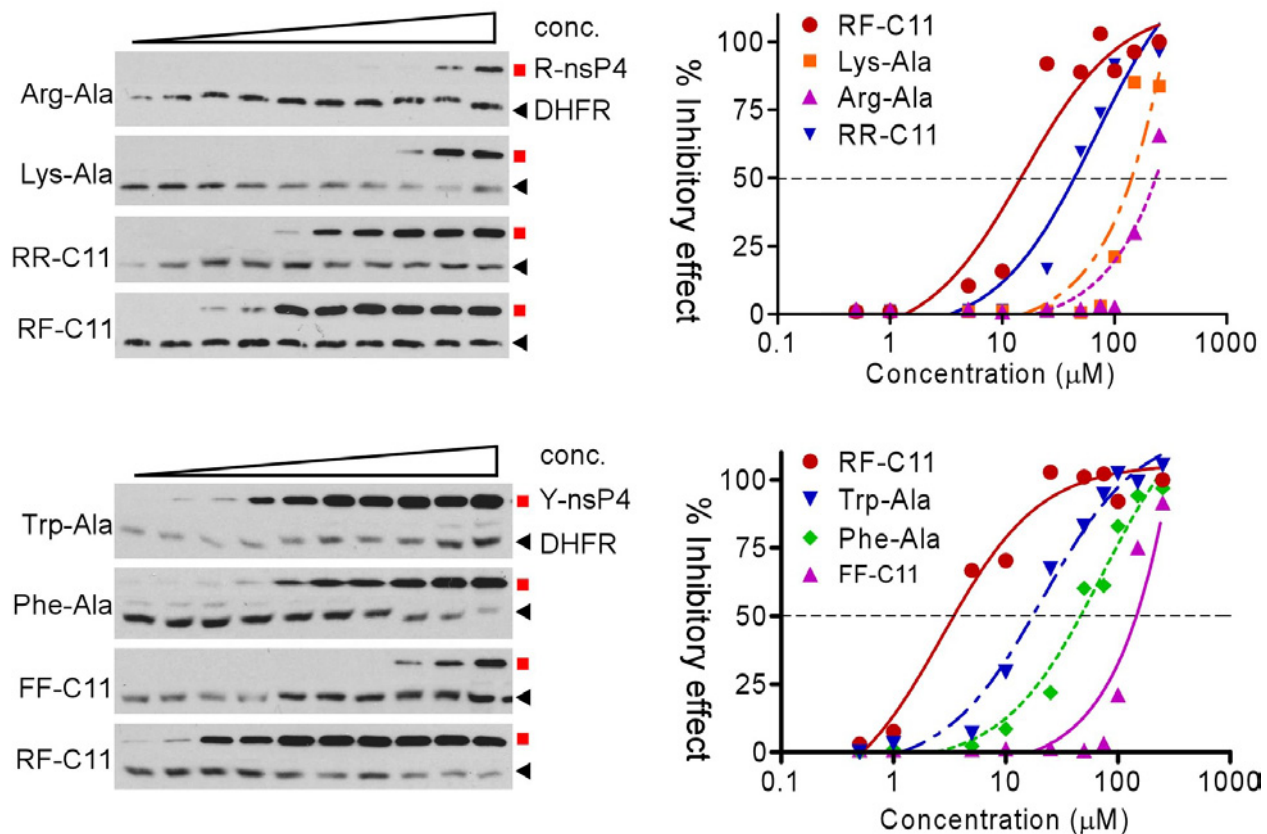Ala) on type 1 (upper panel) and type 2 (lower panel) degradation. Degradation of X-nsP4 was monitored in reticulocyte lysates in the presence of increasing concentrations (0.5, 1, 5, 10, 25, 50, 75, 100, 150, and 250 μM). IC_{50} values were obtained from quantification of relative X-nsP4 intensity and sigmoidal dose-response model.

initially evaluated for optimal immobilization onto Ni^{++}-coated microwell plates (Fig. 49C). Under optimized conditions, direct binding of RF-C11b with immobilized UBR box-1 fragment was observed in concentration-dependent manner (Fig. 50A). GV-C11b showed no detectable binding to UBR box-1. The bound RF-C11 and UBR box-1 was not dissociated by adding up to 500 μM dipeptides. A reciprocal experiment using immobilized biotinylated bivalent inhibitors on streptavidin-coated microwell was also performed and showed specific interaction only between RF-C11 and UBR box (Fig. 50B). A negative control matrix and GV-C11 were used as controls. To determine whether RF-C11 could bind to endogenous UBR box proteins, from pull-down assay using rat testis extracts, streptavidin-immobilized RF-C11b was bound to UBR1 and UBR5 identified by Western blotting with individual antibodies, while no UBR protein was detected binding to GV-C11b (Fig. 50C). In the presence of dipeptide inhibitors, the binding of UBR1 was reduced by Arg-Ala and/or Trp-Ala, but Ala-Arg was not displaced from the RF-

83
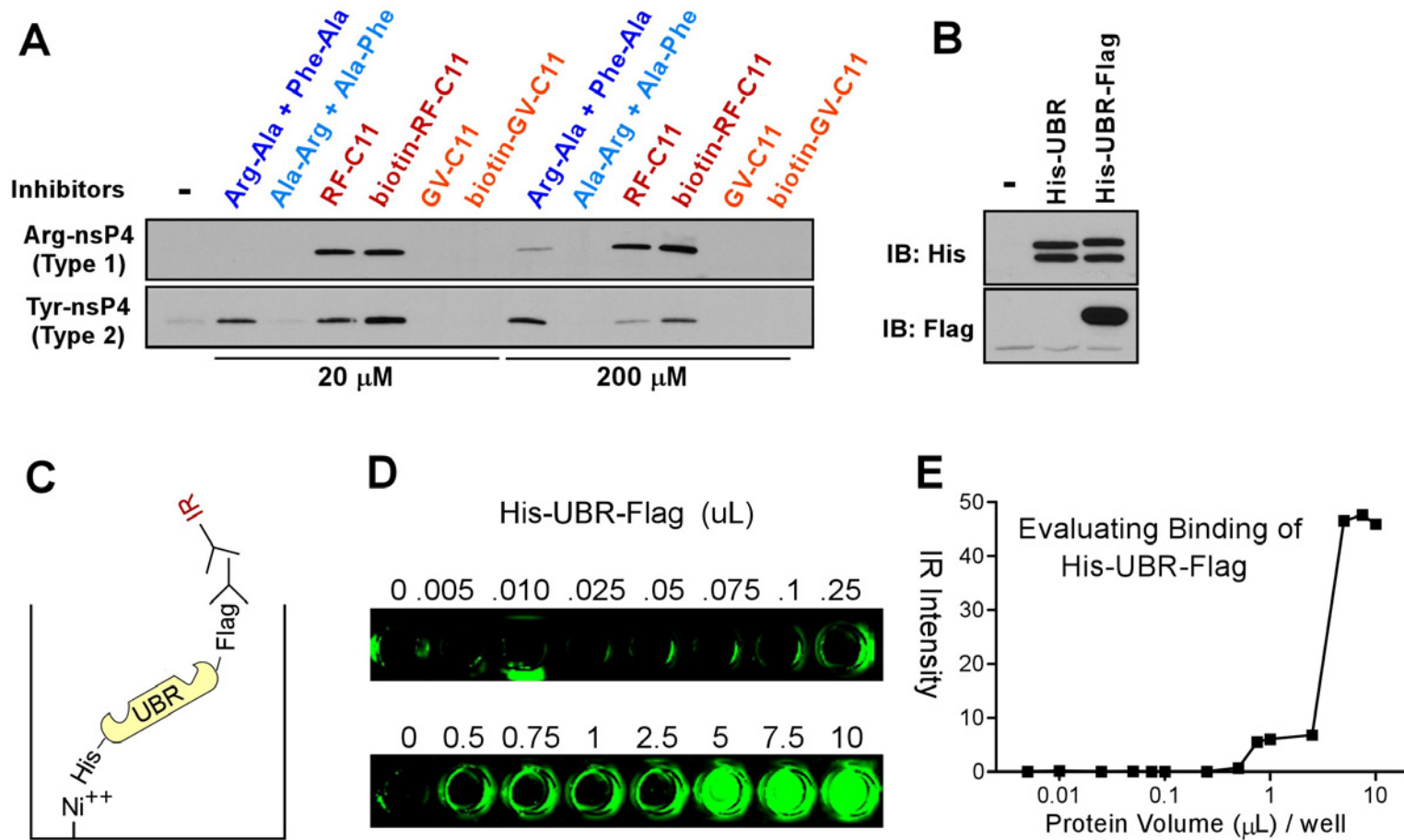
Figure 49. RF-C11b and ELISA-like direct binding assay. (A) Examining *in vitro* inhibitory activity of biotinylated inhibitors. (B) Expression and epitope detection of UBR box proteins. (C) Diagram of ELSA-like binding assay between UBR box and bivalent inhibitors. Preliminary results suggested protein amount for future experiment.
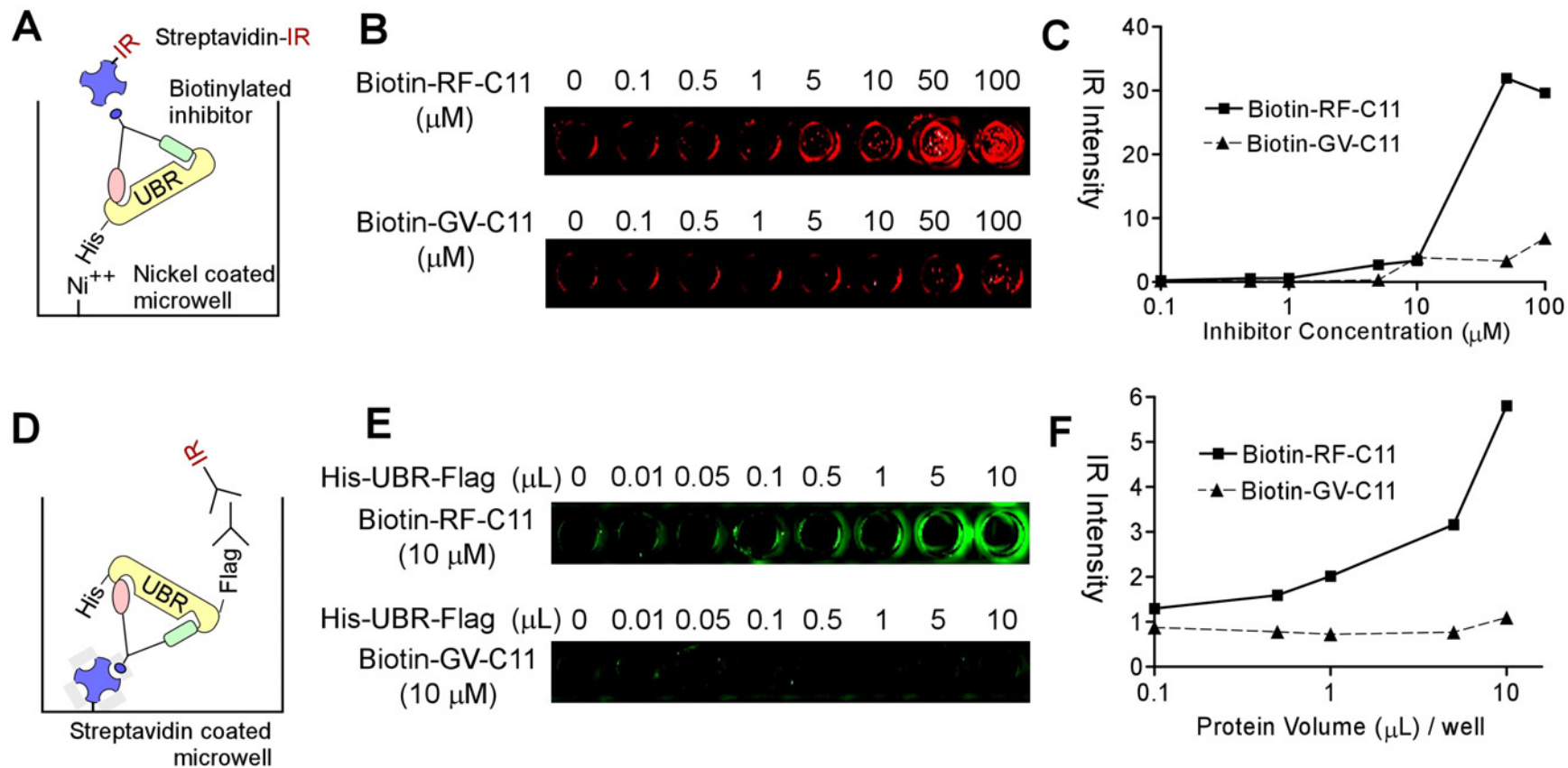
Figure 50. Direct binding assay between bivalent inhibitor and UBR fragment. (A-C) Binding assay using UBR protein immobilized on Nickel coated microwell. Diagram (A), IR detection (B) and its quantification (C). (D-F) Reverse binding assay using immobilized bivalent inhibitors using streptavidin-coated microwell.
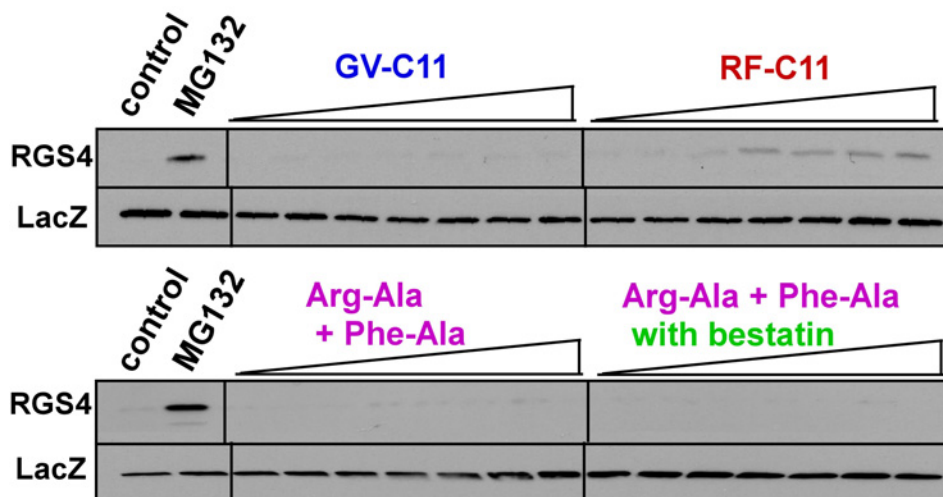
Figure 51. Perturbed RGS4 proteolysis by RF-C11 in mouse embryonic fibroblasts. The levels of overexpressed RGS4 in mouse embryonic fibroblasts in the presence of different inhibitors were determined by immunoblotting. RGS4 and lacZ were transiently expressed in embryonic fibroblasts, and RF-C11 and GV-C11 (0.1, 10, 50, 75, and 100 μM) were treated for 3 h, followed by anti-RGS4 immunoblotting.

C11/UBR protein complex in accordance with the N-degron type-dependent competition and higher affinity of RF-C11. In addition, Trp-Ala did not interfere with the ability of UBR5 binding, indicating that UBR5 is indeed type 1-specific UBR protein (Tasaki et al. 2005). These data strongly suggest that RF-C11 targets UBR proteins (more precisely UBR box) and this is the first identification that endogenous UBR box proteins can be pull-downed by small molecules. It is not clear whether RF-C11 acts as an irreversible inhibitor of UBR protein, but it is predicted to form a 1:1 stoichiometric complex with the UBR box under steady-state conditions with a slow dissociation rate. The availability of highly specific and efficient N-end rule inhibitors will allow us to identify unknown cognate proteins of UBR proteins. Notably, RF-C11 is not a peptide although its major components are amino acids and amide bonds. These data suggest that the identity of the N-degron might not be limited to proteins and that the UBR box is equipped to interact with other biological small molecules. It is possible that N-ligand, such as neurotransmitters and hormones derived from destabilizing amino acids, may regulate non-proteolytic function of the N-end rule pathway.

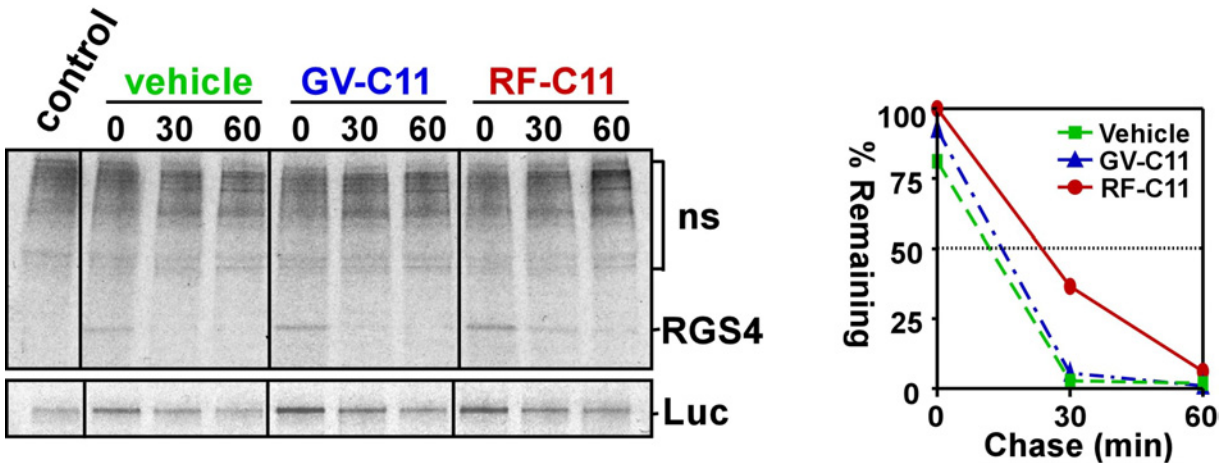### 4.4.6 *In vivo* Application of the Bivalent Inhibitors

Figure 52. Increased half-life of overexpressed RGS4 by RF-C11 in mouse embryonic fibroblasts. Pulse chase analysis of RGS4 and luciferase for control. The transfected cells were labeled for 12 min with ^{35}S-Met/Cys, followed by anti-RGS4 and anti-V5 (for luc) and SDS-PAGE analysis. Quantitation of data using PhosphorImager shown in the right panel. As expected from relatively mild stabilization by RF-C11 *in vivo* (Fig. 51), the half-life of newly synthesized RGS4 in the presence of RF-C11 increased modestly.

Having shown that RF-C11 worked *in vitro* both on type 1 and type 2 and it directly binds to UBR proteins, *in vivo* application of the inhibitor was performed using RGS4 as a substrate in cultured mouse embryonic fibroblasts. RGS4 protein is a negative regulators of Gi- and Gq-mediated signaling pathway by accelerating the rate of Gα-GTP hydrolysis, resulting reassociation of the Gαβγ heterotrimer (Ross and Wilkie 2000; Hollinger and Hepler 2002), and was the first identified *in vivo* N-end rule substrates (Hu et al. 2005; Lee et al. 2005). In physiological condition, overexpressed RGS4 protein was short-lived but its degradation was robustly blocked by MG132 in mouse embryonic fibroblasts (Fig. 51). RF-C11 treatment showed modest but significant stabilization of RGS4 compared with MG132 at the concentration of 25 μM while dipeptides or GV-C11 showed no effect. Pulse-chase analysis was performed to compare half-lives of RGS4 in the presence and absence of RF-C11 and indicated that RF-C11 increased RGS4 stability with modest degree (Fig. 52). Since the internalized RF-C11 was not clearly localized and *in vivo* inhibition effect was observed only in serum-free culture media, it was reasonable to suspect that poor cell permeability of the compound might be the major hurdle for better *in vivo* inhibitor development. Although the intraheterobivalency concept in this work was initially developed as a proof of concept, practical applications may be achievable.

The RGS protein and G protein signaling pathway have been known to have important roles in the cardiac development and in the cardiac function under normal and pathological
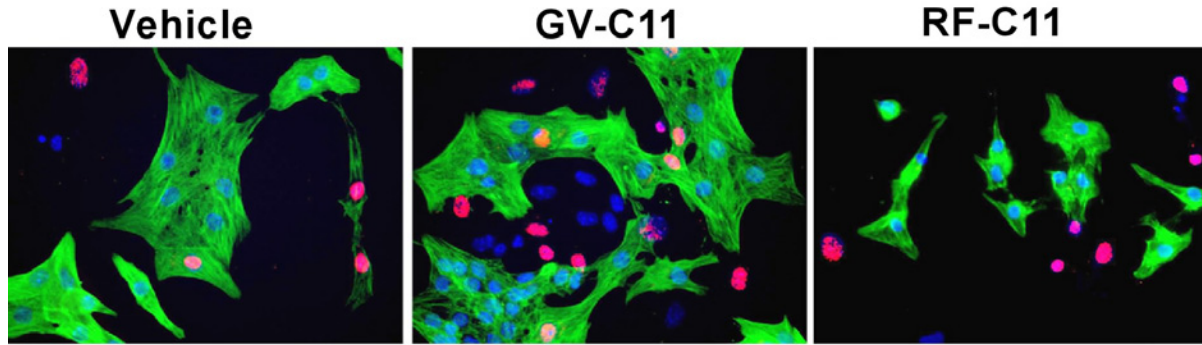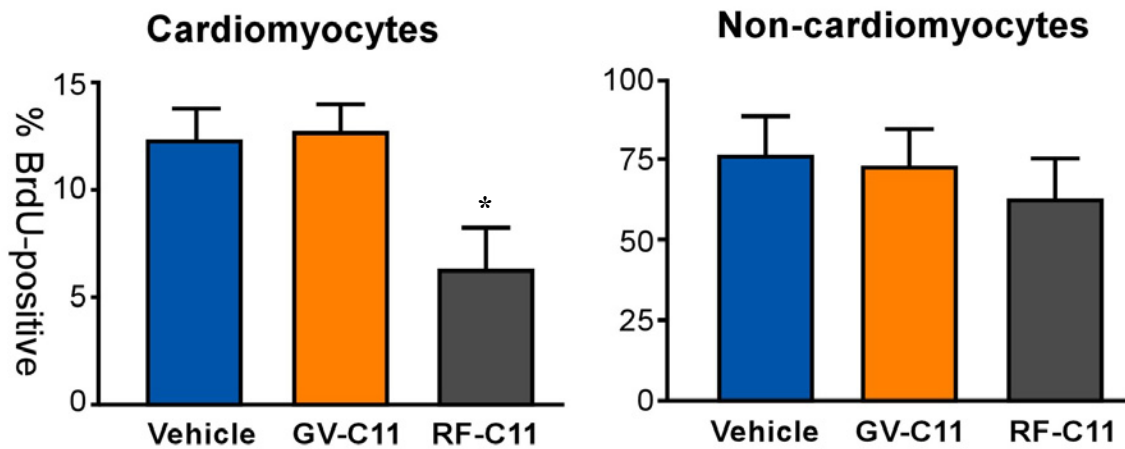
Figure 53. Reduced DNA synthesis of cardiomyocytes with RF-C11 treatment. Cells isolated from mouse embryonic hearts were treated with BrdU for 12 h in the presence of 25 μM RF-C11 or GV-C11, followed by immunostaining troponin I (for cardiomyocytes, green) and BrdU (for S-phase cells, red). BrdU indices were determined by counting BrdU-positive cells for cardiomyocytes (troponin I-positive) and non-cardiomyocytes (troponin I-negative). Data represent mean ± s.e.m. from three independent experiments (*: $p < 0.05$).

condition (Sierra et al. 2000; Riddle et al. 2005). Previously, I reported that the mice deficient ATE1, a component of the N-end rule pathway which regulates RGS proteolysis die in midgestation mainly due to a proliferative deficiency, i.e. decreased DNA synthesis associated with perturbed mitotic activities of cardiomyocytes (see Chapter III). Therefore, initially, The examination of RF-C11's effect on proliferation of primary mouse embryonic cardiomyocytes (MEC) showed that RF-C11 induced not only decreased proliferation of cardiomyocytes, with no effect on non-cardiomyocytes (Fig. 52), but also reduced cardiomyocyte size (Fig. 53). The cytotoxicity of inhibitors was predetermined on both mouse embryonic fibroblasts and embryonic cardiomyocytes (Fig. 54). To further examine RF-C11 regulation of hypertrophism, immunostaining was conducted to detect the production of atrial natriuretic peptide (ANP), a
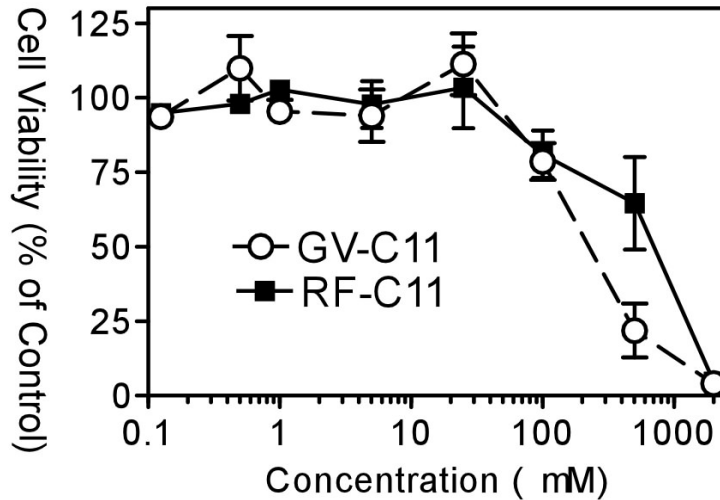
Figure 54. Cytotoxicity of RF-C11. The cytotoxicity of RF-C11 and GV-C11 on mouse embryonic cardiac cells was determined by using MTT (3-(4,5-dimethylthiazolyl-2)-2,5-diphenyltetrazolium bromide) colorimetric dye. 25 μM of RF-C11, the experimental concentration for BrdU assay and hypertrophism, do not affect the viability of primarily cultured mouse embryonic cardiomyocytes

representative hallmark of hypertrophic genetic reprogramming in cardiomyocytes and a prognostic indicator of clinical severity of hypertrophy (Liu and Olson 2002). Notably, decreased peri-nucleic ANP signal was observed in RF-C11 treated cardiomyocytes (Fig. 53). Primary embryonic mouse cardiomyocytes have been known to undergo "autonomous hypertrophy" (Deng et al. 2000) and many *in vivo* studies using rat cardiomyocytes indicate that stimulation of Gq-coupled receptors is sufficient to induce cardiomyocyte hypertrophy (D'Angelo et al. 1997; Adams et al. 1998; Mende et al. 1998; Mittmann et al. 2002).

Transgenic mice overexpressing RGS4 in postnatal ventricular myocardium displayed, upon transverse aortic constriction, left ventricular dilatation, depressed systolic function, and higher postoperative mortality, and failed to induce βMHC expression (Rogers et al. 1999). Therefore, the RF-C11 effect, as a potent inhibitor of the N-end rule pathway, mimics the effect of Gq inhibition or RGS hyperactivation, which is consistent with the study from *ATE1*^{-/-} mouse (Lee et al. 2005). The biological activities of RF-C11 also underscore the fact that cardiomyocyte proliferation and differentiation are complex and coordinated. Together, these observations suggested that RF-C11 inhibits the onset of autonomous hypertrophy in mouse embryonic cardiomyocytes and its mechanism of action, suspected to be related with RGS proteins, may bring new insight of the N-end rule pathway on regulation of G protein signaling for physiological cardiogenesis and pathophysiological hypertrophism. In analogous experiments

GV-C11   **RF-C11**

α-actinin / ANP / DAPI
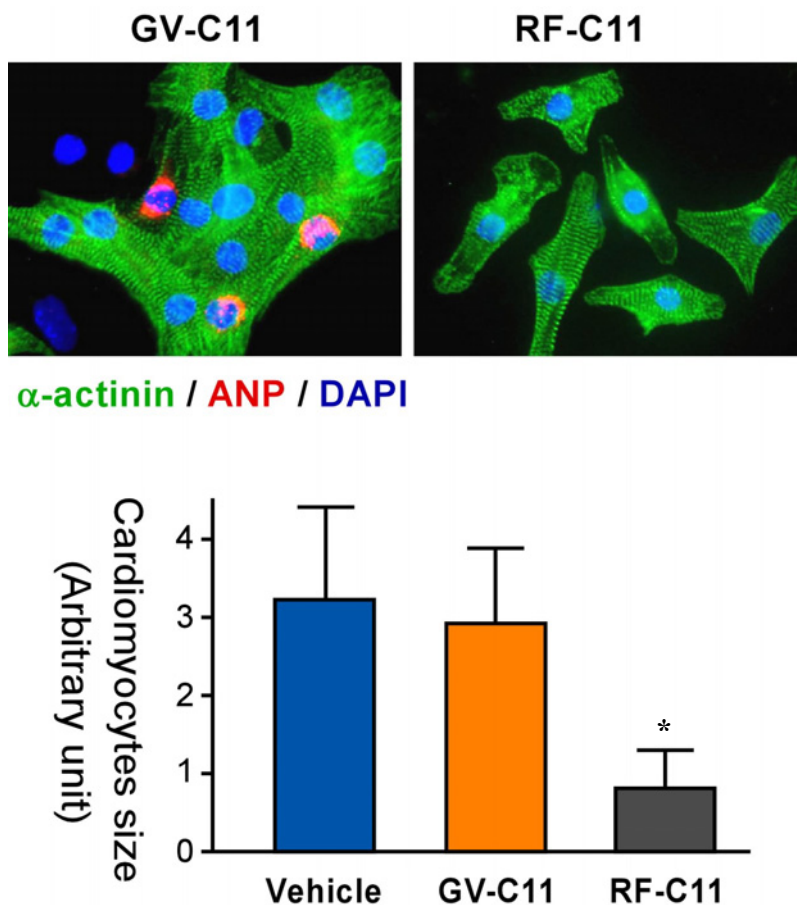
Figure 55. Inhibited hypertrophism by RF-C11. Significantly reduced cell size in RF-C11-treated cardiomyocytes were observed and quantified in the left graph. The surface areas of troponin I-positive cells were determined using ImageJ software version 1.34s (NIH). Data represent mean ± s.e.m. from three independent experiments. Cardiac cells, treated with RF-C11 or GV-C11, were immunostained for sarcomeric α-actinin (for cardiomyocytes, green) and ANP (for hypertrophism, red) with DAPI counterstaining. Data represent mean ± s.e.m. from three independent experiments (See Methods). *: $p < 0.05$.

with rat neonatal cardiac cells, RF-C11 treatment significantly reduced the size of rat cardiomyocytes and the level of ANP expression (data not shown). These results suggest that the N-end rule pathway controls cardiac proliferation and hypertrophy.

4.5   DISCUSSION

Ligand-induced dimerization (or proximity) is one of the key regulatory mechanisms in signal transduction and pioneering organic chemists recognized the potential of synthetic small molecules which can hetero- or homodimerize intracellular proteins and control their cellular

responses for experimental and therapeutic purposes (Austin et al. 1994; Crabtree and Schreiber 1996). Perhaps the most widely used chemical inducer of dimerization (CID) has been rapamycin. The interest in the immunosuppressant has exploded since it were identified that rapamycin is a heterovalent bivalent ligand, which can bind FKBP12 (FK506 binding protein)(Harding et al. 1989; Siekierka et al. 1989) and FRB (FKBP-rapamycin binding domain) (Brown et al. 1994; Sabatini et al. 1994) to form FKBP-rapamycine-FRB ternary complex. This system has been studied not only for its role in the mTOR pathway and cell growth, but also for applications in technology, including conditional protein splicing (for gain-of-function) (Schwartz et al. 2007) and conditional protein degradation (for loss-of-function) (Sakamoto et al. 2001). While CIDs simultaneously bind to two different proteins (interbivalent), intrabivalent bivalirudin, a synthetic, 20-mer oligopeptide anticoagulant, binds to active site and fibrinogen-binding region of a single molecule of thrombin (Warkentin and Koster 2005). A few small molecule-based intrabivalent inhibitors have been synthesized or screened but tested only in a limited set of biochemical analyses (Shuker et al. 1996; Maly et al. 2000; Tsang et al. 2001).

The aim of the this study was to develop small molecule, lipid-based, bivalent inhibitors for the N-end rule pathway through binding to two distinct protein-N-terminal recognition pockets of the UBR system. Existing inhibitors that bind to UBR1 recognition pockets are dipeptides containing either basic (type I inhibitors) or hydrophobic (type II inhibitors) amino acids in the N-terminus. However, structurally they lack the possibility of containing both basic and hydrophobic amino acids simultaneously in the two N-termini because the natural peptides contain only one N-terminus. Synthetic organic molecules have the flexibility of comprising both the N-terminal mimicking sites so they can bind to both the hydrophilic and hydrophobic pockets of UBR1. Therefore, a bivalent inhibitor possessing both type I and II residues will bind UBR1 more effectively and hence be expected to inhibit UBR more efficiently than monovalent inhibitors due to simultaneous and co-operative binding with two binding pockets. The molecule is expected to possess several advantages over existing peptide based inhibitors: 1) *stability*, because there exist no peptide bond that might otherwise be degraded in the presence of peptidases; 2) *bio-admissibility*, owing to its flexibility offered by its lipid-based structure. The lipidic structure offers excellent bio-distribution *in vivo* and effective fusion with the cell membrane, predominantly constituting of lipid-based molecules.

In the bivalent inhibitor molecule RF-C11, the ε-amino group and α-amino group of L-
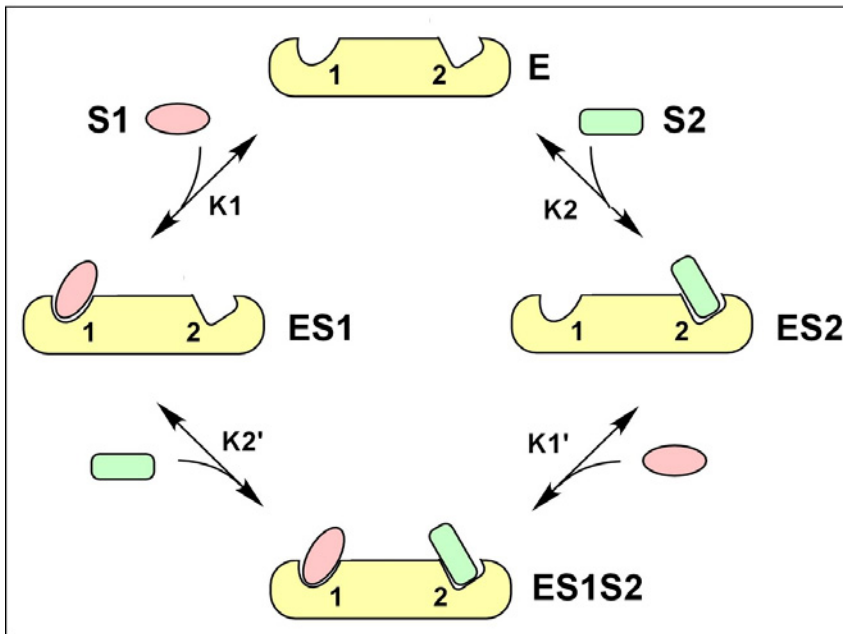
Lys moiety were respectively linked to C-terminal of L- arginine (R) and L- phenylalanine (F) with the help of respective C11 carbon chain linkers. The carboxylic acid group of Lys moiety remained protected as methyl ester to stop any furthering of chemical reactions through this moiety. The overall yield of RFC11 was about 2.8 %. Although the chain length of C11 was chosen arbitrarily, later the chain length was determined by the structure of a UBR box homologue, mouse zinc finger protein 665 (Segal et al. 2006), whose size corresponded to the distance between phenyl group and guanidium group of RF-C11 (~45Å) at the ground state. Crystal structure of the active site indicates relatively spacious binding pocket and conserved hydrophobic residues, including Phe, Leu/Ile, and Tyr, in the inner part of the pocket, which can contribute to both hydrophobic and π–π interactions with type 2 N-degrons.

In order to ascertain the selective inhibitory effect of RF-C11 towards UBR proteins, a negative control called GV-C11 that contains amino acids non-related to either type I or type II N-degrons was synthesized. In this molecule, Arg and Phe were replaced by Gly and Val, respectively. GV-C11 synthetic scheme was comparable of that of RF-C11. To determine the efficacy of bivalent inhibitors, with respect to homovalent inhibitors, two heterovalent inhibitors RR-C11 (containing two arginines) and FF-C11 (containing two phenylalanines), where both the amino acid residues would show binding to either of the type I or type II binding pockets, were also synthesized. A new molecule i.e., RF-C11b (or, RF-C11b) was also prepared by selectively introducing the biotin moiety in the carboxylic acid of the Lys skeleton in RF-C11 with an ethylenediamine linker in between. The molecule was synthesized for the purpose of pulling down both known and yet unknown UBR proteins and to identify unknown substrates (if any) that may interact with UBR proteins.

The progress of combinatorial chemistry and bioinformatics, along with software engineering and automation, allowed us to attempt high throughput and *in silico* screening for drug discovery. However, despite the power of these approaches, such efforts have not been entirely successful because of artifacts, off-target effects, and false positives (McGovern et al. 2002). Moreover, during the high throughput screening, most small interacting molecules, which have low affinity but have a higher chance of binding to the target, will not be detected as "hits" at a typical submicro-molar concentration (Jackson and Harrington 2005). An emerging paradigm in drug development is to develop more sensitive methodologies for screening these molecules and to connect them to generate high-affinity molecules with favorable

Figure 56. Equilibrium Binding Model for the Bivalent Ligands.

pharmacological features (Leach et al. 2006). Increased affinity and selectivity, both thermodynamically and kinetically, by employing cooperative weak interactions (multivalency) plays a key role in recognition for a wide range of functions, and pioneering organic chemists have been intrigued by this ubiquitous but efficient mechanism (Huskens 2006). Most synthetic multivalent molecules developed have targeted surface molecules exposed on virus, bacteria, or cell membrane with tethered identical ligands (homovalency), although a few studies without extensive biological evaluation have unclosed the possibility of molecules with nonidentical ligands (heterovalency) for intracellular proteins (See details in Choi, 2004 (Choi 2004)).

Since the UBR box motif is known to be required and sufficient to bind both type 1 and type 2 and the binding mechanisms are mutually exclusive (Kwon Lab, unpublished data), I examined whether a bivalent small molecule, which contains both type 1 and type 2 N-terminal destabilizing residues, increased binding efficiency compared with those of corresponding homovalent interactions. The prototype bivalent inhibitor, RF-C11, which unites type 1 destabilizing residue, Arg, to type 2, Phe, bridged by a Lys core, showed higher degree of inhibition compared to RR-11 or FF-C11 and was applied to the study of biochemical mechanisms and physiological function of the N-end rule pathway. These data suggest that multivalent inhibition of intracellular proteins is a good strategy for rational drug designs. One of the targets of heterovalent inhibitors can be scaffold proteins in kinase cascades. Although more than 6,000 new inhibitors to regulate kinase pathways are reported every year, there is no evidence of their specificity among the other ~ 500 similar kinases (Frodin 2007). It may be possible to make high specific inhibitors with more affinity by heterovalent inhibitors which block multiple docking sites of a scaffold protein. Continued efforts to improve RF-C11 are being made by modifying the link, destabilizing residue, and core molecules. More biophysical information about the interaction between RF-C11 and its binding protein, UBR protein, will facilitate the development of more sophisticated, drug-like inhibitors which may modulate the functions of the N-end rule pathway *in vivo*.

In summary, the rational design and synthesis of bivalent inhibitors of the N-end rule pathway are described here. This compound afforded the first demonstration of cooperative inhibition of a heterovalent molecule targeting a single enzyme with two different binding sites. The prototype bivalent inhibitor, RF-C11, showed enhanced functional activity *in vitro* both in type 1 and type 2 N-end rule pathways compared with dipeptide inhibitors or homovalent

controls. This hypothesis was further supported by the direct interaction between the bivalent inhibitors and UBR box motif or endogenous UBR proteins. Moreover, the results from *in vivo* applications suggest hitherto unclear links between its hypertrophism and the N-end rule pathway by regulating the RGS proteolysis. A reasonably varied collection of RF-C11 derivatives includes different linker length, linker backbone, linkage identity, and multiple N-degrons. Cell permeability is strongly desirable. Dynamic combinatorial chemistry or "extended tethering" will be a feasible method to identify the second generation of bivalent inhibitors, which is more druglike (Erlanson et al. 2003; Shi et al. 2006). More sophisticated design for bivalent inhibitors may be provided from the identification of X-ray structure of the UBR box. It is expected that further development of bivalent inhibitors, based on this study, will allow a more extensive study of the mechanisms and functions of the N-end rule pathway. Finally, the inhibition of cardiac proliferation and hypertrophy by RF-C11 may be in part through inhibition of multiple N-recognins controlling Gq signaling. In humans, myocardial hypertrophy, associated with hypertension, cardiac valvular disease or ischemia, is typically followed by myocardial diseases, the leading causes of death in western society. Therefore, the N-recognin pathway is a potential target to control cardiac hypertrophy.

SYNTHESIS AND CHARACTERIZATION OF HETEROVALENT INHIBITORS

A.1   RF-C11, GV-C11, RR-C11, AND FF-C11

Synthesis schemes of RF-C11 and related compounds were developed with a collaboration with Banerjee Lab (Indian Institute of Chemical Technology, India) and organic synthesis, purification, and characterization were performed in his group. Z-Arg(Z)$_2$-OH was purchased from Senn chemicals (Dielsdorf, Switzerland). Remaining protected amino acids were purchased from Novabiochem (La Jolla, USA). All other chemicals were purchased from Sigma Chemical Co. (St. Louis, MO). Organic solvents required for synthesis were purchased from Ranbaxy Fine Chemicals Ltd. (New Delhi, India). They were used without further purification. All the intermediates in the synthesis were characterized by ^{1}H NMR and mass spectra. The final molecules were characterized by ESI or FAB or MALDI-TOF Mass spectral analysis and the purity ascertained by HPLC. All the ^{1}H NMR spectra were recorded on a Bruker FT 300 MHz, Varian FT 200 MHz instrument or Varian FT 400MHz instrument. HPLC analysis were performed at 210nm on a Shimadzu LC10A instrument using Whatman Reverse Phase C18 column (4.6×250mm) and either methanol or 5 % water in methanol as mobile phase with a flow rate of 1 mL/min. Figure 57 outlines the synthetic strategy employed for preparing bivalent inhibitor RF-C11, its structural analogue GV-C11, and its homovalent controls, RR-C11 and FF-C11. The strategy for preparing biotinylated inhibitor RF-C11b and its structural analogue GV-C11b is shown in Figure 58.

***tert*-butyl-11-aminoundecanoate, 7.** N,N'-dimethylaminopyridine (1.16 g, 9.51 mmol), EDC (4.00 g, 20.8 mmol) and 11-bromoundecanoic acid **6** (5.00 g, 18.9 mmol) were added sequentially in ice-cold, dry DCM (20 ml), followed by addition of *tert*-butanol (11.0 ml, 115 mmol). After 16 h the organic phase was washed with water, dried and evaporated. The residue was subjected to column chromatographic purification in 1 % ethyl acetate in hexane, yielding *tert*-butyl-11-bromoundecanoate (3.8 g, 62.7 % yield, R_f = 0.80 in 10 % ethyl acetate in hexane). This compound (3.80 g, 11.8 mmol) was reacted with sodium azide (0.77 g, 11.8 mmol) at 70-80 ºC in anhydrous DMF for 18 h. Following cooling, the mixture was taken up in chloroform, washed with water, dried, and evaporated. The crude residue was reacted with triphenylphosphine (4.36 g, 16.6 mmol) with THF/water for 4 h. THF was evaporated, and compound **7** was purified from the crude mixture through column chromatographic purification using 4 % methanol in chloroform (2.8 g, 92.1 % yield, R_f = 0.20 in 5 % methanol in chloroform). ^{1}H NMR (300 MHz, CDCl$_3$): δ 1.28 [s, 12H], 1.43 [s, 9H], 1.49-1.62 [m, 4H], 2.13-2.21 [t, 2H, *J*= 7.5 Hz], 2.76-2.84 [t, 2H, *J*= 7.6 Hz], 2.92-3.10 [bs, 2H]. ESI-MS: m/z 258 ([M+H]$^+$, calculated for C$_{15}$H$_{32}$O$_2$N, 258.2).

R-C11(-CO$_2$H), 8a. HOBt (30 mg, 0.196 mmol), EDC (0.37 g, 1.93 mmol) and Z-Arg-(Z)$_2$-OH (1.00 g, 1.74 mmol) were mixed in ice-cold, dry DCM (5 ml), followed by reaction with compound **7** (0.49 g, 1.91 mmol) for 16 h. R-C11(-CO$_2$Bu^t) was isolated (0.85 g, 60.0 % yield, R_f = 0.80 in 5 % methanol in chloroform) through chromatographic purification in 1 % methanol in chloroform. A DCM solution of this compound (0.85 g, 1.04 mmol) was mixed with TFA (2 ml) to remove *tert*-butyl protecting group, yielding R-C11(-CO$_2$H) **8a** (0.70 g, 89 % yield, R_f = 0.60 in 5 % methanol in chloroform). ^{1}H NMR (200 MHz, DMSO-d$_6$): δ 1.25 [bs, 14H], 1.45-1.76 [m, 6H], 2.11-2.25 [t, 2H, *J*= 7.3 Hz], 2.72-3.11 [m (overlapping with DMSO peak), 2H], 3.82-4.00 [m, 2H], 4.01-4.15 [m, 1H], 4.87-5.21 [m, 6H], 6.56-6.69 [d, 1H, *J*= 8.5 Hz], 7.20-7.44 [m, 15H], 9.20-9.49 [2bs, 2H]. ESI-MS: m/z 761 ([M+H]$^+$, calculated for C$_{41}$H$_{54}$O$_9$N$_5$, 760.4).

F-C11(-CO$_2$H), 8b. Yield: 49.7 % from two steps (R_f = 0.60 in 5 % methanol in chloroform). ^{1}H NMR (500 MHz, DMSO-d$_6$): δ 1.16-1.33 [m, 12H], 1.34-1.41 [m, 2H], 1.53-1.61 [m, 2H], 2.17-2.23 [t, 2H, *J*= 7.7 Hz], 2.86-3.17 [m (partially overlapping with DMSO peak), 4H], 4.27-
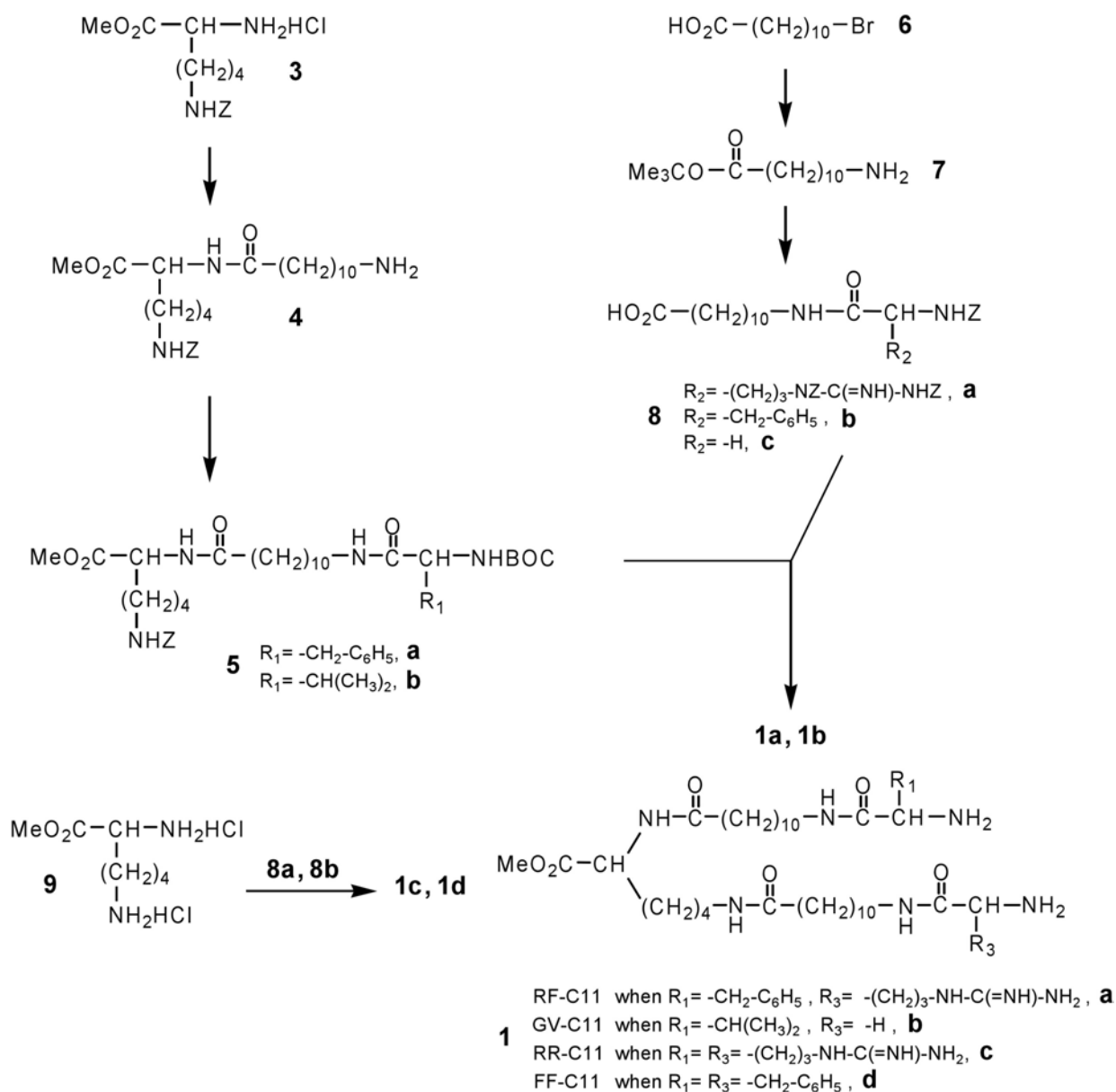
Figure 57. Synthesis scheme of RF-C11, GV-C11, RR-C11 and FF-C11.

4.37 [m, 1H], 5.01 [s, 2H], 7.07-7.33 [m, 10H]. FABMS: m/z 483 ([M+H]$^+$, calculated for C$_{28}$H$_{39}$O$_5$N$_2$, 483.3).

G-C11(-CO$_2$H), 8c. Yield: 50.0 % from two steps (R$_f$ = 0.55 in 5 % methanol in chloroform). ^{1}H NMR (400 MHz, DMSO-d$_6$): δ 1.28 [bs,12H], 1.39-1.49 [m, 2H], 1.51-1.62 [m, 2H], 2.13-2.26 [t, 2H, J= 8.0 Hz], 3.09-3.20 [m (merged with DMSO peak), 2H], 3.67-3.73 [d, 2H, J= 6.0 Hz], 5.07 [s, 2H], 7.23-7.41 [m, 5H]. FABMS: m/z 393 ([M+H]$^+$, calculated for C$_{21}$H$_{33}$O$_5$N$_2$,

393.2).

N(ε)-Z-Lysine(-OMe)C11-NH₂, 4. HOBt (0.28 g, 1.83 mmol), EDC (3.50 g, 18.2 mmol) and 11-bromoundecanoic acid (4.81 g, 18.1 mmol) were mixed in ice-cold, dry DCM (20 ml), followed by addition of N(ε)-Z-lysine methyl ester hydrochloride **3** (5.00 g, 15.1 mmol), drop-wise addition of DIPEA, and reaction for 16 h. N(ε)-Z-Lysine(-OMe)C11-Br (4.92 g, 60.2 % yield, R_f = 0.60 in 5 % methanol in chloroform) was obtained through column chromatographic purification (2 % methanol in chloroform). This product (4.92 g, 9.09 mmol) was reacted with sodium azide (0.60 g, 9.23 mmol) at 70-80 ºC in dry DMF for 18 h. Following cooling, the mixture was taken up in chloroform, washed with water, dried, and evaporated. The crude residue was reacted with triphenylphosphine (3.44 g, 13.1 mmol) with THF/water for 4 h. THF was evaporated, and N(ε)-Z-Lysine(-OMe)C11-NH₂ **4** was purified through column chromatography using 4 % methanol in chloroform (4.0 g, 92.1 % yield, R_f = 0.20 in 5 % methanol in chloroform). ¹H NMR (200 MHz, CDCl₃): δ 1.26 [bs, 14 H], 1.35-1.73 [m, 8H], 2.11-2.23 [t, 2H, J= 7.5 Hz], 2.60-2.71 [t, 2H, J= 6.7 Hz], 3.10-3.23 [m, 2H], 3.72 [s, 3H], 4.46-4.61 [m, 1H], 4.95-5.04 [t, 1H, J= 6.0 Hz], 5.05 [s, 2H], 6.08-6.18 [d, 1H, J= 7.7 Hz], 7.30 [s, 5H].

N(ε)-Z-Lysine(-OMe)C11F, 5a. HOBt (0.13 g, 0.85 mmol), EDC (1.61 g, 8.40 mmol) and Boc-Phe-OH (2.00 g, 7.55 mmol) were mixed in ice-cold, dry DCM (10 ml) followed by addition of compound **4** (4.00 g, 8.38 mmol) and then reacted at r.t. for 16 h. The product N(ε)-Z-Lysine(-OMe)C11F **5a** was obtained through column chromatography using 2% methanol in chloroform (3.30 g, 60.3 % yield, R_f = 0.55 in 5 % methanol in chloroform).
¹H NMR (300 MHz, CDCl₃): δ 1.11-1.40 [m, 14 H], 1.43 [s, 9H], 1.48-1.75 [m, 8H], 2.15-2.26 [t, 2H, J= 7.6 Hz], 2.97-3.25 [m, 6H], 3.75 [s, 3H], 4.16-4.28 [m, 1H], 4.52-4.63 [m, 1H], 4.98-5.06 [t, 1H, J= 6.1Hz], 5.08 [s, 2H], 5.15-5.25 [bs, 1H], 5.78-5.88 [bs, 1H], 6.22-6.30 [d, 1H, J= 7.5 Hz], 7.15-7.37 [m, 10H]. ESI-MS: m/z 725.8 ([M+H]⁺, calculated for $C_{40}H_{61}O_8N_4$, 725.4).

N(ε)-Z-Lysine(-OMe)C11V, 5b. Yield: 59.9 % (R_f = 0.55 in 5 % methanol in chloroform).
¹H NMR (300 MHz, CDCl₃): δ 0.86-0.97 [t, 6H, J= 6.0 Hz], 1.24 [bs, 12H], 1.41 [s, 9H], 1.50-1.88 [m, 10H], 1.94-2.06 [m, 1H], 2.12-2.21 [t, 2H, J= 7.6Hz], 3.08-3.26 [m, 4H], 3.71 [s, 3H],

3.78-3.86 [t, 1H, J = 8.0 Hz], 4.48-4.59 [m, 1H], 5.05 [s, 2H], 7.21-7.33 [s, 5H]. FABMS: m/z 677 ([M+H]$^+$, calculated for $C_{36}H_{61}O_8N_4$, 677.4).

PRF-C11, precursor of 1a. Compound **5a** (1.00 g, 1.38 mmol) was subjected to Z-deprotection by conventional hydrogenation with 10 % Pd on charcoal in methanol, yielding Lysine(-OMe)C11F (0.61 g, 75.3 % yield, R_f = 0.25 in 5 % methanol in chloroform). This product (0.60 g, 1.02 mmol) was added to an ice cold, dry DCM mixture containing HOBt (15 mg, 0.098 mmol), EDC (0.20 g, 1.04 mmol) and compound **8a** (0.70 g, 0.92 mmol), followed by reaction at r.t. for 48 h. PRF-C11 was obtained through column chromatographic purification using 2% methanol in chloroform (0.65 g, 53.3 % yield, R_f = 0.20 in 70 % ethyl acetate in hexane). ^{1}H NMR (300 MHz, CDCl$_3$ + CD$_3$OD): δ 1.26 [bs, 32 H], 1.45-1.75 [m, 10H], 2.11-2.28 [two triplets, 4H, J = 7.6 and 7.5 Hz], 2.91-3.23 [m, 8H], 3.73 [s, 3H], 3.91-4.03 [m, 2H], 4.12-4.28 [m, 2H], 4.45-4.54 [m, 1H], 5.01-5.18 [m, 4H], 5.24 [s, 2H], 7.12-7.41 [m, 20H]. ESI-MS: m/z 1,334 ([M+2H]$^+$, calculated for $C_{73}H_{107}O_{14}N_9$, 1,333.8) and 667 ([M+2H]$^{2+}$, calculated 666.9)

PGV-C11, precursor of 1b. Yield: 42.6 % from two steps (R_f = 0.60 in 10 % methanol in chloroform). ^{1}H NMR (400 MHz, CDCl$_3$ + CD$_3$OD): δ 0.88-0.98 [t, 6H, J = 7.5 Hz], 1.28 [bs, 24H], 1.43 [s, 9H], 1.46-1.85 [m, 15H], 2.10-2.26 [two triplets, 4H, J = 8.5 and 9.0 Hz], 3.06-3.31 [m, 6H], 3.68-3.80 [d, 6H, J = 8.7 Hz], 4.40 [m (overlapped with CD$_3$OD solvent peak), 1H], 5.08 [s, 2H], 7.25-7.39 [m, 5H]. FABMS: m/z 917 ([M+H]$^+$, calculated for $C_{49}H_{85}O_{10}N_6$, 917.6).

PRR-C11, precursor of 1c. HOBt (0.01 g, 0.065 mmol), EDC (0.12 g, 0.626 mmol) and compound **8a** (0.42 g, 0.552 mmol) were dissolved in cold, dry DCM (5 ml), followed by dropwise addition of DMSO solution containing L-lysine methyl ester dihydrochloride **9** (0.05 g, 0.215 mmol) and DIPEA. The resulting solution was stirred at r.t. for 48 h. PRR-C11 was obtained through column chromatographic purification using 1 % methanol in chloroform (0.22 g, 62.3 % yield, R_f = 0.70 in 5 % methanol in chloroform). ^{1}H NMR (200 MHz, CDCl$_3$ + CD$_3$OD): δ 1.08-1.37 [m, 32H], 1.42-1.83 [m, 14H], 2.07-2.28 [two triplets, 4H, J = 7.8 and 7.1 Hz], 2.88-3.07 [m, 4H], 3.08-3.19 [t, 2H, J = 6.3 Hz], 3.72 [s, 3H], 3.76-4.02 [m, 6H], 4.36-4.47

[m, 1H], 4.97-5.26 [m, 12H], 7.20-7.40 [m, 30H]. ESI-MS: m/z 1645 ([M+H]$^+$, calculated for $C_{89}H_{119}O_{18}N_{12}$, 1644.9), and 823 ([M+2H]$^{2+}$, calculated 822.5).

PFF-C11, precursor of 1d. Yield 59.8 % (R_f = 0.60 in 10 % methanol in chloroform). ^{1}H NMR (400 MHz, CDCl$_3$ + CD$_3$OD): δ 1.11-1.38 [m, 28H], 1.42-1.83 [m,10H], 2.09-2.25 [two triplets, J = 7.4 and 7.8 Hz, 4H], 2.85-3.18 [m, 10H], 3.71 [s, 3H], 4.22-4.32 [m (partially overlapped with CD$_3$OD solvent peak), 3H], 4.95-5.08 [m, 4H], 7.11-7.34 [m, 20H]. ESIMS: m/z 1,090 ([M+H]$^+$, calculated for $C_{63}H_{89}O_{10}N_6$, 1,089.7).

RF-C11, 1a. PRF-C11 (0.10 g, 0.075 mmol) and TFA (2.0 ml) were mixed under N$_2$ and stirred on ice. Thioanisole (0.4 ml, 3.4 mmol) and TMSOTf (0.6 ml, 3.3 mmol) were added sequentially to the cold mixture, followed by stirring at r.t. for 24 h. HPLC grade methanol (1.0 ml) was added, and the organic phase was flushed out with N$_2$. The residue was four times re-precipitated from methanol-diethyl ether (1:8) system. By using chloride ion exchange chromatography with Amberlite IRA400Cl resin and repeated re-precipitations, the pure product RF-C11 **1a** was isolated as a yellowish white semi-solid (0.044 g, 71.0 % yield, R_f = 0.0-0.10 in methanol:chloroform:acetic acid (30:70:0.1)). ESI-HRMS: m/z 830.6219 ([M+H]$^+$, calculated for $C_{44}H_{80}O_6N_9$, 830.6231), and 415.8151 ([M+2H]$^{2+}$ calculated, 415.8155). RP-HPLC: Rt = 5.8 min (100 % methanol), purity > 99 %.

GV-C11, 1b. Yield: 60.5 % (R_f = 0.20 in 10 % methanol in chloroform). ESI-HRMS: m/z 683.5426 ([M+H]$^+$, calculated for $C_{36}H_{71}O_6N_6$, 683.5435), and 342.2738 ([M+2H]$^{2+}$calculated, 342.2757). RP-HPLC: Rt = 6.2 min (100 % methanol), purity > 92 %

RR-C11. 1c. Yield: 39.2 % (Rf = 0.00, compound lies in the base for TLC at methanol:chloroform:acetic acid (30:70:0.1)). ESI-HRMS: m/z 420.3330 ([M+2H]$^{2+}$calculated for $[C_{41}H_{84}O_6N_{12}]/2$, 420.3312). RP-HPLC: Rt = 2.2 min (0.05 % TFA in methanol), purity > 98 %.

FF-C11, 1d. Yield: 33.1 % (R_f = 0.25 in 10 % methanol in chloroform). ESI-HRMS: m/z 821.5909 ([M+H]$^+$, calculated for $C_{47}H_{77}O_6N_6$, 821.5899), and 411.2942 ([M+2H]$^{2+}$ calculated,

411.2989). RP-HPLC: Rt = 2.3 min (0.05 % TFA in methanol), purity > 99 %.

A.2   SYNTHESIS AND CHARACTERIZATION OF RF-C11B AND GV-C11B

Biotinylated versions of bivalent inhibitors, RF-C11b and GV-C11b, were synthesized using the similar synthesis scheme as RF-C11 and GV-C11, mainly using conventional protocols of amide bond formation using EDC and HOBt. However, for biotin-labeled inhibitors, ethylenediamine-coupled biotinwas initially conjugated with $N(\varepsilon)$-Z-Lysine(-OMe)C11-NH$_2$ prior to further reactions.

Boc-protected biotinylated ethylenediamine. 11. HOBt (0.19 g, 1.24 mmol), EDC (0.23 g, 1.20 mmol) and biotin (0.20 g, 0.82 mmol) was added in cold, dry DMF (5 ml), followed by addition of DMF solution of mono-BOC-ethylenediamine (0.20 g, 1.25 mmol) and DIPEA dropwise. The resulting solution was stirred at r.t. for 16 h. Compound **11** was obtained through column chromatographic purification using 4 % methanol in chloroform (0.21 g, 66.4 % yield, R_f = 0.40 in 10 % methanol in chloroform). ^{1}H NMR (300 MHz, CDCl$_3$ + CD$_3$OD): δ 1.25 [s, 2H], 1.41 [s, 9H], 1.51-1.78 [m, 4H], 2.16-2.23 [t, 2H], 2.68-2.97 [m, 2H], 3.11-3.37 [m, 5H], 4.23-4.35 [m, 2H].

$N(\varepsilon)$-Z-lysine(-O-biotinylated ethylenediamine)-C11F, 12. Compound **5a** was demethylated using LiOH in THF:water:methanol (3:1:1) solvent mixture, yielding $N(\varepsilon)$-Z-Lysine(OH)-C11F (78.1 % yield, R_f = 0.30 in 5 % methanol in chloroform). Compound **11** was subjected to BOC deprotection using TFA, yielding biotinylated ethylenediamine (97.1 % yield). HOBt (0.043 g, 0.28 mmol), EDC (0.065 g, 0.34 mmol) and $N(\varepsilon)$-Z-Lysine(-OH)-C11F (0.20 g, 0.28 mmol) were added in cold, dry DMF (2 ml), followed by addition of DMF solution of biotinylated ethylenediamine (0.135 g, 0.34 mmol) and dropwise addition of DIPEA. The resulting solution was stirred at r.t. for 48 h. After washing with 0.5 N HCl in brine solution and column chromatography using 3 % methanol in chloroform, compound **12** was obtained in pure form (0.144 g, 52.2 %, R_f = 0.40 in 10 % methanol in chloroform. ^{1}H NMR (200 MHz, CDCl$_3$ +
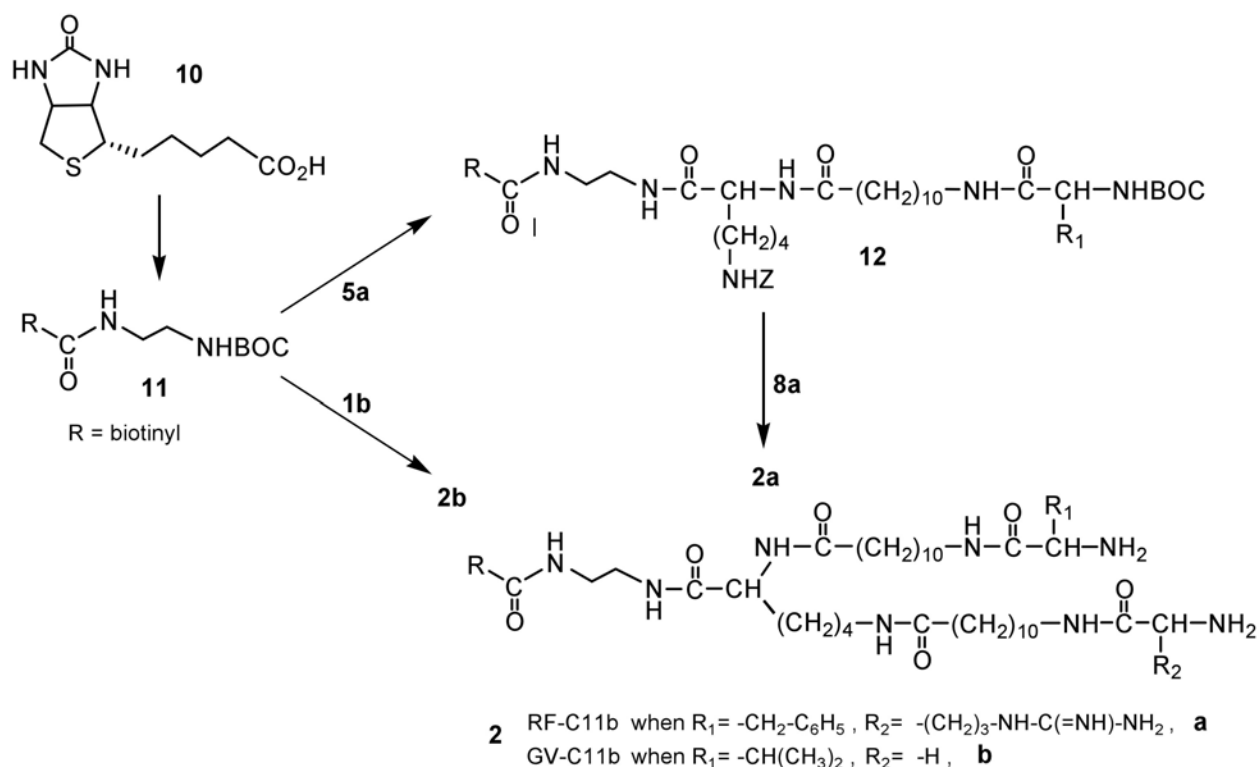
Figure 58. Synthesis scheme of biotinylated version of compounds, RF-C11b and GV-C11b.

CD$_3$OD): δ 1.10-1.34 [bs, 18H], 1.38 [s, 9H], 1.50-1.79 [m, 10H], 2.09-2.32 [m, 4H], 2.57-3.57 [m, 13H], 4.06-4.36 [m, 3H], 4.38-4.54 [m, 1H], 5.05 [s , 2H], 7.12-7.43 [m, 10H]

PRF-C11b, precursor of 2a. Compound **12** was subjected to Z-deprotection using hydrogenolysis with 10 % Pd on charcoal in methanol afforded Lysine(-O-biotinylated ethylenediamine)-C11F (78.8 % yield). HOBt (6 mg, 0.039 mmol), EDC (9 mg, 0.047 mmol) and compound **8a** (30 mg, 0.039 mmol) was added in cold, dry DMF (1 ml), followed by addition of DMF solution of Lysine(-O-biotinylated ethylenediamine)-C11F (0.05 g, 0.059 mmol) and dropwise addition of DIPEA. The resulting solution was stirred at r.t. for 72 h. Washing with 0.5 N HCl in brine solution and column chromatographic purification using 5 % methanol in chloroform yielded PRF-C11b in pure form (0.028 g, 44.8 % yield, R$_f$ = 0.50 in 10 % methanol in chloroform). ^{1}H NMR (200 MHz, CDCl$_3$ + CD$_3$OD): δ 1.20-1.39 [bs, 34H], 1.42 [s, 9H], 1.53-1.81 [m, 14H], 2.14-2.39 [m, 6H], 2.62-3.42 [m, 13H], 3.81-4.62 [m, 5H, ring junction protons], 5.08-5.19 [m, 4H], 5.28 [s, 2H], 7.17-7.58 [m, 20H].

PGV-C11b, precursor of 2b. PGV-C11 was demethylated using the same method as described above. Demethylated PGV-C11 and compound **12** were coupled using HOBt and EDC in DMF as described above (42.3 % yield from two steps, R_f = 0.35 in 10 % methanol in chloroform). ^{1}H NMR (200 MHz, CDCl$_3$ + CD$_3$OD): δ 0.82-0.97 [d, 6H, J= 6.8 Hz], 1.28 [bs, 34H], 1.43 [s, 9H], 1.50-1.78 [m, 11H], 2.01-2.30 [m, 6H], 2.65-3.78 [m, 15H], 4.00-4.39 [m, 4H, ring junction protons], 5.08 [s, 2H], 7.31 [s, 5H].

RF-C11b, 2a. PRF-C11b was deprotected and purified through selective precipitation using methanol/diethyl ether solvent mixture, yielding pure RF-C11b **2a** (58.4 % yield). ESI-MS: m/z 1,085 ([M+H]$^+$, calculated for C$_{55}$H$_{98}$O$_7$N$_{13}$S, 1,084.7), and 543 ([M+2H]$^{2+}$ calculated, 542.9). RP-HPLC: Rt = 4.1 min (5 % water in methanol), purity > 98 %.

GV-C11b, 2b. Yield: 43.6 %. ESI-MS: m/z 937.6 ([M+H]$^+$, calculated for C$_{47}$H$_{89}$O$_7$N$_{10}$S, 937.7), and 469.4 ([M+2H]$^{2+}$ calculated, 469.3). RP-HPLC: Rt = 3.3 min (10 % water in methanol), purity > 94 %.

BIBLIOGRAPHY

Adams, J.W. and Brown, J.H. 2001. G-proteins in growth and apoptosis: lessons from the heart. *Oncogene* **20**(13): 1626-1634.

Adams, J.W., Migita, D.S., Yu, M.K., Young, R., Hellickson, M.S., Castro-Vargas, F.E., Domingo, J.D., Lee, P.H., Bui, J.S., and Henderson, S.A. 1996. Prostaglandin F2 alpha stimulates hypertrophic growth of cultured neonatal rat ventricular myocytes. *J Biol Chem* **271**(2): 1179-1186.

Adams, J.W., Sakata, Y., Davis, M.G., Sah, V.P., Wang, Y., Liggett, S.B., Chien, K.R., Brown, J.H., and Dorn, G.W., 2nd. 1998. Enhanced Galphaq signaling: a common pathway mediates cardiac hypertrophy and apoptotic heart failure. *Proc Natl Acad Sci U S A* **95**(17): 10140-10145.

Akhter, S.A., Luttrell, L.M., Rockman, H.A., Iaccarino, G., Lefkowitz, R.J., and Koch, W.J. 1998. Targeting the receptor-Gq interface to inhibit in vivo pressure overload myocardial hypertrophy. *Science* **280**(5363): 574-577.

An, J.Y., Seo, J.W., Tasaki, T., Lee, M.J., Varshavsky, A., and Kwon, Y.T. 2006. Impaired neurogenesis and cardiovascular development in mice lacking the E3 ubiquitin ligases UBR1 and UBR2 of the N-end rule pathway. *Proc Natl Acad Sci U S A* **103**(16): 6212-6217.

Austin, D.J., Crabtree, G.R., and Schreiber, S.L. 1994. Proximity versus allostery: the role of regulated protein dimerization in biology. *Chem Biol* **1**(3): 131-136.

Bachmair, A., Finley, D., and Varshavsky, A. 1986. In vivo half-life of a protein is a function of its amino-terminal residue. *Science* **234**(4773): 179-186.

Baker, R.T., Tobias, J.W., and Varshavsky, A. 1992. Ubiquitin-specific proteases of Saccharomyces cerevisiae. Cloning of UBP2 and UBP3, and functional analysis of the UBP gene family. *J Biol Chem* **267**(32): 23364-23375.

Baker, R.T. and Varshavsky, A. 1995. Yeast N-terminal amidase. A new enzyme and component of the N-end rule pathway. *J Biol Chem* **270**(20): 12065-12074.

Balzi, E., Choder, M., Chen, W.N., Varshavsky, A., and Goffeau, A. 1990. Cloning and functional analysis of the arginyl-tRNA-protein transferase gene ATE1 of Saccharomyces cerevisiae. *J Biol Chem* **265**(13): 7464-7471.

Baumeister, W., Walz, J., Zuhl, F., and Seemuller, E. 1998. The proteasome: paradigm of a self-compartmentalizing protease. *Cell* **92**(3): 367-380.

Berman, D.M., Wilkie, T.M., and Gilman, A.G. 1996. GAIP and RGS4 are GTPase-activating proteins for the Gi subfamily of G protein alpha subunits. *Cell* **86**(3): 445-452.

Bertozzi, C.R. and Kiessling, L.L. 2001. Chemical glycobiology. *Science* **291**(5512): 2357-2364.

Botbol, V. and Scornik, O.A. 1983. Peptide intermediates in the degradation of cellular proteins. Bestatin permits their accumulation in mouse liver in vivo. *J Biol Chem* **258**(3): 1942-1949.

Brooks, G., Poolman, R.A., and Li, J.M. 1998. Arresting developments in the cardiac myocyte cell cycle: role of cyclin-dependent kinase inhibitors. *Cardiovasc Res* **39**(2): 301-311.

Brown, E.J., Albers, M.W., Shin, T.B., Ichikawa, K., Keith, C.T., Lane, W.S., and Schreiber, S.L. 1994. A mammalian protein targeted by G1-arresting rapamycin-receptor complex. *Nature* **369**(6483): 756-758.

Byrd, C., Turner, G.C., and Varshavsky, A. 1998. The N-end rule pathway controls the import of peptides through degradation of a transcriptional repressor. *Embo J* **17**(1): 269-277.

Carrithers, M.D. and Lerner, M.R. 1996. Synthesis and characterization of bivalent peptide ligands targeted to G-protein-coupled receptors. *Chem Biol* **3**(7): 537-542.

Cherian, S., Whitelaw, A., Thoresen, M., and Love, S. 2004. The pathogenesis of neonatal post-hemorrhagic hydrocephalus. *Brain Pathol* **14**(3): 305-311.

Cho, H., Kozasa, T., Bondjers, C., Betsholtz, C., and Kehrl, J.H. 2003. Pericyte-specific expression of Rgs5: implications for PDGF and EDG receptor signaling during vascular maturation. *Faseb J* **17**(3): 440-442.

Choi, S.-k. 2004. *Synthetic multivalent molecules: concepts and biomedical applications*. Wiley-Interscience, Hoboken, N.J.

Ciechanover, A. 2005. Intracellular protein degradation: from a vague idea thru the lysosome and the ubiquitin-proteasome system and onto human diseases and drug targeting. *Cell Death Differ* **12**(9): 1178-1190.

Ciechanover, A. 2005. Proteolysis: from the lysosome to ubiquitin and the proteasome. *Nat Rev Mol Cell Biol* **6**(1): 79-87.

Clark, K.L., Yutzey, K.E., and Benson, D.W. 2006. Transcription factors and congenital heart defects. *Annu Rev Physiol* **68**: 97-121.

Coux, O., Tanaka, K., and Goldberg, A.L. 1996. Structure and functions of the 20S and 26S proteasomes. *Annu Rev Biochem* **65**: 801-847.

Crabtree, G.R. and Schreiber, S.L. 1996. Three-part inventions: intracellular signaling and induced proximity. *Trends Biochem Sci* **21**(11): 418-422.

D'Angelo, D.D., Sakata, Y., Lorenz, J.N., Boivin, G.P., Walsh, R.A., Liggett, S.B., and Dorn, G.W., 2nd. 1997. Transgenic Galphaq overexpression induces cardiac contractile failure in mice. *Proc Natl Acad Sci U S A* **94**(15): 8121-8126.

Davydov, I.V. and Varshavsky, A. 2000. RGS4 is arginylated and degraded by the N-end rule pathway in vitro. *J Biol Chem* **275**(30): 22931-22941.

de Groot, R.J., Rumenapf, T., Kuhn, R.J., Strauss, E.G., and Strauss, J.H. 1991. Sindbis virus RNA polymerase is degraded by the N-end rule pathway. *Proc Natl Acad Sci U S A* **88**(20): 8967-8971.

Deng, X.F., Rokosh, D.G., and Simpson, P.C. 2000. Autonomous and growth factor-induced hypertrophy in cultured neonatal mouse cardiac myocytes. Comparison with rat. *Circ Res* **87**(9): 781-788.

Derrien, A., Zheng, B., Osterhout, J.L., Ma, Y.C., Milligan, G., Farquhar, M.G., and Druey, K.M. 2003. Src-mediated RGS16 tyrosine phosphorylation promotes RGS16 stability. *J Biol Chem* **278**(18): 16107-16116.

Deshaies, R.J. 1999. SCF and Cullin/Ring H2-based ubiquitin ligases. *Annu Rev Cell Dev Biol* **15**: 435-467.

Ditzel, M., Wilson, R., Tenev, T., Zachariou, A., Paul, A., Deas, E., and Meier, P. 2003. Degradation of DIAP1 by the N-end rule pathway is essential for regulating apoptosis. *Nat Cell Biol* **5**(5): 467-473.

Dorn, G.W., 2nd and Hahn, H.S. 2004. Genetic factors in cardiac hypertrophy. *Ann N Y Acad Sci* **1015**: 225-237.

Doupnik, C.A., Xu, T., and Shinaman, J.M. 2001. Profile of RGS expression in single rat atrial myocytes. *Biochim Biophys Acta* **1522**(2): 97-107.

Erbse, A., Schmidt, R., Bornemann, T., Schneider-Mergener, J., Mogk, A., Zahn, R., Dougan, D.A., and Bukau, B. 2006. ClpS is an essential component of the N-end rule pathway in Escherichia coli. *Nature* **439**(7077): 753-756.

Eriste, E., Norberg, A., Nepomuceno, D., Kuei, C., Kamme, F., Tran, D.T., Strupat, K., Jornvall, H., Liu, C., Lovenberg, T.W., and Sillard, R. 2005. A novel form of neurotensin post-translationally modified by arginylation. *J Biol Chem* **280**(42): 35089-35097.

Erlanson, D.A., Lam, J.W., Wiesmann, C., Luong, T.N., Simmons, R.L., DeLano, W.L., Choong, I.C., Burdett, M.T., Flanagan, W.M., Lee, D., Gordon, E.M., and O'Brien, T. 2003. In situ assembly of enzyme inhibitors using extended tethering. *Nat Biotechnol* **21**(3): 308-314.

Findeis, M.A. 2001. *Nonviral vectors for gene therapy: methods and protocols*. Humana Press, Totowa, N.J.

Finley, D., Ciechanover, A., and Varshavsky, A. 2004. Ubiquitin as a central cellular regulator. *Cell* **116**(2 Suppl): S29-32, 22 p following S32.

Fishman, M.C. and Chien, K.R. 1997. Fashioning the vertebrate heart: earliest embryonic decisions. *Development* **124**(11): 2099-2117.

Fredj, S., Bescond, J., Louault, C., and Potreau, D. 2005. Interactions between cardiac cells enhance cardiomyocyte hypertrophy and increase fibroblast proliferation. *J Cell Physiol* **202**(3): 891-899.

Frodin, M. 2007. A RSK kinase inhibitor reporting its selectivity in vivo. *Nat Chem Biol* **3**(3): 138-139.

Gargano, J.M., Ngo, T., Kim, J.Y., Acheson, D.W., and Lees, W.J. 2001. Multivalent inhibition of AB(5) toxins. *J Am Chem Soc* **123**(51): 12909-12910.

Gestwicki, J.E., Strong, L.E., and Kiessling, L.L. 2000. Tuning chemotactic responses with synthetic multivalent ligands. *Chem Biol* **7**(8): 583-591.

Gil, P., Dewey, E., Friml, J., Zhao, Y., Snowden, K.C., Putterill, J., Palme, K., Estelle, M., and Chory, J. 2001. BIG: a calossin-like protein required for polar auxin transport in Arabidopsis. *Genes Dev* **15**(15): 1985-1997.

Glickman, M.H. and Ciechanover, A. 2002. The ubiquitin-proteasome proteolytic pathway: destruction for the sake of construction. *Physiol Rev* **82**(2): 373-428.

Gonda, D.K., Bachmair, A., Wunning, I., Tobias, J.W., Lane, W.S., and Varshavsky, A. 1989. Universality and structure of the N-end rule. *J Biol Chem* **264**(28): 16700-16712.

Graciet, E., Hu, R.G., Piatkov, K., Rhee, J.H., Schwarz, E.M., and Varshavsky, A. 2006. Aminoacyl-transferases and the N-end rule pathway of prokaryotic/eukaryotic specificity in a human pathogen. *Proc Natl Acad Sci U S A* **103**(9): 3078-3083.

Grigoryev, S., Stewart, A.E., Kwon, Y.T., Arfin, S.M., Bradshaw, R.A., Jenkins, N.A., Copeland, N.G., and Varshavsky, A. 1996. A mouse amidase specific for N-terminal asparagine. The gene, the enzyme, and their function in the N-end rule pathway. *J Biol Chem* **271**(45): 28521-28532.

Harding, M.W., Galat, A., Uehling, D.E., and Schreiber, S.L. 1989. A receptor for the immunosuppressant FK506 is a cis-trans peptidyl-prolyl isomerase. *Nature* **341**(6244): 758-760.

Hardy, S., Kitamura, M., Harris-Stansil, T., Dai, Y., and Phipps, M.L. 1997. Construction of adenovirus vectors through Cre-lox recombination. *J Virol* **71**(3): 1842-1849.

Hein, L., Barsh, G.S., Pratt, R.E., Dzau, V.J., and Kobilka, B.K. 1995. Behavioural and cardiovascular effects of disrupting the angiotensin II type-2 receptor in mice. *Nature* **377**(6551): 744-747.

Heller, H. and Hershko, A. 1990. A ubiquitin-protein ligase specific for type III protein substrates. *J Biol Chem* **265**(12): 6532-6535.

Hershko, A., Ciechanover, A., and Varshavsky, A. 2000. Basic Medical Research Award. The ubiquitin system. *Nat Med* **6**(10): 1073-1081.

Hiol, A., Davey, P.C., Osterhout, J.L., Waheed, A.A., Fischer, E.R., Chen, C.K., Milligan, G., Druey, K.M., and Jones, T.L. 2003. Palmitoylation regulates regulators of G-protein signaling (RGS) 16 function. I. Mutation of amino-terminal cysteine residues on RGS16 prevents its targeting to lipid rafts and palmitoylation of an internal cysteine residue. *J Biol Chem* **278**(21): 19301-19308.

Hochstrasser, M. 2006. Lingering mysteries of ubiquitin-chain assembly. *Cell* **124**(1): 27-34.

Hollinger, S. and Hepler, J.R. 2002. Cellular regulation of RGS proteins: modulators and integrators of G protein signaling. *Pharmacol Rev* **54**(3): 527-559.

Hondermarck, H., Sy, J., Bradshaw, R.A., and Arfin, S.M. 1992. Dipeptide inhibitors of ubiquitin-mediated protein turnover prevent growth factor-induced neurite outgrowth in rat pheochromocytoma PC12 cells. *Biochem Biophys Res Commun* **189**(1): 280-288.

Hu, R.-G., Brower, C.S., Wang, H., Davydov, I.V., Sheng, J., Zhou, J., Kwon, Y.T., and Varshavsky, A. 2006. Arginyl-transferase, its specificity, putative substrates, bidirectional promoter, and splicing-derived isoforms. *J Biol Chem* **281**(43): 32559-32573

Hu, R.G., Sheng, J., Qi, X., Xu, Z., Takahashi, T.T., and Varshavsky, A. 2005. The N-end rule pathway as a nitric oxide sensor controlling the levels of multiple regulators. *Nature* **437**(7061): 981-986.

Huang, L., Kinnucan, E., Wang, G., Beaudenon, S., Howley, P.M., Huibregtse, J.M., and Pavletich, N.P. 1999. Structure of an E6AP-UbcH7 complex: insights into ubiquitination by the E2-E3 enzyme cascade. *Science* **286**(5443): 1321-1326.

Huibregtse, J.M., Scheffner, M., Beaudenon, S., and Howley, P.M. 1995. A family of proteins structurally and functionally related to the E6-AP ubiquitin-protein ligase. *Proc Natl Acad Sci U S A* **92**(7): 2563-2567.

Hunyady, L. and Catt, K.J. 2006. Pleiotropic AT1 receptor signaling pathways mediating physiological and pathogenic actions of angiotensin II. *Mol Endocrinol* **20**(5): 953-970.

Huskens, J. 2006. Multivalent interactions at interfaces. *Curr Opin Chem Biol* **10**(6): 537-543.

Ivan, M., Kondo, K., Yang, H., Kim, W., Valiando, J., Ohh, M., Salic, A., Asara, J.M., Lane, W.S., and Kaelin, W.G., Jr. 2001. HIFalpha targeted for VHL-mediated destruction by proline hydroxylation: implications for O2 sensing. *Science* **292**(5516): 464-468.

Izumi, Y., Kim, S., Zhan, Y., Namba, M., Yasumoto, H., and Iwao, H. 2000. Important role of angiotensin II-mediated c-Jun NH(2)-terminal kinase activation in cardiac hypertrophy in hypertensive rats. *Hypertension* **36**(4): 511-516.

Jackson, P.D. and Harrington, J.J. 2005. High-throughput target discovery using cell-based genetics. *Drug Discov Today* **10**(1): 53-60.

Joazeiro, C.A. and Weissman, A.M. 2000. RING finger proteins: mediators of ubiquitin ligase activity. *Cell* **102**(5): 549-552.

Jung, J., Kim, T.G., Lyons, G.E., Kim, H.R., and Lee, Y. 2005. Jumonji regulates cardiomyocyte proliferation via interaction with retinoblastoma protein. *J Biol Chem* **280**(35): 30916-30923.

Kaji, H., Novelli, G.D., and Kaji, A. 1963. A Soluble Amino Acid-Incorporating System From Rat Liver. *Biochim Biophys Acta* **76**: 474-477.

Karakozova, M., Kozak, M., Wong, C.C., Bailey, A.O., Yates, J.R., 3rd, Mogilner, A., Zebroski, H., and Kashina, A. 2006. Arginylation of beta-actin regulates actin cytoskeleton and cell motility. *Science* **313**(5784): 192-196.

Kendall, R.L. and Bradshaw, R.A. 1992. Isolation and characterization of the methionine aminopeptidase from porcine liver responsible for the co-translational processing of proteins. *J Biol Chem* **267**(29): 20667-20673.

Krumins, A.M., Barker, S.A., Huang, C., Sunahara, R.K., Yu, K., Wilkie, T.M., Gold, S.J., and Mumby, S.M. 2004. Differentially regulated expression of endogenous RGS4 and RGS7. *J Biol Chem* **279**(4): 2593-2599.

Kwon, Y.T., Balogh, S.A., Davydov, I.V., Kashina, A.S., Yoon, J.K., Xie, Y., Gaur, A., Hyde, L., Denenberg, V.H., and Varshavsky, A. 2000. Altered activity, social behavior, and spatial memory in mice lacking the NTAN1p amidase and the asparagine branch of the N-end rule pathway. *Mol Cell Biol* **20**(11): 4135-4148.

Kwon, Y.T., Kashina, A.S., Davydov, I.V., Hu, R.G., An, J.Y., Seo, J.W., Du, F., and Varshavsky, A. 2002. An essential role of N-terminal arginylation in cardiovascular development. *Science* **297**(5578): 96-99.

Kwon, Y.T., Kashina, A.S., and Varshavsky, A. 1999. Alternative splicing results in differential expression, activity, and localization of the two forms of arginyl-tRNA-protein transferase, a component of the N-end rule pathway. *Mol Cell Biol* **19**(1): 182-193.

Kwon, Y.T., Reiss, Y., Fried, V.A., Hershko, A., Yoon, J.K., Gonda, D.K., Sangan, P., Copeland, N.G., Jenkins, N.A., and Varshavsky, A. 1998. The mouse and human genes encoding the recognition component of the N-end rule pathway. *Proc Natl Acad Sci U S A* **95**(14): 7898-7903.

Kwon, Y.T., Xia, Z., An, J.Y., Tasaki, T., Davydov, I.V., Seo, J.W., Sheng, J., Xie, Y., and Varshavsky, A. 2003. Female lethality and apoptosis of spermatocytes in mice lacking the UBR2 ubiquitin ligase of the N-end rule pathway. *Mol Cell Biol* **23**(22): 8255-8271.

Kwon, Y.T., Xia, Z., Davydov, I.V., Lecker, S.H., and Varshavsky, A. 2001. Construction and analysis of mouse strains lacking the ubiquitin ligase UBR1 (E3alpha) of the N-end rule pathway. *Mol Cell Biol* **21**(23): 8007-8021.

LaMorte, V.J., Thorburn, J., Absher, D., Spiegel, A., Brown, J.H., Chien, K.R., Feramisco, J.R., and Knowlton, K.U. 1994. Gq- and ras-dependent pathways mediate hypertrophy of neonatal rat ventricular myocytes following alpha 1-adrenergic stimulation. *J Biol Chem* **269**(18): 13490-13496.

Larminie, C., Murdock, P., Walhin, J.P., Duckworth, M., Blumer, K.J., Scheideler, M.A., and Garnier, M. 2004. Selective expression of regulators of G-protein signaling (RGS) in the human central nervous system. *Brain Res Mol Brain Res* **122**(1): 24-34.

Leach, A.R., Hann, M.M., Burrows, J.N., and Griffen, E.J. 2006. Fragment screening: an introduction. *Mol Biosyst* **2**(9): 430-446.

Lecker, S.H., Solomon, V., Price, S.R., Kwon, Y.T., Mitch, W.E., and Goldberg, A.L. 1999. Ubiquitin conjugation by the N-end rule pathway and mRNAs for its components increase in muscles of diabetic rats. *J Clin Invest* **104**(10): 1411-1420.

Lee, M.J., Tasaki, T., Moroi, K., An, J.Y., Kimura, S., Davydov, I.V., and Kwon, Y.T. 2005. RGS4 and RGS5 are in vivo substrates of the N-end rule pathway. *Proc Natl Acad Sci U S A* **102**(42): 15030-15035.

Lepic, E., Burger, D., Lu, X., Song, W., and Feng, Q. 2006. Lack of endothelial nitric oxide synthase decreases cardiomyocyte proliferation and delays cardiac maturation. *Am J Physiol Cell Physiol* **291**(6): C1240-1246.

Levy, F., Johnsson, N., Rumenapf, T., and Varshavsky, A. 1996. Using ubiquitin to follow the metabolic fate of a protein. *Proc Natl Acad Sci U S A* **93**(10): 4907-4912.

Liu, Z.P. and Olson, E.N. 2002. Suppression of proliferation and cardiomyocyte hypertrophy by CHAMP, a cardiac-specific RNA helicase. *Proc Natl Acad Sci U S A* **99**(4): 2043-2048.

Madura, K. and Varshavsky, A. 1994. Degradation of G alpha by the N-end rule pathway. *Science* **265**(5177): 1454-1458.

Maly, D.J., Choong, I.C., and Ellman, J.A. 2000. Combinatorial target-guided ligand assembly: identification of potent subtype-selective c-Src inhibitors. *Proc Natl Acad Sci U S A* **97**(6): 2419-2424.

Matrosovich, M.N. 1989. Towards the development of antimicrobial drugs acting by inhibition of pathogen attachment to host cells: a need for polyvalency. *FEBS Lett* **252**(1-2): 1-4.

McGovern, S.L., Caselli, E., Grigorieff, N., and Shoichet, B.K. 2002. A common mechanism underlying promiscuous inhibitors from virtual and high-throughput screening. *J Med Chem* **45**(8): 1712-1722.

Meinnel, T., Serero, A., and Giglione, C. 2006. Impact of the N-terminal amino acid on targeted protein degradation. *Biol Chem* **387**(7): 839-851.

Mende, U., Kagen, A., Cohen, A., Aramburu, J., Schoen, F.J., and Neer, E.J. 1998. Transient cardiac expression of constitutively active Galphaq leads to hypertrophy and dilated cardiomyopathy by calcineurin-dependent and independent pathways. *Proc Natl Acad Sci U S A* **95**(23): 13893-13898.

Milano, C.A., Dolber, P.C., Rockman, H.A., Bond, R.A., Venable, M.E., Allen, L.F., and Lefkowitz, R.J. 1994. Myocardial expression of a constitutively active alpha 1B-adrenergic receptor in transgenic mice induces cardiac hypertrophy. *Proc Natl Acad Sci U S A* **91**(21): 10109-10113.

Mittmann, C., Chung, C.H., Hoppner, G., Michalek, C., Nose, M., Schuler, C., Schuh, A., Eschenhagen, T., Weil, J., Pieske, B., Hirt, S., and Wieland, T. 2002. Expression of ten RGS proteins in human myocardium: functional characterization of an upregulation of RGS4 in heart failure. *Cardiovasc Res* **55**(4): 778-786.

Mogk, A., Schmidt, R., and Bukau, B. 2007. The N-end rule pathway for regulated proteolysis: prokaryotic and eukaryotic strategies. *Trends Cell Biol* **17**(4): 165-172.

Molkentin, J.D. and Dorn, I.G., 2nd. 2001. Cytoplasmic signaling pathways that regulate cardiac hypertrophy. *Annu Rev Physiol* **63**: 391-426.

Neves, S.R., Ram, P.T., and Iyengar, R. 2002. G protein pathways. *Science* **296**(5573): 1636-1639.

Offermanns, S., Zhao, L.P., Gohla, A., Sarosi, I., Simon, M.I., and Wilkie, T.M. 1998. Embryonic cardiomyocyte hypoplasia and craniofacial defects in G alpha q/G alpha 11-mutant mice. *Embo J* **17**(15): 4304-4312.

Olson, E.N. and Schneider, M.D. 2003. Sizing up the heart: development redux in disease. *Genes Dev* **17**(16): 1937-1956.

Ota, I.M. and Varshavsky, A. 1993. A yeast protein similar to bacterial two-component regulators. *Science* **262**(5133): 566-569.

Owen, V.J., Burton, P.B., Mullen, A.J., Birks, E.J., Barton, P., and Yacoub, M.H. 2001. Expression of RGS3, RGS4 and Gi alpha 2 in acutely failing donor hearts and end-stage heart failure. *Eur Heart J* **22**(12): 1015-1020.

Pandey, G.N., Dwivedi, Y., SridharaRao, J., Ren, X., Janicak, P.G., and Sharma, R. 2002. Protein kinase C and phospholipase C activity and expression of their specific isozymes is decreased and expression of MARCKS is increased in platelets of bipolar but not in unipolar patients. *Neuropsychopharmacology* **26**(2): 216-228.

Papa, F.R. and Hochstrasser, M. 1993. The yeast DOA4 gene encodes a deubiquitinating enzyme related to a product of the human tre-2 oncogene. *Nature* **366**(6453): 313-319.

Peng, J., Schwartz, D., Elias, J.E., Thoreen, C.C., Cheng, D., Marsischky, G., Roelofs, J., Finley, D., and Gygi, S.P. 2003. A proteomics approach to understanding protein ubiquitination. *Nat Biotechnol* **21**(8): 921-926.

Pickart, C.M. 2001. Mechanisms underlying ubiquitination. *Annu Rev Biochem* **70**: 503-533.

Rai, R. and Kashina, A. 2005. Identification of mammalian arginyltransferases that modify a specific subset of protein substrates. *Proc Natl Acad Sci U S A* **102**(29): 10123-10128.

Rao, H., Uhlmann, F., Nasmyth, K., and Varshavsky, A. 2001. Degradation of a cohesin subunit by the N-end rule pathway is essential for chromosome stability. *Nature* **410**(6831): 955-959.

Rao, J., Lahiri, J., Isaacs, L., Weis, R.M., and Whitesides, G.M. 1998. A trivalent system from vancomycin.D-ala-D-Ala with higher affinity than avidin.biotin. *Science* **280**(5364): 708-711.

Rasband, W.S. 1997-2006. ImageJ. In. U. S. National Institutes of Health, Bethesda, Maryland, USA.

Rechsteiner, M., Hoffman, L., and Dubiel, W. 1993. The multicatalytic and 26 S proteases. *J Biol Chem* **268**(9): 6065-6068.

Riddle, E.L., Schwartzman, R.A., Bond, M., and Insel, P.A. 2005. Multi-tasking RGS proteins in the heart: the next therapeutic target? *Circ Res* **96**(4): 401-411.

Rogers, J.H., Tamirisa, P., Kovacs, A., Weinheimer, C., Courtois, M., Blumer, K.J., Kelly, D.P., and Muslin, A.J. 1999. RGS4 causes increased mortality and reduced cardiac hypertrophy in response to pressure overload. *J Clin Invest* **104**(5): 567-576.

Rogers, J.H., Tsirka, A., Kovacs, A., Blumer, K.J., Dorn, G.W., 2nd, and Muslin, A.J. 2001. RGS4 reduces contractile dysfunction and hypertrophic gene induction in Galpha q overexpressing mice. *J Mol Cell Cardiol* **33**(2): 209-218.

Romero, D.G., Plonczynski, M.W., Gomez-Sanchez, E.P., Yanes, L.L., and Gomez-Sanchez, C.E. 2006. RGS2 is regulated by angiotensin II and functions as a negative feedback of aldosterone production in H295R human adrenocortical cells. *Endocrinology* **147**(8): 3889-3897.

Ross, E.M. and Wilkie, T.M. 2000. GTPase-activating proteins for heterotrimeric G proteins: regulators of G protein signaling (RGS) and RGS-like proteins. *Annu Rev Biochem* **69**: 795-827.

Rubin, D.M., van Nocker, S., Glickman, M., Coux, O., Wefes, I., Sadis, S., Fu, H., Goldberg, A., Vierstra, R., and Finley, D. 1997. ATPase and ubiquitin-binding proteins of the yeast proteasome. *Mol Biol Rep* **24**(1-2): 17-26.

Sabatini, D.M., Erdjument-Bromage, H., Lui, M., Tempst, P., and Snyder, S.H. 1994. RAFT1: a mammalian protein that binds to FKBP12 in a rapamycin-dependent fashion and is homologous to yeast TORs. *Cell* **78**(1): 35-43.

Sakamoto, K.M., Kim, K.B., Kumagai, A., Mercurio, F., Crews, C.M., and Deshaies, R.J. 2001. Protacs: chimeric molecules that target proteins to the Skp1-Cullin-F box complex for ubiquitination and degradation. *Proc Natl Acad Sci U S A* **98**(15): 8554-8559.

Saric, T., Graef, C.I., and Goldberg, A.L. 2004. Pathway for degradation of peptides generated by proteasomes: a key role for thimet oligopeptidase and other metallopeptidases. *J Biol Chem* **279**(45): 46723-46732.

Saunders, D.N., Hird, S.L., Withington, S.L., Dunwoodie, S.L., Henderson, M.J., Biben, C., Sutherland, R.L., Ormandy, C.J., and Watts, C.K. 2004. Edd, the murine hyperplastic disc gene, is essential for yolk sac vascularization and chorioallantoic fusion. *Mol Cell Biol* **24**(16): 7225-7234.

Schunkert, H., Sadoshima, J., Cornelius, T., Kagaya, Y., Weinberg, E.O., Izumo, S., Riegger, G., and Lorell, B.H. 1995. Angiotensin II-induced growth responses in isolated adult rat hearts. Evidence for load-independent induction of cardiac protein synthesis by angiotensin II. *Circ Res* **76**(3): 489-497.

Schwartz, E.C., Saez, L., Young, M.W., and Muir, T.W. 2007. Post-translational enzyme activation in an animal via optimized conditional protein splicing. *Nat Chem Biol* **3**(1): 50-54.

Sedmera, D. and Thomas, P.S. 1996. Trabeculation in the embryonic heart. *Bioessays* **18**(7): 607.

Segal, D.J., Crotty, J.W., Bhakta, M.S., Barbas, C.F., 3rd, and Horton, N.C. 2006. Structure of Aart, a designed six-finger zinc finger peptide, bound to DNA. *J Mol Biol* **363**(2): 405-421.

Shi, B., Stevenson, R., Campopiano, D.J., and Greaney, M.F. 2006. Discovery of glutathione S-transferase inhibitors using dynamic combinatorial chemistry. *J Am Chem Soc* **128**(26): 8459-8467.

Shrader, T.E., Tobias, J.W., and Varshavsky, A. 1993. The N-end rule in Escherichia coli: cloning and analysis of the leucyl, phenylalanyl-tRNA-protein transferase gene aat. *J Bacteriol* **175**(14): 4364-4374.

Shuker, S.B., Hajduk, P.J., Meadows, R.P., and Fesik, S.W. 1996. Discovering high-affinity ligands for proteins: SAR by NMR. *Science* **274**(5292): 1531-1534.

Siekierka, J.J., Hung, S.H., Poe, M., Lin, C.S., and Sigal, N.H. 1989. A cytosolic binding protein for the immunosuppressant FK506 has peptidyl-prolyl isomerase activity but is distinct from cyclophilin. *Nature* **341**(6244): 755-757.

Sierra, D.A., Popov, S., and Wilkie, T.M. 2000. Regulators of G-protein signaling in receptor complexes. *Trends Cardiovasc Med* **10**(6): 263-268.

Sin, N., Meng, L., Wang, M.Q., Wen, J.J., Bornmann, W.G., and Crews, C.M. 1997. The anti-angiogenic agent fumagillin covalently binds and inhibits the methionine aminopeptidase, MetAP-2. *Proc Natl Acad Sci U S A* **94**(12): 6099-6103.

Solomon, V., Baracos, V., Sarraf, P., and Goldberg, A.L. 1998. Rates of ubiquitin conjugation increase when muscles atrophy, largely through activation of the N-end rule pathway. *Proc Natl Acad Sci U S A* **95**(21): 12602-12607.

Song, J.J. and Lee, Y.J. 2005. Dissociation of Akt1 from its negative regulator JIP1 is mediated through the ASK1-MEK-JNK signal transduction pathway during metabolic oxidative stress: a negative feedback loop. *J Cell Biol* **170**(1): 61-72.

Srivastava, D. and Olson, E.N. 2000. A genetic blueprint for cardiac development. *Nature* **407**(6801): 221-226.

Stewart, A.E., Arfin, S.M., and Bradshaw, R.A. 1995. The sequence of porcine protein NH2-terminal asparagine amidohydrolase. A new component of the N-end Rule pathway. *J Biol Chem* **270**(1): 25-28.

Struthers, A.D. and MacDonald, T.M. 2004. Review of aldosterone- and angiotensin II-induced target organ damage and prevention. *Cardiovasc Res* **61**(4): 663-670.

Sucov, H.M., Dyson, E., Gumeringer, C.L., Price, J., Chien, K.R., and Evans, R.M. 1994. RXR alpha mutant mice establish a genetic basis for vitamin A signaling in heart morphogenesis. *Genes Dev* **8**(9): 1007-1018.

Sundgren, N.C., Giraud, G.D., Stork, P.J., Maylie, J.G., and Thornburg, K.L. 2003. Angiotensin II stimulates hyperplasia but not hypertrophy in immature ovine cardiomyocytes. *J Physiol* **548**(Pt 3): 881-891.

Taban, C.H., Hondermarck, H., Bradshaw, R.A., and Biolly, B. 1996. Effect of a dipeptide inhibiting ubiquitin-mediated protein degradation nerve-dependent limb regeneration in the newt. *Experientia* **52**(9): 865-870.

Tamirisa, P., Blumer, K.J., and Muslin, A.J. 1999. RGS4 inhibits G-protein signaling in cardiomyocytes. *Circulation* **99**(3): 441-447.

Tasaki, T., Mulder, L.C., Iwamatsu, A., Lee, M.J., Davydov, I.V., Varshavsky, A., Muesing, M., and Kwon, Y.T. 2005. A family of mammalian E3 ubiquitin ligases that contain the UBR box motif and recognize N-degrons. *Mol Cell Biol* **25**(16): 7120-7136.

Tasaki, T., Mulder, L.C.F., Iwamatsu, A., Lee, M.J., Davydov, I.V., Varshavsky, A., Muesing, M., and Kwon, Y.T. 2005. A family of mammalian E3 ubiquitin ligases that contain the UBR box motif and recognize N-degrons. *Mol Cell Biol* **25**: 7120-7136.

Tasaki, T., Sohr, R., Xia, Z., Hellweg, R., Hortnagl, H., Varshavsky, A., and Kwon, Y.T. 2007. Biochemical and genetic studies of UBR3, a ubiquitin ligase with a function in olfactory and other sensory systems. *J Biol Chem* **282**(25): 18510-18520.

Thomas, W.G., Brandenburger, Y., Autelitano, D.J., Pham, T., Qian, H., and Hannan, R.D. 2002. Adenoviral-directed expression of the type 1A angiotensin receptor promotes cardiomyocyte hypertrophy via transactivation of the epidermal growth factor receptor. *Circ Res* **90**(2): 135-142.

Tobias, J.W., Shrader, T.E., Rocap, G., and Varshavsky, A. 1991. The N-end rule in bacteria. *Science* **254**(5036): 1374-1377.

Toyoda, M., Shirato, H., Nakajima, K., Kojima, M., Takahashi, M., Kubota, M., Suzuki-Migishima, R., Motegi, Y., Yokoyama, M., and Takeuchi, T. 2003. jumonji downregulates cardiac cell proliferation by repressing cyclin D1 expression. *Dev Cell* **5**(1): 85-97.

Tsang, S.K., Cheh, J., Isaacs, L., Joseph-McCarthy, D., Choi, S.K., Pevear, D.C., Whitesides, G.M., and Hogle, J.M. 2001. A structurally biased combinatorial approach for discovering new anti-picornaviral compounds. *Chem Biol* **8**(1): 33-45.

Varshavsky, A. 1996. The N-end rule: functions, mysteries, uses. *Proc Natl Acad Sci U S A* **93**(22): 12142-12149.

Varshavsky, A. 1996. The N-end rule: functions, mysteries, uses. *Proc Natl Acad Sci USA* **93**: 12142-12149.

Varshavsky, A. 2000. Recent studies of the ubiquitin system and the N-end rule pathway. *Harvey Lect* **96**: 93-116.

Varshavsky, A. 2006. The early history of the ubiquitin field. *Protein Sci* **15**(3): 647-654.

Wang, X., Li, F., Said, S., Capasso, J.M., and Gerdes, A.M. 1996. Measurement of regional myocardial blood flow in rats by unlabeled microspheres and Coulter channelyzer. *Am J Physiol* **271**(4 Pt 2): H1656-1665.

Warkentin, T.E. and Koster, A. 2005. Bivalirudin: a review. *Expert Opin Pharmacother* **6**(8): 1349-1371.

Wieland, T. and Mittmann, C. 2003. Regulators of G-protein signalling: multifunctional proteins with impact on signalling in the cardiovascular system. *Pharmacol Ther* **97**(2): 95-115.

Zenker, M., Mayerle, J., Lerch, M.M., Tagariello, A., Zerres, K., Durie, P.R., Beier, M., Hulskamp, G., Guzman, C., Rehder, H., Beemer, F.A., Hamel, B., Vanlieferinghen, P., Gershoni-Baruch, R., Vieira, M.W., Dumic, M., Auslender, R., Gil-da-Silva-Lopes, V.L., Steinlicht, S., Rauh, M., Shalev, S.A., Thiel, C., Ekici, A.B., Winterpacht, A., Kwon, Y.T., Varshavsky, A., and Reis, A. 2005. Deficiency of UBR1, a ubiquitin ligase of the N-end rule pathway, causes pancreatic dysfunction, malformations and mental retardation (Johanson-Blizzard syndrome). *Nat Genet* **37**(12): 1345-1350.

Zhang, S., Watson, N., Zahner, J., Rottman, J.N., Blumer, K.J., and Muslin, A.J. 1998. RGS3 and RGS4 are GTPase activating proteins in the heart. *J Mol Cell Cardiol* **30**(2): 269-276.

Zhou, J., Moroi, K., Nishiyama, M., Usui, H., Seki, N., Ishida, J., Fukamizu, A., and Kimura, S. 2001. Characterization of RGS5 in regulation of G protein-coupled receptor signaling. *Life Sci* **68**(13): 1457-1469.